THE UNIVERSITY
of LIVERPOOL

THE CONTROL OF HELICOPTERS WITH UNDERSLUNG EXTERNAL LOADS

Thesis submitted in accordance with the
requirements of the University of Liverpool
for the degree of Doctor of Philosophy

by

K.K.T.Thanapalan B.Eng (Hons), MIEE, MIEEE

July 2004

THE CONTROL OF HELICOPTERS WITH UNDERSLUNG EXTERNAL LOADS

by

K.K.T.Thanapalan

Acknowledgements

It is my pleasure to express my sincere thanks to my supervisor Dr Jihong Wang for her invaluable support and intellectual guidance, both academically and personally, for this research project. Her assiduous supervision and healthy criticisms made it possible for me to complete the project successfully.

Thanks is offered to my co-supervisors Professor Gareth Padfield and Dr Keith Nuttall for many helpful discussions and much valuable advice; also to the members of the Flight Science & Technology Research group and Intelligence Engineering & Automation Research group, especially Dr Emmanuel Prempain, Dr Binoy Manimala, and Mr Jianlin Wei for their friendly help and valuable discussions.

I am grateful to the University of Liverpool, for providing the research facilities, making it possible for me to conduct this research.

Finally, I am greatly indebted to my best friends Elizabeth, Lisa, and Shanthi for their undying love and encouragement, also to my family for their moral support and encouragement during the whole period of my postgraduate life.

Abstract

The Control of Helicopters with
Underslung External Loads

By

K. K. T. Thanapalan

This thesis addresses some of the issues associated with the dynamics of helicopters with an external underslung load, and development of robust control strategies to ensure the positioning of the underslung load, whilst the helicopter maintains the hover condition.

The helicopter dynamics are studied with reference to a general dynamical model of a generic helicopter which is then adapted to model a UH-60 helicopter. Validation of the model has been performed by comparison with flight test data for a UH-60 helicopter for small perturbations about the hover condition. The dynamics of that helicopter with an external underslung load are investigated by developing an underslung load model as a driven pendulum with the helicopter motion as the input. First, the influence of the motion of the helicopter on the dynamics of the underslung load is analysed, then the influence of the load on the dynamics of the helicopter is investigated.

An overview of flight control design techniques that have been applied to helicopter control has been undertaken. An experimental study has been conducted to demonstrate the application of fuzzy logic control as an example of an intelligent flight control method. For the experimental study a twin rotor MIMO system has been used, which is an experimental system with complex nonlinearities, similar to a helicopter.

For the control of a helicopter with an underslung load, a nonlinear stabilizing feedback control for uncertain dynamical systems has been applied to a helicopter and its load treated as a composite system. In general, two main approaches are often adopted for the control of an uncertain dynamical system. If the uncertainty in the system model is assumed to have statistical characterization and the desired behaviour of the system is described in a statistical sense, a stochastic approach is feasible. Otherwise, if structural properties and bounds relating to the uncertainties are known, then a deterministic approach is appropriate. Considering the control of a helicopter and its load the dynamic models of both helicopter and load have some terms that are uncertain. The uncertainties may arise

from the unknown parameters in the dynamical models or from inadequate modelling of aspects such as the aerodynamics of the load. Therefore, for a realistic model, uncertainties must be taken into account during the controller design. There are always some restrictions on the control input limits, so- called bounds on the control inputs levels. Hence the deterministic control approach has been chosen. Using the deterministic control law design method, a nonlinear state stabilizing feedback control law has been designed.

Contents

List of Figures

List of Tables

Chapter 1

Introduction

Helicopters have the ability to carry large and bulky loads externally on a sling. This capability is important in many applications, ranging from lifting heavy load to saving life. Importantly, when lives are under risk and rapid rescue operations are needed this operation is vital. The stability of the helicopter will be disturbed by the underslung load, which slows or even prevents an accurate pick up or placement of the loads. The goal of this work is to study the dynamics of helicopters with an external underslung load, in particular, at a hover condition and to develop a robust control strategy to ensure the positioning of the load at the hover condition.

1.1 General description of the problem

Helicopter operators over the world gain benefits such as large freight transportation, fire fighting and life saving missions by carrying payloads externally, underslung beneath the helicopter. Furthermore the load weight limit is often greater than the load carried internally when it is carried externally on a sling. The bulky loads can be carried and the process of picking up and droping off is relatively straightforward. Once the load is on the ground, these benefits are offset by the piloting difficulties, the increased workload, and the attendant reduction in flight safety arising from carrying underslung loads. Piloting problems arise from the adverse coupling between the helicopter and the load. The nature of this problem can be easily appreciated by trying to place a weight hanging from a piece of string accurately on the squares of a chequer-board. As the pivot point is accelerated away from rest, the weight begins to swing, the precision is degraded and the control becomes more difficult. Similarly, if the pilot of a helicopter manoeuvres the helicopter too quickly while trying to place an underslung load precisely on a spot, the load will start to swing. Moreover, the swinging load can couple with the helicopter motion and pilot control so that there is the potential for instability. This is all exacerbated by the fact that the pilot cannot see the load under the helicopter and often has to rely on a second crew member to call out positioning instructions. If weather conditions are poor and/or visibility degraded,

the task difficulty is further increased. The way in which the operators typically cope with these piloting problems is to restrict operations to be taken under good conditions.

A second problem arises when a pilot tries to manoeuvre the helicopter when flying in forward flight. Generally high speed is not allowed because of the potential hazards associated with the load flying. At mid speeds the pilot still needs to manoeuvre the aircraft to climb/descent and turn. Here again, the pilot needs to manoeuvre the helicopter gently to avoid exciting the oscillatory aircraft/load mode.

The dynamics of a helicopter with an external suspended load received considerable attention since the late 70's and early 90's. This interest has been renewed recently, prompted by the re-evaluation and extension of the ADS-33 [Anonymous, 1996] helicopter handling qualities specification to compact helicopters, and in the expectation of new cargo helicopter procurements [Fusato *et al,* 1999]. Gubbles [Gubbles, 2001] investigated the effect of an external slung load on helicopter dynamics and handling qualities. The objective of that work was to compare helicopter dynamics and handling qualities for two cases. The first case involved an externally carried load on a single sling. The second case consisted of the same aircraft mass, with the load carried internally. Through this investigation the dynamic problems of carrying an external load on a sling were addressed.

The challenges of control of dynamics of a helicopter with an underslung external load are traditionally studied by means of simulations. The essence of flight simulation is in creating an illusion of reality for the pilot to experience. The quality or fidelity of this illusion will ultimately determine the boundary for what can and cannot be accomplished in terms of read-across to the real world. To demonstrate this fact, NASA has conducted both simulation and flight trials using UH-60 helicopter with an instrumented 8-by-6-by-6-ft cargo container [Cicolani *et al,* 2001, Sahai, *et al,* 1999, Tyson, *et at,* 1999, McCoy, 1998].

A variety of literature has been published concerning various aspects of underslung load operations. Broader details of the subject can be found in various reports, which summarise the problems experienced in helicopters. These reports also suggest some

technical solutions and analysis methods for some of the problems [e.g. Shaughnessy, *et al* 1979, Sheldon, 1977, Watkins, *et al* 1974].

Previous research considered mainly single point suspensions, where the load is connected to the helicopter at only one point. The single point suspension restrains the motion of the load to pendulous oscillations in the longitudinal (pitch) plane and in the lateral (roll) plane. But it gives no restoring moment in the yaw plane, and the load motion in that plane is governed only by the aerodynamic forces and moments that act on the load [Fusato *et al,* 1999].

Many of the dynamic models for a single-point suspension approximate the load as a point mass, sometime with aerodynamics drag force acting on it. The helicopter is usually treated as a rigid body with various degrees of complexity [Dukes, 1973, Gupta, *et al* 1976]. In many cases, the model is simplified by de-coupling the longitudinal modes from the lateral modes, especially near hover [e.g. Dukes, 1973]. Early research shows that approximating the helicopter as a rigid body and neglecting rotor dynamics is accurate enough for the slung load problem analysis [Nagabhushan, 1977].

The emphasis in most of the recent research has shifted to the study of multiple point suspensions see for example, [Cicolani, *et al* 1995, Cicolani, *et al* 1990, Prabhakar 1978]. The shift is motivated by the need to stabilise the yaw motion of the load. In multiple point suspensions the load is attached to the helicopter at two or more points thereby providing some restraint in yaw.

The dynamic models for multiple point suspensions are usually more rigorous than models for a single point suspension. They usually account for six degrees of freedom of the helicopter motion, and account for rigid body motion of the load. The suspension cables are usually assumed extensible and modelled as springs. However the multiple point suspensions do not necessarily solve the problems of yaw instabilities. First, they give only static restoring moment, and cannot eliminate problems due to dynamic yaw instabilities. Second and even more important, their usage is limited since these suspensions may create large variations in the longitudinal centre of gravity of the helicopter, which most of the helicopters cannot handle.

Hence most helicopters have only a single rotor, and must continue to use single point suspensions. So it is necessary to continue to study the yaw instabilities and single point suspensions, which have appeared to be neglected in the 80's and the interest has been renewed recently. Now there is considerable interest in this problem.

In this thesis, a study of dynamics of helicopters and the dynamics extended to helicopter with underslung external loads are carried out in order to gain insight into the dynamic characteristics of a helicopter with an underslung load. The analysis begins with the study of helicopter mathematical model, and then the development of a mathematical model of an underslung load, by considering the helicopter dynamics are the input to the load model is carried out in order to investigate the load dynamics. The work then proceeds to investigate the flight stability of the helicopter with an underslung load attached. Simulation studies have been performed using the simulation software FLIGHTLAB. The results reveal how the stability of the helicopter is degraded by the influences of the load. The stability deceases as both the load weight and sling length are increased. Secondly, the stability problem is addressed. A good controller is vital for maintaining the stability of the system while performing the underslung load operation. Controller development is addressed starting from an overview of flight control design techniques applied to develop a control law for helicopter. For the control of helicopter with underslung load problem, a nonlinear stabilizing feedback control for uncertain dynamical systems is studied and initial investigation for the possibility of applying this method to helicopter control with underslung load composite system is carried out.

1.2 Control of helicopters with an underslung load

A helicopter with an underslung load is a complex dynamic system in which its subsystems and components are interact each other dynamically and exhibit great deal of nonlinearities. The adequate system dynamic performance is highly depending on the proper performance of controller of the system. Today's aviation industry offers a range of flight control design techniques to develop control laws for helicopters. These methods are ranging from linear quadratic regulator control (LQR), eigenstructure assignment to H-infinity optimisation etc. For example, linear quadratic regulator (LQR) control theory has provided an important tool for helicopter

control law design [Gribble, 1993]. The design freedoms in the LQR method are two matrices which penalise excursions of states and input vectors from desired values. Innocenti [Innocenti *et al,* 1984] gives an example of classical SISO methods application to a flight control design. The use of eigenstructure assignment for helicopter control system design has been considered by several researchers; see for instance [Manness *et al,* 1990]. Turner [Turner, 2000] gives an account of success of H-infinity method and shows the successful application of H-infinity approach to helicopter control.

The use of intelligent control methods for helicopter control system design has also been considered by several researchers; especially some form of fuzzy control development is widely considered, for example see [Kadmiry *et al,* 2001], [Steinberg, 1992]. Recently, Ledin [Ledin *et al,* 2003] presents a PID (Proportional-Integral-Derivative) controller to drive the helicopter to a specified point in a space by considering that the helicopter possesses a navigation system that tracks the vehicle's position, velocity and angular orientation without error. However, it should be noted that in reality such error –free navigation systems are difficult to realise. Furthermore, Enns [Enns, *et al,* 1986] used the MIMO generalization PI technique to design a MIMO PI control law for YAH-64 helicopter. Many researchers have applied PID or some form of PID control law to scaled size helicopter control (for example see [Sanders *et al,* 1998, Woodley, *et al,* 1997]). But tuning the PID controller is one of the most common problems for a control Engineer.

The design of flight control systems for actively controlled helicopters presents problems, which are associated not only with the complex nature of the dynamics of the helicopter itself, but also with the range of design objectives which must be satisfied. Usually, the military rotorcraft handling qualities specification ADS-33D [Anonymous, 1996] is used to assess the capability of the control law. Generally speaking what is required from the control law, it should be able to stabilize the aircraft while controlling.

Linear or nonlinear control methods can be adapted to design a control law for a helicopter system. A brief introduction to the linear and nonlinar control systems and control methods are presented in the following subsections.

1.2.1 Linear control systems

Linear control system theories provide the fundamental background needed for controller design of dynamical systems. Linear control system theories are widely used for the analysis and synthesis of feedback control systems. Linear control is a subject with a variety of powerful methods and a long history of successful applications [Slotine *et al,* 1991].

Linear systems are often described in the form of linear differential equations. If the coefficients of the differential equations are constants then the system is linear time invariant. If the coefficients of differential equations governing the system are functions of time then the system is linear time varying. The differential equations of a linear time invariant system can be transformed into different mathematical descriptions, such as state space representation for the convenience of analysis. For example, in the case of single input single output system analysis, transfer function (s-domain equation) can be obtained by taking Laplace transform of the differential equations governing the system with zero initial conditions and rearranging the resulting algebraic equations to get the ratio of output to input.

In the early days, the classical Bode, Nyquist, and Nichols frequency response plots has been of immense use in frequency domain analysis and synthesis of linear control systems. Bhattacharyya [Bhattacharyya *et al,* 1995] gave details exposition of these tools. Many important applications found in practice involve stability problems. Gain and phase margins are popularly used as stability specifications in classical methods of analysis and synthesis of linear control systems. These specifications basically related to the maximum allowable variation in the open loop gain or phase of the system to conserve closed loop stability. The system models found in classical approaches to linear systems usually have fixed parameters values. However, for most real life system some uncertainty is present in the model parameters due to the modelling error etc. The uncertainty can be included in the model and then the stability analysis, such as gain and phase margin analysis must be carried out by considering the uncertainty, leading to the concept of robust stability of the system [Barve, 2003].

Time domain approach is also used for analyses of responses and designing control systems. Analysis of response means to see the variation of output with respect to time. The evaluation of system is based on the analysis of such responses. This output behaviour with respect to time should be within specified limits to have satisfactory performance of the system. The complete base of stability analysis lies in the time response analysis. The system stability, system accuracy and complete evaluation is always based on the time response analysis and corresponding results.

Classical control theory, which deals with techniques developed before 1950, and embodies such methods as root locus, etc. These methods have in common the use of transfer functions in the complex frequency domain, emphasis on the use of graphical techniques, the use of feedback, and the use of simplifying assumptions to approximate the time response. The essence of classical design is successive loop closure technique. Such a one-loop at a time design approach become increasingly difficult as more loops are added and do not guarantee success when the dynamics are multivariable.

Modern control refers to state space based methods developed in the early 1960s (e.g. LQ, LQR etc.). In modern control theory, system models are directly written in the time domain. Analysis and design are also based in the time domain. Modern control methods provided a lot of insight into system structure and properties; however, the row back of most modern control methods is that they inherently require a precise model of the system. To overcome this difficulty during the late 1970s a methods so-called robust control is emerged that tried to provide answers to the system uncertainty problem. Robust controls are a combination of modern state space and classical frequency domain techniques [Bhattacharyya *et al,* 1995].

In this work, for the investigation of the stability characteristics of a helicopter with underslung load system, linear control system theory is applied. The linearised system is expressed in the state space description form and the system stability was assessed by reference to the location of the system poles on a root locus diagram. However, it should be noted that the linear model is only an approximation to the true system dynamics. Thus, in this thesis considerable attention is paid into the nonlinear system and analysis.

1.2.2 Nonlinear control systems

Nonlinear systems have been shown to exhibit surprising and complex effects that would never be anticipated by a scientist trained only in linear techniques for example chaos, and bifurcation etc. Nonlinearity has its most profound effects on dynamical systems. There are essentially nonlinear phenomena that can take place in the presence of nonlinearity, hence they can not be described or predicted by linear models. For example, nonlinear systems may exhibit autonomous constant amplitude closed loop oscillations, known as limit cycles. The describing function approach [Atherton, 1975] is traditionally employed to predict the existence of the limit cycles. If limit cycles are predicted, it is also of interest to know the number of limit cycles, their frequencies and amplitudes, and key characteristics such as stability or instability. Describing function analysis occasionally fails to predict the limit cycles, particularly when the system under consideration does not satisfy the assumption of filtering out the higher order harmonics. It is also possible for describing function analysis to predict no limit cycles, even when a limit cycle actually exists. Despite these limitations, describing function analysis has been successfully used in many practical applications [Newman, 1995, Anthony, *et al,* 1990].

Many other nonlinear phenomena that may exhibit in the presence of nonlinearities such as finite escape time and multiple equilibria etc. these problems can be dealt with system analyses and controller development. The effect of nonlinearities on a dynamical system can be studied by employing modern dynamical system techniques such as global bifurcation theory. The global bifurcation theory is useful to detect large scale phenomena such as deterministic chaos etc. however, usually the primary concern in the analysis of nonlinear dynamical system is that the determination and predication of steady states or stationary motions and stability of the system. Stability analyses of a nonlinear system can be carried out using input-output (frequency) method, such as deriving the gain of the system and analyse the stability propriety of the system using passivity techniques etc, whereas the passivity idea is that the increase in stored energy is less than or equal to added energy. On the other hand Lyapunov's methods can be used for stability analysis, whereas storage function is a generalisation of Lyapunov function and the idea of Lyapunov's method is that the

energy is decreasing. Lyapunov was interested in showing how to discover if a solution to a dynamical system is stable or not for all time. Since the linear stability theory was not good enough for long time response analysis, because the small errors due to linearization would pile up and make the approximation invalid. Lyapunov developed concepts (now called Lyapunov stability) to over come these difficulties. In this work, Lyapunov function based control design method is developed for helicopter with underslung load system i.e., for the control system analyses, in this thesis the development of a nonlinear stabilisation feedback control via deterministic approach is studied and initial investigation for the possibility of applying this method to helicopter control with an external slung load is addressed. Firstly, stabilisations of uncertain dynamical systems are introduced. Then the case of deterministic control of cascade connection of uncertain nonlinear systems is investigated with application to control of helicopter with underslung load system.

1.3 Outline of the thesis

The thesis is organised as follows.

Chapter 2: Study of helicopter mathematical model

In chapter 2, firstly the fundamental concept of helicopter dynamics and modelling aspects of helicopters are discussed. Then a study of general models of a helicopter is presented, which started from a nonlinear dynamic model to a simplified linear model. Finally a simulation model of a UH-60 alike helicopter model (FGR model) is realised to be used to validate flight test data for the UH-60 helicopters at hover.

Chapter 3: Study on the influences of the undreslung load dynamics to the stability of helicopter.

This chapter, investigate the influences of an underslung load on flight handling performance and stability of the system. Stability of the helicopter is investigated with the presence of an underslung load, using FGR model. To conduct the combined system (helicopter with load) stability analysis a simulation model of an underslung load is implemented in FLIGHTLAB software and attached to the UH-60 alike FGR model. Linear and nonlinear analyses are conducted. The analysis shows how the stability of the helicopter is affected by the influences of the addition of the underslung load.

Chapter 4: Influence of helicopter dynamics to the dynamics of the underslung load.
In this chapter, an investigation of the dynamic behaviour of helicopter with underslung load is presented. A mathematical model of an underslung load is developed and applied to study the behaviour of the suspended load in response to in-flight helicopter manoeuvres. The simulation results show the importance of pilot control actions in positioning the load.

Chapter 5: Helicopter control methods and application of fuzzy control.
In chapter 5, an overview of flight control design techniques applied to develop a control law for helicopters are discussed. A review of the use of some popular methods such as PID control, LQ methods, nonlinear feedback linearization, eigenstructure assignment, classical SISO techniques, H-infinity optimisation and intelligent control methods for helicopter control system design are presented for example purpose, to show the wider scope of the topic. An experimental study is conducted to the development of a Fuzzy set point weighting PID control for the twin rotor MIMO system is also presented.

Chapter 6: Nonlinear deterministic control of a helicopter with an underslung load.
This chapter addresses a development of a nonlinear stabilization feedback control, using deterministic control approach. Firstly, deterministic control of uncertain dynamical system is introduced. Then for the control of helicopter with underslung load problem, the system is considered as a cascade connection of uncertain nonlinear systems and initial investigation for the possibility of applying the deterministic control method to helicopter control with underslung load composite system is carried out.

Chapter 7: Concluding remarks
The last chapter includes concluding remarks and some suggestions for further research work.

Chapter 2

Study of Helicopter Mathematical Model

2.1 Introduction

A helicopter has six degrees of freedom in its motions: up/down, fore/aft (longitudinal motion), left/right (lateral motion), pitching, rolling, and yawing. The motions of a helicopter are achieved by 1) collectively changing the pitch of all the main rotor blades, thus increasing rotor thrust (collective pitch); 2) cyclically changing the pitch as a sinusoidal function of azimuth which tilts the tip-path-plane fore/aft or left/right and changes the thrust vector direction (cyclic pitch); and 3) collectively changing the tail rotor pitch, which changes tail rotor thrust and thus the yaw moment. A helicopter pilot must simultaneously control three forces and moments, hence, control of a helicopter, is a difficult task indeed. A helicopter pilot typically has at his disposal a cyclic stick to control both fore/aft motions (pitch control) and left/right motion (roll control), a collective lever to control up and down motions (vertical control), and pedals to control left and right yawing motions (yaw control). Lift, thrust, pitching, and rolling control comes from the main rotor while yawing control comes from the tail rotor [Bramwell *et al,* 2001].

To analyse the dynamic problems of controlling a helicopter and develop control schemes for alleviating these problems, it is necessary to have a dynamic model for helicopters. The dynamic model should be well suited to stability and control analysis, which may involve linearised equations of motion about possible equilibrium positions.

In this chapter, the fundamental concept of helicopter dynamics, such as the principles of rotary flight and controls are studied, and also a mathematical model of a single main rotor helicopter is presented. The forces and moments from the different elements of helicopter are discussed in details. Then this generic model is bridging to a UH-60 like Flightlab Generic Rotorcraft Model (FGR), which is available in the University of Liverpool, Flight Simulation Laboratory. Simulation studies have been conducted using

FGR model with flight test data for UH-60 helicopters, simulations that illustrate the validity of the FGR model.

2.2 Fundamental concept of helicopter dynamics

2.2.1 Principles of rotary flight

The essential requirements for any flying machines are:

1. The lift force must be equal or exceed the aircraft's weight and be capable of being controlled.
2. The propulsive thrust in a forward flight direction must equal or exceed the aircraft's drag and be capable of being controlled.
3. There must be control forces and moments, which are capable of altering the aircraft's attitude in pitch, roll and yaw.

Rotorcrafts produce their lift force by means of rotors, which are rotating wings, and consequently these rotors must be able to supply the above three requirements. The single main rotor provides that vertical thrust necessary for the aircraft to leave the ground and control it in vertical direction [Leishman, 2000, Newman, 1994].

Considering the complexity of a helicopter in relation to fixed wing aircraft, there are two fundamental differences. Firstly, the helicopter possesses the ability to fly at low speeds and even to hover. As a result of these unique abilities, the helicopter is able to precisely follow a planned trajectory. This low speed and hover capability can only be achieved at the expense of payload and operating cost [Thomson *et al,* 1998] as low speed flight implies that there is less lift from the aerodynamics surfaces, hence the maximum payload is considerably less than that of a fixed wing aircraft. Secondly, the helicopter is controlled in a manner very different from that of the fixed wing aircraft, due not just to the vehicle configuration, but also because of the complex cross-coupling between the longitudinal and lateral states [Cameron, 2002].

A helicopter is equipped with one or more power-driven rotors (horizontal propellers) in lieu of fixed wings. It is able to take off and land vertically, to move in any direction, or to remain stationary in the air. The lift developed by a conventional aircraft wing depends

on two factors: the angle of attack of the wing and the velocity of the air in relation to the wing. To obtain the necessary lift the aircraft must have a forward movement. In the case of the helicopter, the (relative) air velocity is produced by the rotation of the rotor blades when the angle of attack attains a certain value, the lift overcomes the weight of the aircraft. Then the aircraft takes off vertically. To achieve horizontal flight, the pilot tilts the rotor forward at a certain angle, which is achieved by what is known as cycle pitch change, i.e., changing the pitch of each blade once per revolution. More particularly, the angle of attack of each blade is increased every time when it sweeps over the tail of the machine, thereby temporarily developing a greater amount of thrust then the other blades. The thrust developed by the rotor can be resolved into a vertical component (the actual lift that keeps the machine in the air) and a forward component (which propels the machine horizontally). Each blade can swivel about its longitudinal axis and its pitch is changed cyclically, through a linkage system, by a so-called swash-plate, which performs a sort of wobbling rotary motion around the shaft and swivels the blades to and from as they rotate. The tilt of the swash plate can be varied by the pilot, and the tilt of the rotor follows the tilt of the plate.

The blade root hinges are called as lag hinges. If there were no hinges, tilting of the plane of rotation of the rotor blades relative to the helicopter causes a periodic change in the speed of the blades. This would produce severe stresses in the blades; which are relieved and cancelled by the hinge. Motion about the hinge enables the blade to rotate at a constant speed irrespective of how much the rotor is tilted. In forward movement of the helicopter, the velocity due to blade rotation and due to forward speed are added together, i.e., they intensify each other, on the advancing side of the rotor; on the retreating side, however, they are subtracted from each other. If the rotor blades were rigidly fixed to the shaft, the lift would vary cyclically and cause the helicopter to roll. This is prevented by the hinge. Instead, the blade flaps cyclically as it rotates.

The rotation of the rotor tends to cause the fuselage of the aircraft to rotate in the opposite direction (on the principle that any action calls forth a reaction). To prevent this, the single-rotor helicopter is provided at its tail with a small propeller producing a counteracting sideways thrust. Alternatively, the helicopter may have two rotors, which revolve in opposite directions and thus counterbalance each other.

2.2.2 Controls of a helicopter

To control completely the position and attitude of a helicopter (body) requires control of the forces and moments about all three axes. This involves six independent controls thus, if the body drifts to the side, a force may be exerted to return it to its original position. If it rolls over, a moment may be exerted to right it again. It would be exceedingly difficult, however, for a man to co-ordinate the controls of any machine having six independent control systems. Fortunately, it is possible to reduce this number by coupling together independent controls [Bramwell, 1976, Stepniewski, *et al,* 1984]. Actually, four independent controls are adequate for the helicopter, which are:

1) Vertical control: This is necessary to fix the position of the helicopter in the vertical direction. It is achieved by increasing or decreasing the pitch of the rotor so as to increase or decrease the thrust.
2) Directional control: Directional control fixes the attitude of the helicopter in rotation about the vertical axis, permitting the pilot to point the ship in any horizontal direction.
3) Lateral control: Lateral control involves the application of both moments and forces. When the pilot applies lateral control a rolling moment is produced about the aircraft centre of gravity which tilts the helicopter. As a consequence of the tilt, a component of the rotor thrust vector acts in the direction of tilt. The application of lateral control has therefore resulted in a tilt and sideward motion of the helicopter.
4) Longitudinal control: Longitudinal control is identical in nature to lateral control. Pitching moments are coupled with longitudinal forces.

In order to maintain these controls, while the helicopter flying, there are three main controls required to fly a helicopter, which are collective pitch control, cyclic pitch control, and Rudder pedals, which are briefly described below.

Collective pitch control can only be found in helicopters. Moving the collective pitch up and down changes the pitch of the main rotors and moves the helicopter up and down. This is linked to the engine power. As the pitch is increased, and more power is required from the engine so the rotor speed is kept at the same level.

Cyclic pitch control is the central control column. When it is moved forward or backward it will point the nose of the helicopter up or down. It does this by varying the angle of the rotor blades as they go round, tilting the rotor back and forth. When it is moved left or right, the rotor tilts in that direction and the helicopter banks and rolls.

Rudder pedals control the tail rotor. Moving the left pedal makes the helicopter to go left and moving the right pedal makes it to go right. This action is achieved actually by changing the pitch of the tail rotor.

Rotor blades are the helicopter's equivalent to the wings of an aeroplane. Like any wings, the shape of the blades is very important. It is designed so that the air passing over the upper surface moves faster, causing a difference in pressure between the upper and lower surfaces, creating an upwards force known as lift.

Most helicopters have a single main rotor on the top and a smaller tail rotor at the back, controlling the direction of the helicopter flies. The tail rotor is very important, when spin a rotor using an engine, the rotor will rotate, but the engine and the helicopter will try to rotate in the opposite direction. This is called torque reaction. The tail rotor is used like a small propeller, to pull against torque reaction and hold the helicopter straight. By applying more or less pitch (angle) to the tail rotor blades it can be used to make the helicopter turn left or right, becoming a rudder. The tail rotor is connected to the main rotor through a gearbox.

2.3 Study of helicopter models

The six rigid body degrees of freedom are the basic motion involved in the analysis of flight dynamics. The rotor is also a major factor in the dynamic response characteristics of helicopters; therefore the dynamic model of helicopter must take account of these facts for the adequate replicate of the system and its behaviour.

2.3.1 Dynamic model of a helicopter

The forces and moments from the different elements of a helicopter, such as main rotor, tail rotor, fuselage and empennage, are considered. The helicopter has six degree of

freedom in its motion and it has nine state variables in general, which are u, v, w the aircraft velocity components at centre of gravity, p, q, r the aircraft roll, pitch and yaw rates about body reference axes, and θ, ϕ, ψ the Euler angles. The Euler angles define the orientation of the fuselage with respect to earth axes system [Padfield, 1996]. To derive the equations of the translational and rotational motions of a helicopter, the helicopter is assumed to be a rigid body referred to an axes system fixed at the centre of mass of the aircraft, as shown in Figure 2.1, so the axes move with time varying velocity components under the action of the applied forces. Firstly, a structure block diagram of a helicopter system from control point of view is shown in Figure 2.2. In Figure 2.2, downward arrows are used to indicate the flow of the system functionality. The flow of functions starts with the four control inputs, which are, longitudinal cyclic (θ_{1s}) lateral cyclic (θ_{1c}), collective (θ_c) and pedal (θ_{0T}), which control the basic nine states of the system such as $p, q, r, \phi, \theta, \psi, u, v,$ and w. The block diagram shows how the helicopter motion is achieved through the overall external forces X, Y and Z along x, y, z axes and moments L, M, N about x, y, z axes. It can be noted that the main contributions to helicopter motion are from the rotors, especially from the main rotor.

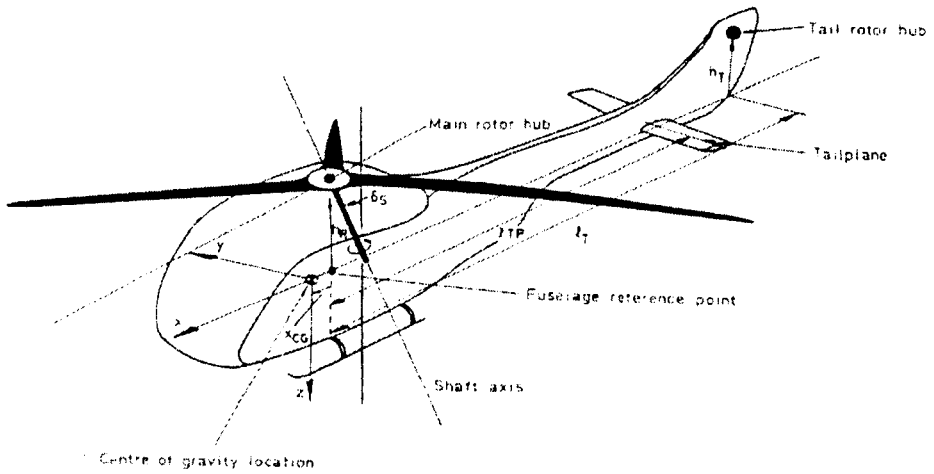

Fig.2.1 Helicopter elements with defined *x, y, z* axes coordinate system [Padfield, 1981]

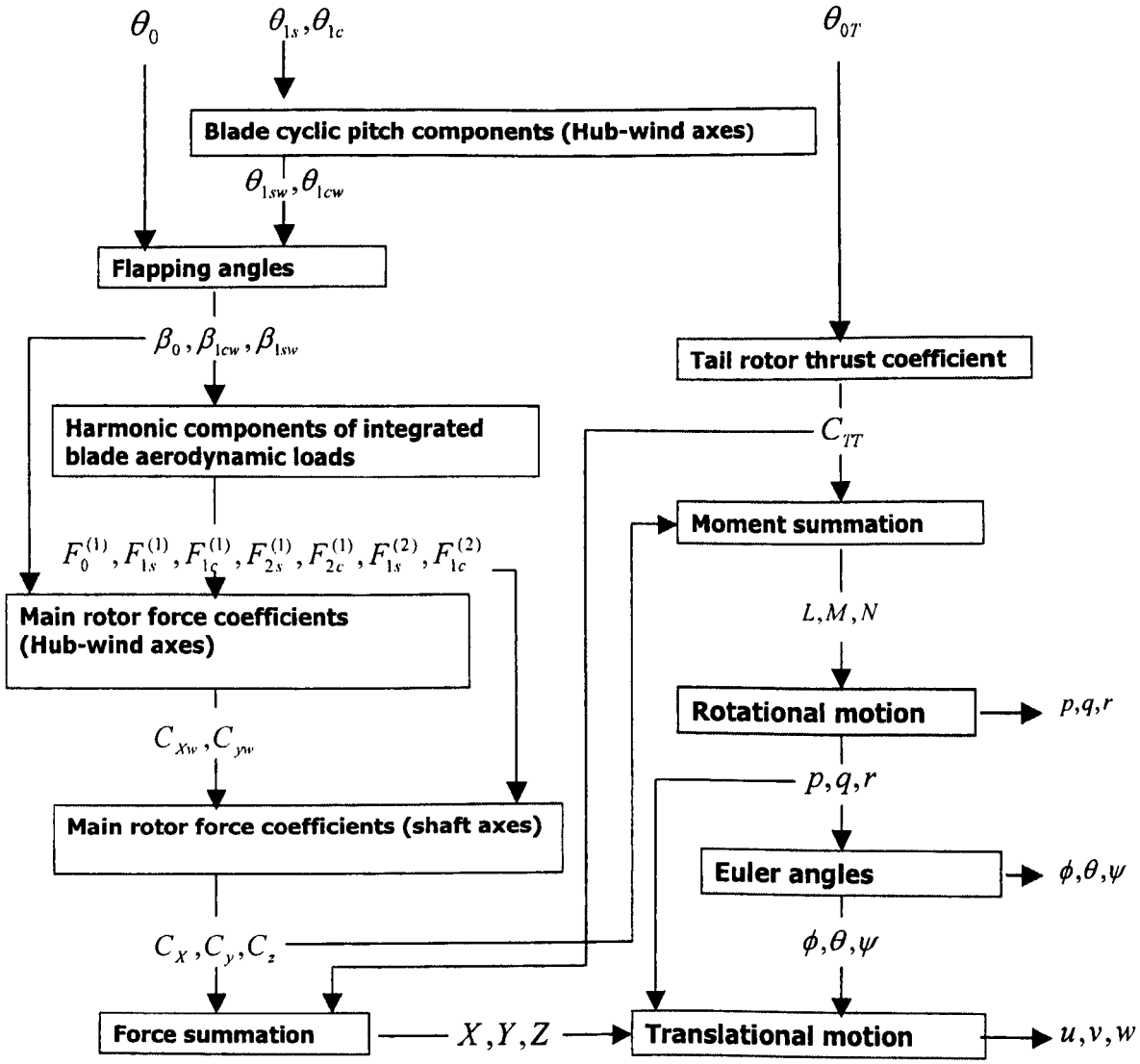

Fig 2.2 Structure block diagram of a helicopter system

The mathematical model of helicopter motion can be derived which is a set of complicated nonlinear differential equations. Initially the basic nine state equations are written which involves the overall external forces and moments. It follows the overall forces and moment's equation, in which individual element's (e.g. main rotor) contribution to produce the overall forces and moments for the helicopter motion is expressed then details description of their contribution is discussed.

The equations govern the translational motions are given below [Padfield, 1996]

$$\dot{u} = rv - qw - g\sin\theta + X/M_a \tag{2.1a}$$

$$\dot{v} = pw - ru + g\cos\theta\sin\phi + Y/M_a \tag{2.1b}$$

$$\dot{w} = qu - pv + g\cos\theta\cos\phi + Z/M_a \tag{2.1c}$$

The equations describe the rotational motion are as follows:

$$\dot{p} = \frac{(I_{yy} - I_{zz})qr}{I_{xx}} + \frac{I_{xz}(pq(I_{xx} - I_{yy}) + rq + I_{yy} - I_{zz}) + I_{xx}^2 pq}{(I_{xx}^2 + I_{xx}I_{zz})} + pq + \frac{I_{xz}(N - L)}{(I_{xx}^2 + I_{xx}I_{zz})} + L \tag{2.2a}$$

$$\dot{q} = \frac{1}{I_{yy}}\left[(I_{zz} - I_{xx})pr - I_{xz}(p^2 - r^2)\right] + \frac{1}{I_{yy}}M \tag{2.2b}$$

$$\dot{r} = \frac{I_{xz}(rq - I_{yy} - I_{zz}) - I_{xz}^2 pq + pq(I_{xx} - I_{yy})}{(I_{xz}^2 + I_{xx}I_{zz})} + \frac{N - I_{xz}L}{(I_{xz}^2 + I_{xx}I_{zz})} \tag{2.2c}$$

The resulted Euler angles from the motion can be obtained from

$$\dot{\phi} = p + q\sin\phi\tan\theta + r\cos\phi\tan\theta \tag{2.3a}$$

$$\dot{\theta} = q\cos\phi - r\sin\phi \tag{2.3b}$$

$$\dot{\psi} = q\sin\phi\sec\theta + r\cos\phi\sec\theta \tag{2.3c}$$

The mathematical symbols used in above equations can be found in the list of notions. M_a and g are the mass of the helicopter and acceleration due to gravity, I_{xx}, I_{yy}, I_{zz} are the moment of inertia of the helicopter about x, y and z axes, and I_{xz} the aircraft product of inertia.

The overall external forces X, Y and Z along x, y, z axes can be written as

$$\begin{aligned} X = {} & \frac{1}{2}\rho(\Omega R)^2 \pi R^2 a_0 s \cos\gamma_s \frac{2C_x}{a_0 s} - \frac{1}{2}\rho(\Omega R)^2 \pi R^2 a_0 s \sin\gamma_s \frac{2C_Z}{a_0 s} \\ & + \frac{1}{2}\rho(\Omega R)^2 \pi R^2 a_0 s S_p \overline{V}_F^2 C_{XF}(\alpha_F) \end{aligned} \tag{2.4}$$

$$\begin{aligned} Y = {} & \frac{1}{2}\rho(\Omega R)^2 \pi R^2 a_0 s\left(\frac{2C_Y}{a_0 s}\right) + \frac{1}{2}\rho(\Omega R)^2 \overline{V}_{FN}^2 S_{FN} C_{YFN}(\beta_{FN}) \\ & + \frac{1}{2}\rho(\Omega_T R_T)^2 a_{0T} s_T (\pi R_T)^2 \left(\frac{2C_{TT}}{a_0 s_T}\right) F_T \\ & + \frac{1}{2}\rho(\Omega R)^2 S_S \overline{V}_F^2 C_{YS} \frac{v_A}{V_F} \end{aligned} \tag{2.5}$$

$$Z = \frac{1}{2}\rho(\Omega R)^2 \pi R^2 a_0 s\left(\sin\gamma_s\left(\frac{2C_X}{a_0 s}\right) + \cos\gamma_s\left(\frac{2C_Z}{a_0 s}\right)\right) + \frac{1}{2}\rho(\Omega R)^2 \overline{V}_T^2 S_{TP} C_{ZTP}(\alpha_{TP}) + S_P \overline{V}_F^2 C_{ZF}(\alpha_F) \tag{2.6}$$

The moments L, M, N about x, y, z axes can be written as

$$L = \frac{-b}{2} K_\beta \beta_{1s} + h_R\left(\frac{1}{2}\rho\pi R^2 (\Omega R)^2 a_0 s\left(\frac{2C_Y}{a_0 s}\right)\right) + h_T \cdot \frac{1}{2}\rho(\Omega_T R_T)^2 a_{0T} s_T (\pi R_T)^2\left(\frac{2C_{TT}}{a_{0T} s_T}\right) F_T + h_{FN} \cdot \frac{1}{2}\rho(\Omega R)^2 \overline{V}_{FN}^2 S_{FN} C_{YFN}(\beta_{FN}) \tag{2.7}$$

$$M = \frac{-b}{2} K_\beta \beta_{1s} - h_R \cdot \frac{1}{2}\rho\pi R^2 (\Omega R)^2 a_0 s\left(\cos\gamma_s\left(\frac{2C_X}{a_0 s}\right) - \sin\gamma_s\left(\frac{2C_Z}{a_0 s}\right)\right) + x_{cg} \cdot \frac{1}{2}\rho\pi R^2 (\Omega R)^2 a_0 s\left(\sin\gamma_s\left(\frac{2C_X}{a_0 s}\right) + \cos\gamma_s\left(\frac{2C_Z}{a_0 s}\right)\right) + (l_{TP} + x_{cg})\frac{1}{2}\rho(\Omega R)^2 \overline{V}_T^2 S_{TP} C_{ZTP}(\alpha_{TP}) + \frac{1}{2}\rho(\Omega R)^2 S_P l_F \overline{V}_F^2 C_{MF}(\alpha_F) \tag{2.8}$$

$$N = \frac{1}{2}\rho(\Omega R)^2 \pi R^3 s a_0\left(\frac{2C_Q}{a_0 s} + \left(\frac{2I_R}{bI_\beta}\right)\frac{\overline{\Omega}'}{\gamma}\right) - x_{cg}\left(\frac{1}{2}\rho\pi R^2 (\Omega R)^2 a_0 s\left(\frac{2C_Y}{a_0 s}\right)\right) - (l_T + x_{cg})\frac{1}{2}\rho(\Omega_T R_T)^2 a_{0T} s_T (\pi R_T)^2\left(\frac{2C_{TT}}{a_0 s_T}\right) F_T - (l_{FN} + x_{cg})\frac{1}{2}(\Omega R)^2 \overline{V}_{FN}^2 S_{FN} C_{YFN}(\beta_{FN}) + \frac{1}{2}\rho(\Omega R)^2 S_S l_F \overline{V}_F^2 C_{NF}(\beta_F) \tag{2.9}$$

where ρ is air density, R and Ω are the main rotor blade radius and speed, a_0 and s the main rotor blade lift curve slope and solidity, and C_x, C_y, C_z are the main rotor force coefficients in shaft axes. They can be obtained by

$$\begin{bmatrix} C_X \\ C_Y \end{bmatrix} = \begin{bmatrix} \cos\Psi_w & -\sin\Psi_w \\ \sin\Psi_w & \cos\Psi_w \end{bmatrix} \begin{bmatrix} C_{XW} \\ C_{YW} \end{bmatrix} \tag{2.10}$$

$$\left(\frac{2C_Z}{a_0 s}\right) = -\left(\frac{2C_T}{a_0 s}\right) = -F_0^{(1)} \tag{2.11}$$

where Ψ_w is the side-slip angle and C_T is the main rotor thrust coefficient given by

$$C_T = \frac{T}{\rho(\Omega R)^2 \pi R^2} \tag{2.12}$$

The main rotor force coefficients in the hub-wind axes C_{XW} and C_{YW} are can be obtained through equations (2.13) and (2.14) in terms of harmonic components of integrated blade aerodynamic loads and harmonics of flapping.

$$\left(\frac{2C_{XW}}{a_0 s}\right) = \left(\frac{F_0^{(1)}}{2} + \frac{F_{2c}^{(1)}}{4}\right)\beta_{1cw} + \frac{F_{1c}^{(1)}}{2}\beta_0 + \frac{F_{2s}^{(1)}}{4}\beta_{1sw} + \frac{F_{1s}^{(2)}}{2} \tag{2.13}$$

$$\left(\frac{2C_{YW}}{a_0 s}\right) = \left(\frac{F_0^{(1)}}{2} + \frac{F_{2c}^{(1)}}{4}\right)\beta_{1sw} - \frac{F_{1s}^{(1)}}{2}\beta_0 - \frac{F_{2s}^{(1)}}{4}\beta_{1cw} + \frac{F_{1c}^{(2)}}{2} \tag{2.14}$$

where β_0 is the coning angle and β_{1cw}, β_{1sw} are the first harmonic cyclic flapping angles.

The harmonic components of integrated blade aerodynamic loads are given by the following expressions

$$F_0^{(1)} = \theta_0\left(\frac{1}{3} + \frac{\mu^2}{2}\right) + \frac{\mu}{2}\left(\theta_{1sw} + \frac{\bar{p}_w}{2}\right) + \left(\frac{\mu_z - \lambda_0}{2}\right) + \frac{1}{4}\left(1 + \mu^2\right)\theta_{tw} \tag{2.15}$$

$$F_{1s}^{(1)} = \frac{\alpha_{sw} + \theta_{1sw}}{3} + \mu\left(\theta_0 + \mu_z - \lambda_0 + \frac{2}{3}\theta_{tw}\right) \tag{2.16}$$

$$F_{1c}^{(1)} = \frac{\alpha_{cw} + \theta_{1cw}}{3} - \frac{\mu\beta_0}{2} \tag{2.17}$$

$$F_{2s}^{(1)} = \frac{\mu}{2}\left\{\theta_{1cw} - \beta_{1sw} + \frac{\bar{q}_w - \lambda_{1cw}}{2} - \mu\beta_0\right\} \tag{2.18}$$

$$F_{2c}^{(1)} = -\frac{\mu}{2}\left\{\theta_{1sw} + \beta_{1cw} + \frac{\bar{p}_w - \lambda_{1sw}}{2} + \mu\left(\theta_0 + \frac{\theta_{tw}}{2}\right)\right\} \tag{2.19}$$

$$\begin{aligned} F_{1s}^{(2)} &= \frac{\mu^2}{2}\beta_0\beta_{1sw} + \left(\mu_z - \lambda_0 - \frac{\mu}{4}\beta_{1cw}\right)\alpha_{sw} - \frac{\mu}{4}\beta_{1sw}\alpha_{cw} \\ &+ \theta_0\left(\frac{\alpha_{sw}}{3} + \mu(\mu_z - \lambda_0) - \frac{\mu^2}{4}\beta_{1cw}\right) + \left(\frac{\alpha_{sw}}{4} + \frac{\mu}{2}\left(\mu_z - \lambda_0 - \frac{\beta_{1c}\mu}{4}\right)\right)\theta_{tw} \\ &+ \theta_{1sw}\left(\frac{\mu_z - \lambda_0}{2} + \mu\left(\frac{3}{8}(\bar{p}_w - \lambda_{1sw}) + \frac{\beta_{1cw}}{4}\right)\right) \\ &+ \frac{\mu}{4}\theta_{1cw}\left(\frac{\bar{q}_w - \lambda_{1cw}}{2} - \beta_{1sw} - \mu\beta_0\right) - \frac{\delta\mu}{a_0} \end{aligned} \tag{2.20}$$

$$\begin{aligned} F_{1c}^{(2)} &= -2\beta_0\mu\left(\mu_z - \lambda_0 - \frac{4}{3}\mu\beta_{1cw}\right) + \left(\mu_z - \lambda_0 - \frac{3}{4}\beta_{1cw}\mu\right)\alpha_{cw} \\ &- \frac{\mu}{4}\beta_{1sw}\alpha_{sw} + \theta_0\left(\frac{\alpha_{cw}}{3} - \frac{\mu}{2}\left(\beta_0 + \frac{\mu}{2}\beta_{1sw}\right)\right) + \theta_{tw}\left(\frac{\alpha_{cw}}{4} - \mu\left(\frac{\beta_0}{3} + \frac{\mu}{8}\beta_{1sw}\right)\right) \\ &+ \theta_{1cw}\left(\frac{\mu_z - \lambda_0}{2} + \frac{\mu}{4}\left(\frac{\bar{p}_w - \lambda_{1sw}}{2} - \beta_{1cw}\right)\right) \\ &+ \frac{\mu}{4}\theta_{1sw}\left(\frac{\bar{q}_w - \lambda_{1cw}}{2} - \beta_{1sw} - \mu\beta_0\right) \end{aligned} \tag{2.21}$$

The flapping is written in the form, such as

$$\beta = \beta_0 + \beta_{1cw}\cos\psi + \beta_{1sw}\sin\psi \tag{2.22}$$

and the flapping angles are given by

$$[\beta_0] = \frac{n_\beta}{\lambda_\beta^2}\left\{\left[1+\mu^2, \frac{4}{5}+\frac{2}{3}\mu^2, \frac{4}{3}\mu, 0\right]\begin{bmatrix}\theta_0\\ \theta_{tw}\\ \theta_{1sw}\\ \theta_{1cw}\end{bmatrix} + \left[\frac{4}{3}, \frac{-2}{3}\mu, 0\right]\begin{bmatrix}\mu_z - \lambda_0\\ \lambda_{1sw}\\ \lambda_{1cw}\end{bmatrix} + \left[0, 0, \frac{2}{3}\mu, 0\right]\begin{bmatrix}\bar{p}'_w\\ \bar{q}'_w\\ \bar{p}_w\\ \bar{q}_w\end{bmatrix}\right\} \tag{2.23}$$

$$\begin{bmatrix}\beta_{1cw}\\ \beta_{1sw}\end{bmatrix}=\frac{-n_\beta}{\lambda_\beta^2\left(1+S_\beta^2\right)}\left\{\begin{bmatrix}\frac{4}{3}\mu\left(S_\beta+\frac{2\lambda_\beta^2}{n_\beta}\right), 2\mu\left(\frac{\lambda_\beta^2}{n_\beta}+\frac{8}{15}S_\beta\right), \left(1+2\mu^2\right)\frac{\lambda_\beta^2}{n_\beta}+\left(\frac{4}{3}\mu\right)^2 S_\beta, -\frac{\lambda_\beta^2}{n_\beta}S_\beta\left(1+\frac{\mu^2}{2}\right)\\ \frac{4}{3}\mu\left(1-2S_\beta\frac{\lambda_\beta^2}{n_\beta}\right), 2\mu\left(\frac{8}{15}-S_\beta\frac{\lambda_\beta^2}{n_\beta}\right), \left(\frac{4}{3}\mu\right)^2-S_\beta\frac{\lambda_\beta^2}{n_\beta}\left(1+\frac{3}{2}\mu^2\right), -\frac{\lambda_\beta^2}{n_\beta}\end{bmatrix}\begin{bmatrix}\theta_0\\ \theta_{1w}\\ \theta_{1sw}\\ \theta_{1cw}\end{bmatrix}+\right.$$
$$\begin{bmatrix}\mu\left(\left(\frac{4}{3}\right)^2 S_\beta+\frac{2\lambda_\beta^2}{n_\beta}\right), -\left(\frac{\lambda_\beta^2}{n_\beta}\left(1+\frac{\mu^2}{2}\right)+\frac{S_\beta}{2}\left(\frac{4}{3}\mu\right)^2\right), \frac{\lambda_\beta^2}{n_\beta}S_\beta\\ \mu\left(\left(\frac{4}{3}\right)^2-2S_\beta\frac{\lambda_\beta^2}{n_\beta}\right), -\frac{1}{2}\left(\frac{4}{3}\mu\right)^2+\frac{\lambda_\beta^2}{n_\beta}S_\beta, -\frac{\lambda_\beta^2}{n_\beta}\left(\frac{\mu^2}{2}-1\right)\end{bmatrix}\begin{bmatrix}\mu_z-\lambda_0\\ \lambda_{1sw}\\ \lambda_{1cw}\end{bmatrix}+$$
$$\left.\begin{bmatrix}\left(\frac{\lambda_\beta}{n_\beta}\right)^2\left(1+\frac{\mu^2}{2}\right), -\left(\frac{\lambda_\beta}{n_\beta}\right)^2 S_\beta, \frac{\lambda_\beta^2}{n_\beta}\left(1+\frac{\mu^2}{2}-\frac{2S_\beta}{n_\beta}\right)+\frac{S_\beta}{2}\left(\frac{4}{3}\mu\right)^2, \frac{\lambda_\beta^2}{n_\beta}\left(S_\beta+\frac{2}{n_\beta}\left(1+\frac{\mu^2}{2}\right)\right)\\ -\left(\frac{\lambda_\beta}{n_\beta}\right)^2 S_\beta, \left(\frac{\lambda_\beta}{n_\beta}\right)^2\left(\frac{\mu^2}{2}-1\right), \frac{\lambda_\beta^2}{n_\beta}\left(\frac{2}{n_\beta}\left(\frac{\mu^2}{2}-1\right)-S_\beta\right)+\frac{1}{2}\left(\frac{4}{3}\mu\right)^2, \frac{\lambda_\beta^2}{n_\beta}\left(\frac{2S_\beta}{n_\beta}+\frac{\mu^2}{2}-1\right)\end{bmatrix}\begin{bmatrix}\bar{p}_w\\ \bar{q}_w\\ \bar{p}_w\\ \bar{q}_w\end{bmatrix}\right\} \tag{2.24}$$

where θ_0 is the main rotor collective pitch and $\theta_{1cw}, \theta_{1sw}$ blade cyclic pitch components in hub-wind axes are defined by

$$\begin{bmatrix}\theta_{1sw}\\ \theta_{1cw}\end{bmatrix}=\begin{bmatrix}\cos\Psi_w & \sin\Psi_w\\ -\sin\Psi_w & \cos\Psi_w\end{bmatrix}\begin{bmatrix}\theta_{1s}\\ \theta_{1c}\end{bmatrix}, \tag{2.25}$$

where θ_{1s}, θ_{1c} are the longitudinal and lateral cyclic pitch.

The tail rotor provides control for the *yaw*, whose only responsibility is to provide a sideways thrust force and thereby produce a yawing moment about the main rotor shaft [Newman, 1994, Leishman, 2000] i.e. contributes the external force Y, moments L, and M (see equations (2.5), (2.7) and (2.9)). Tail rotor contribution can be determined by

$$\left(\frac{2C_T}{a_{0T}s_T}\right)=\frac{1}{3}\cdot\frac{\theta_{0T}+K_3\left(\frac{n_\beta}{\lambda_\beta^2}\right)_T\frac{4}{3}\left(\mu_{zT}-\lambda_{0T}\right)}{1-K_3\left(\frac{n_\beta}{\lambda_\beta^2}\right)_T\left(1+\mu_T^2\right)}\cdot\left(1+\frac{3}{2}\mu_T^2\right)+\left(\frac{\mu_{zT}-\lambda_{0T}}{2}\right), \tag{2.26}$$

where θ_{0T} is a tail rotor pitch (control input).

The detailed description and explanation to the complete helicopter mathematical model can be found in [Padfield, 1981, Prouty, 1986 Padfield, 1996]. From the above description, it can be seen that the mathematical model is very complicated and nonlinear. Apart from simulation study, it is difficult to conduct any theoretic analysis

based on this version of system model. In some cases, the simplified linear model may provide a helpful description to the helicopter to reveal some aspects of helicopter dynamics. So a linearised version of helicopter model is discussed in next section.

2.3.2 Linear approximation to a helicopter model

The mathematical model presented in section 2.3.1 may be too complicated for analysis. Sometime it is necessary to make use of the well developed theory of linearisation to learn more about the behaviour of a nonlinear system [Khalil, 1992]. Linearisation is an approximation in the neighbourhood of an operating point; it can only predict the local behaviour of the nonlinear system in the vicinity of that point. In this study, the behaviour of the helicopter system at hover condition (operating point) is considered thus the linear model may be suitable for the analysis of a helicopter at a hover condition.

The helicopter equations of motion described in Section 2.3.1 can be written as follows

$$\dot{\bar{x}} = \bar{F}(\bar{x}, \bar{u}, t) \ , \tag{2.27}$$

where $\bar{x} = [\phi \quad \theta \quad \psi \quad u \quad v \quad w \quad p \quad q \quad r]^T$ is the state variable vector, $\bar{u} = [\theta_{1c} \quad \theta_{1s} \quad \theta_0 \quad \theta_{0T}]^T$ is the control vector, and $\bar{F}$ represents the nonlinear relationship of the system state variables. To derive the linearised equations of motion using small perturbation theory, the helicopter behaviour can be described as a perturbation from the trim, written in the form

$$\bar{x} = \bar{x}_e + \delta\bar{x} \tag{2.28}$$

For linearization, it is assumed that the external forces X, Y and Z and moments L, M and N can be represented as analytic functions of the disturbed motion variables and their derivatives. Thus the forces and moments can then be written in the Taylor's expansion form. Then, the linearized equations of motion about a general trim condition can be written as in the state space form $\dot{\bar{x}} = A\bar{x} + B\bar{u}$ and the system matrix A and control matrix B are derived from the partial derivatives of the nonlinear function $\bar{F}$, i.e.

$$A = \left(\frac{\partial \bar{F}}{\partial \bar{x}} \right)_{\bar{x}=\bar{x}_e} \tag{2.29}$$

and

$$B = \left(\frac{\partial \bar{F}}{\partial \bar{u}} \right)_{\bar{x}=\bar{x}_e} \tag{2.30}$$

So the fully expanded form of the linear helicopter mathematical model has the following structure:

$$\begin{bmatrix} \dot{\phi} \\ \dot{\theta} \\ \dot{\psi} \\ \dot{u} \\ \dot{v} \\ \dot{w} \\ \dot{p} \\ \dot{q} \\ \dot{r} \end{bmatrix} = \begin{bmatrix} 0 & 0 & 0 & 0 & 0 & 0 & 1 & 0 & 0 \\ 0 & 0 & 0 & 0 & 0 & 0 & 0 & 1 & 0 \\ 0 & 0 & 0 & 0 & 0 & 0 & 0 & 0 & 1 \\ 0 & -g\cos\theta_e & 0 & X_u & X_v & X_w & X_p & (X_q - w_e) & (X_r - v_e) \\ g & 0 & 0 & Y_u & Y_v & Y_w & (Y_p + w_e) & Y_q & (Y_r - u_e) \\ 0 & -g\sin\theta_e & 0 & Z_u & Z_v & Z_w & (Z_p - v_e) & (Z_q + u_e) & Z_r \\ 0 & 0 & 0 & L_u & L_v & L_w & L_p & L_q & L_r \\ 0 & 0 & 0 & M_u & M_v & M_w & M_p & M_q & M_r \\ 0 & 0 & 0 & N_u & N_v & N_w & N_p & N_q & N_r \end{bmatrix} \begin{bmatrix} \phi \\ \theta \\ \psi \\ u \\ v \\ w \\ p \\ q \\ r \end{bmatrix}$$

$$+ \begin{bmatrix} 0 & 0 & 0 & 0 \\ 0 & 0 & 0 & 0 \\ 0 & 0 & 0 & 0 \\ X_{\theta_{1c}} & X_{\theta_{1s}} & X_{\theta_0} & X_{\theta_{0T}} \\ Y_{\theta_{1c}} & Y_{\theta_{1s}} & Y_{\theta_0} & Y_{\theta_{0T}} \\ Z_{\theta_{1c}} & Z_{\theta_{1s}} & Z_{\theta_0} & Z_{\theta_{0T}} \\ L_{\theta_{1c}} & L_{\theta_{1s}} & L_{\theta_0} & L_{\theta_{0T}} \\ M_{\theta_{1c}} & M_{\theta_{1s}} & M_{\theta_0} & M_{\theta_{0T}} \\ N_{\theta_{1c}} & N_{\theta_{1s}} & N_{\theta_0} & N_{\theta_{0T}} \end{bmatrix} \begin{bmatrix} \theta_{1c} \\ \theta_{1s} \\ \theta_0 \\ \theta_{0T} \end{bmatrix} \tag{2.31}$$

In order to investigate the longitudinal and lateral stability, the linear model can be reduced to longitudinal and lateral motion, by assuming that at hover trim condition, position, attitude and velocities are zero and longitudinal and lateral motion can be decoupled.

Decoupling longitudinal and lateral modes are common practices in the fixed wing aircraft, the cross coupling derivatives would be zero. However, this is not the case for the helicopter as these cross-coupling terms influence the vehicle modes, and the handling qualities. But this decoupling or weakly coupled assumption leads to investigate the longitudinal and lateral modes separately as two distinctive sets. Phugoid, pitch and heave modes are identified as longitudinal modes and spiral, roll and dutch roll modes are identified as lateral modes [Padfield, 1996].

Equation of longitudinal motion

$$\begin{bmatrix} \dot{\theta} \\ \dot{u} \\ \dot{w} \\ \dot{q} \end{bmatrix} = \begin{bmatrix} 0 & 0 & 0 & 1 \\ -g\cos\theta_e & X_u & X_w & (X_q - w_e) \\ -g\sin\theta_e & Z_u & Z_w & (Z_q + u_e) \\ 0 & M_u & M_w & M_q \end{bmatrix} \begin{bmatrix} \theta \\ u \\ w \\ q \end{bmatrix} + \begin{bmatrix} 0 & 0 \\ X_{\theta_{1s}} & X_{\theta_0} \\ Z_{\theta_{1s}} & Z_{\theta_0} \\ M_{\theta_{1s}} & M_{\theta_0} \end{bmatrix} \begin{bmatrix} \theta_{1s} \\ \theta_0 \end{bmatrix} \tag{2.32}$$

where, longitudinal motion of the helicopter is uncoupled from lateral dynamics and described by four vector elements. It is assumed that the collective and (longitudinal) cyclic controls are mainly influence the longitudinal motion.

Equation of lateral motion

$$\begin{bmatrix} \dot{\phi} \\ \dot{\psi} \\ \dot{v} \\ \dot{p} \\ \dot{r} \end{bmatrix} = \begin{bmatrix} 0 & 0 & 0 & 1 & 0 \\ 0 & 0 & 0 & 0 & 1 \\ g & 0 & Y_v & (Y_p + w_e) & (Y_r - u_e) \\ 0 & 0 & L_v & L_p & L_r \\ 0 & 0 & N_v & N_p & N_r \end{bmatrix} \begin{bmatrix} \phi \\ \psi \\ v \\ p \\ r \end{bmatrix} + \begin{bmatrix} 0 & 0 \\ 0 & 0 \\ Y_{\theta_{1c}} & Y_{\theta_{0T}} \\ L_{\theta_{1c}} & L_{\theta_{0T}} \\ N_{\theta_{1c}} & N_{\theta_{0T}} \end{bmatrix} \begin{bmatrix} \theta_{1c} \\ \theta_{0T} \end{bmatrix} \tag{2.33}$$

Similarly, where lateral motion of the helicopter is uncoupled from longitudinal dynamics and described by five vector elements. It is assumed that the pedal (tail rotor collective) and (lateral) cyclic controls are mainly influence the lateral motion. Usually the heading angle ψ is omitted from the matrices, as the direction of flight in horizontal plane has no bearing on the aerodynamic forces and moments [Fletcher, 1995]. Detailed discussion of state, control and stability derivatives of the matrices can be found in Padfield [Padfield, 1996] who discusses in detail some of their characteristics.

The stability and control derivatives contained in the linear equations of motion aid in the understanding of helicopter flight dynamics. Analysis of the model takes place by considering that for small deviations from trim, the helicopter model can be determined from the system eigenvalues which are calculated from the stability matrix A.

To investigate the influences of a control input for a particular mission task, the state space representation can be transformed into a transfer function relationship between the states and controls. This is achieved simply by taking the state space representation.

$$\dot{\bar{x}} = A\bar{x} + B\bar{u} \tag{2.34}$$

and transforming it to the frequency domain to give

$$\mathbf{s}\bar{X}(\mathbf{s}) = A\bar{X}(\mathbf{s}) + B\bar{U}(\mathbf{s}) \tag{2.35}$$

Finally, rearranging to relate the state variables to the control inputs gives

$$(\mathbf{s}I - A)\bar{X}(\mathbf{s}) = B\bar{U}(\mathbf{s})$$

$$\bar{X}(\mathbf{s}) = (\mathbf{s}I - A)^{-1} B\bar{U}(\mathbf{s}) \tag{2.36}$$

The helicopter handling qualities are strongly influenced by the stability of the normal modes, where stability of the mode is determined by whether or not the real part of the eigenvalue is positive or negative (stable modes having a negative real eigenvalue). Emphasis will be placed on the stability assessment in the following chapter.

2.4 UH-60 helicopter model (FGR model) and simulation study

The generic mathematical model is bridging to a simulation model, which is available in the University of Liverpool, Flight Simulation Laboratory. Simulation studies have been conducted using the simulation model with flight test data for UH-60 helicopters to examine the validity of the simulation model. The helicopter simulation model used in this study is implemented in FLIGHTLAB software [Padfield *et al*, 2001]. The aircraft model employed, as a basis to this study is the FLIGHTLAB Generic Rotorcraft model (FGR) configured approximately as a UH-60 Black Hawk helicopter. The UH-60 helicopter is a multi-mission helicopter and has been utilised in various missions such as air assault, air cavalry, command and control, electronic warfare and medical evacuations etc., so the UH-60 model is chosen for this study.

An approach similar to the mathematical model presented in section 2.3.1 has been taken for modelling the FGR model. However, in FLIGHTLAB, tail rotor components implemented is based on a simplified theoretical method of determining the characteristics of a lifting rotor in forward flight which is called Bailey rotor. The coordinate system of the Bailey rotor has X forward into the free-stream airflow and Z in the direction of thrust. Rotor thrust and torque are calculated as a function of a blade tip loss factor by making the following assumptions:

- Uniform induced flow over the rotor
- Unsteady aerodynamic effects are neglected
- Compressibility effects are ignored
- Linear lift with constant lift curve slope
- Constant chord and linear twist

Bailey derived rotor thrust and torque by analytically integrating the air-loads over the rotor blade span and averaging them over the azimuth. For the main rotor, in Flightlab model aerodynamics effect has been taken into account in more details. It considered that the aerodynamic components are numeric components that allow the computation of airloads, inflow, and interference. Airloads are computed to give the motion of the attached structural component and inflow is computed based on the airloads. Additionally, interference between the aerodynamic components can be computed.

Fuselage and empennage components are implemented in Flightlab model, by using aerodynamics laws, in which the forces and moments from these elements are given by functions of incident and sideslip angles. In the process of modelling due to the complex flow field around helicopter fuselages and the interaction of the main rotor wake with the fuselage, some difficulties are caused to construct the forces and moments equations. So the direct results from wind tunnel test data gathered from various sources are used. The model also has a basic control system with mixing unit and actuators plus limited authority stability augmentation system (SAS).

In summary, the model is modelled with four rigid blades with offset flap hinge and the blade element rotor with look-up tables of quasi-steady, nonlinear lift, drag and pitching moment as functions of incidence and Mach number.

Validation of the model is an important issue and, to this end, comparisons are made with flight test data for UH-60 helicopter at hover [Fletcher, 1993], [Fletcher, 1995]. FGR model is set to hover condition with the model parameters values (UH-60 helicopter data) tabulated in Tables 2.1~2.4 and the control input responses are applied to the FGR model from the flight test data and the outputs are compared with the flight test data responses. Comparisons are made for all four control inputs, which are lateral, longitudinal, collective and pedal. The results are presented below.

Table 2.1: Parameters for aircraft mass and inertia

Description	Symbol	UH-60 value	Units
mass of the helicopter	M_a	15350	*lb*
aircraft roll inertia	I_{xx}	5629	*slug ft²*
aircraft pitch inertia	I_{yy}	40000	*slug ft²*
aircraft yaw inertia	I_{zz}	37200	*slug ft²*
product of inertia	I_{xz}	1670	*slug ft²*
c.g. location	-	(36.0 0 24.7)	*ft*
Fuselage reference pt.	-	(34.6 0 23.4)	*ft*

Table 2.2: Parameters for main rotor group

Description	Symbol	UH-60 value	Units
main rotor speed	Ω	27.0	*rad* / sec
main rotor blade radius	R	26.83	*ft*
blade lift curve slope	a_0	5.73	rad^{-1}
main rotor solidity	s	0.08210	-
rotor shaft forward tilt	γ_s	0.05236	*rad*
rotor thrust coefficient	C_T	0.1846	-
number of blades	b	4	-
blade lock number	$\gamma(\gamma_0)$	8.1936	-
rotor inertia number	η_β	1.0242	-
flap frequency ratio	λ_β	1	-
linear blade twist	θ_{tw}	-0.3142	*rad*
z co-ordinate of rotor hub	h_R	31.5	*ft*
mixing angle	ψ_F	0.175	*rad*
blade chord	c	1.73	*ft*
flapping spring const.	K_β	0	-
c.g. location fwd. of fuselage ref. Point	x_{cg}	1.4	*ft*
Stiffness number	S_β	0	-
Blade profile drag coefficient	δ_0	-0.0216	-
air density	ρ	0.002473	*slug* / ft^3
blade flapping moment of inertia	I_β	3.10	*slug ft²*

Table 2.3: Parameters for empennage

Description	Symbol	UH-60 value	Units
tail plane area	S_{TP}	45.0	ft
lift curve slope at zero incident	a_{0TP}	4	-
Location aft of fuselage reference point	l_{TP}, l_{FN}	70.0	ft
fin area	S_{FN}	32.3	ft^2

Table 2.4: Parameters for tail rotor group

Description	Symbol	UH-60 value	Units
tail rotor blade radius	R_T	5.5	ft
tail rotor speed	Ω_T	124.62	$rad/\sec$
blade lift curve slope	a_{0T}	5.73	rad^{-1}
tail rotor solidity	s_T	0.1875	-
fin blockage factor	F_T	-0.402	-
tail rotor inertia number	$(n_\beta)_T$	0.4223	-
flap frequency ratio	$(\lambda_\beta)_T$	1.0	-
tail rotor location aft of fuselage reference point	l_T	73.2	ft
Negative z co-ordinate of hub	h_T	32.5	ft
linear blade twist	θ_{tw}	-18.0	deg
Number of rotor blade	b	4	-
blade profile drag coefficient	δ_{0T}	-0.0216	-
blade lift dependent drag coefficient	δ_{2T}	0.40	-
pitch/flap coupling (δ_3)	k_3	0.700	-
blade lock number	$(\gamma)_T$	3.378	-

With the helicopter parameters shown in Table 2.1~2.4, the simulation studies have been carried out and the simulation results are summarised in Figures 2.3~2.6. The discussion of the simulation results are followed by the results for different input cases

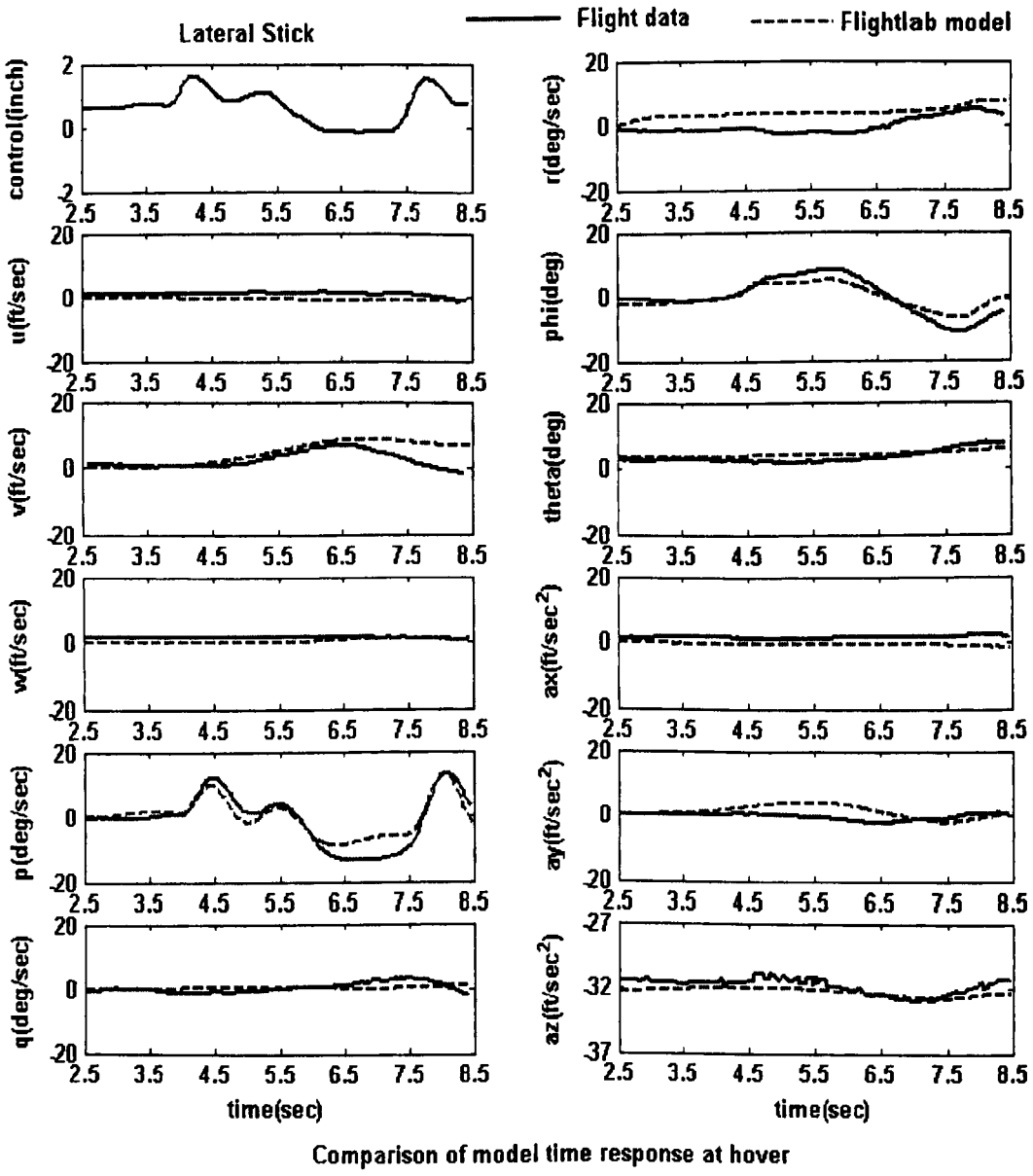

Figure 2.3 Comparison of helicopter dynamic responses at hover between flight test data and FGR model for lateral stick input

In Figure 2 .3 the pilot's lateral stick input was used to drive the model in hover condition and the time responses to the lateral control input have been compared. The responses show quite reasonable agreement. In Figure 2.3 the model response for the lateral translational velocity (v) initially follows the flight data response but in the long term it tends to be stable while the flight data has variation in its response. Furthermore the yaw rate (r) from the simulation was almost stable and steady throughout the motion while the flight data response has some variation, which might indicate that the model has been

simulated in an ideal environment while the flight test data is generated from the real environment.

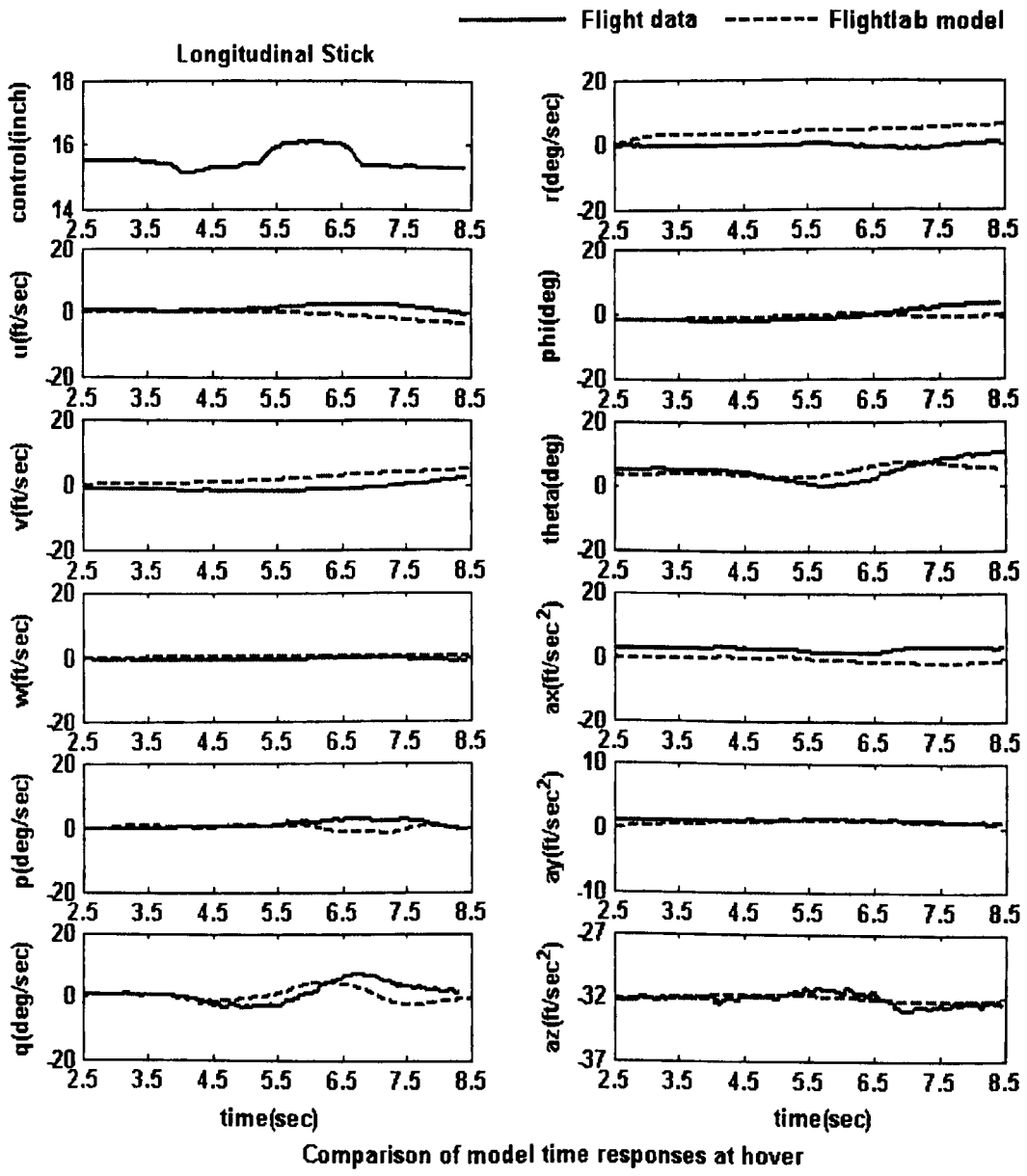

Figure 2.4 Comparison of helicopter dynamic responses at hover between flight test data and FGR model for longitudinal stick input

In Figure 2.4 the pilot's longitudinal stick input was used to drive the model in hover condition again there exists reasonably acceptable correlation with the flight data responses. However some discrepancies are evident in the pitch rate (q), and so the pitch angle (θ), initially it was a good agreement but tends to differ in the long term. The simulation curve seems to follow the changes in input faster than the flight test results in q. This result is reasonable because it should have some unknown resistance in reality but

not being included into the flightlab model. This reason may explain the discrepancy in pitch angle θ as well.

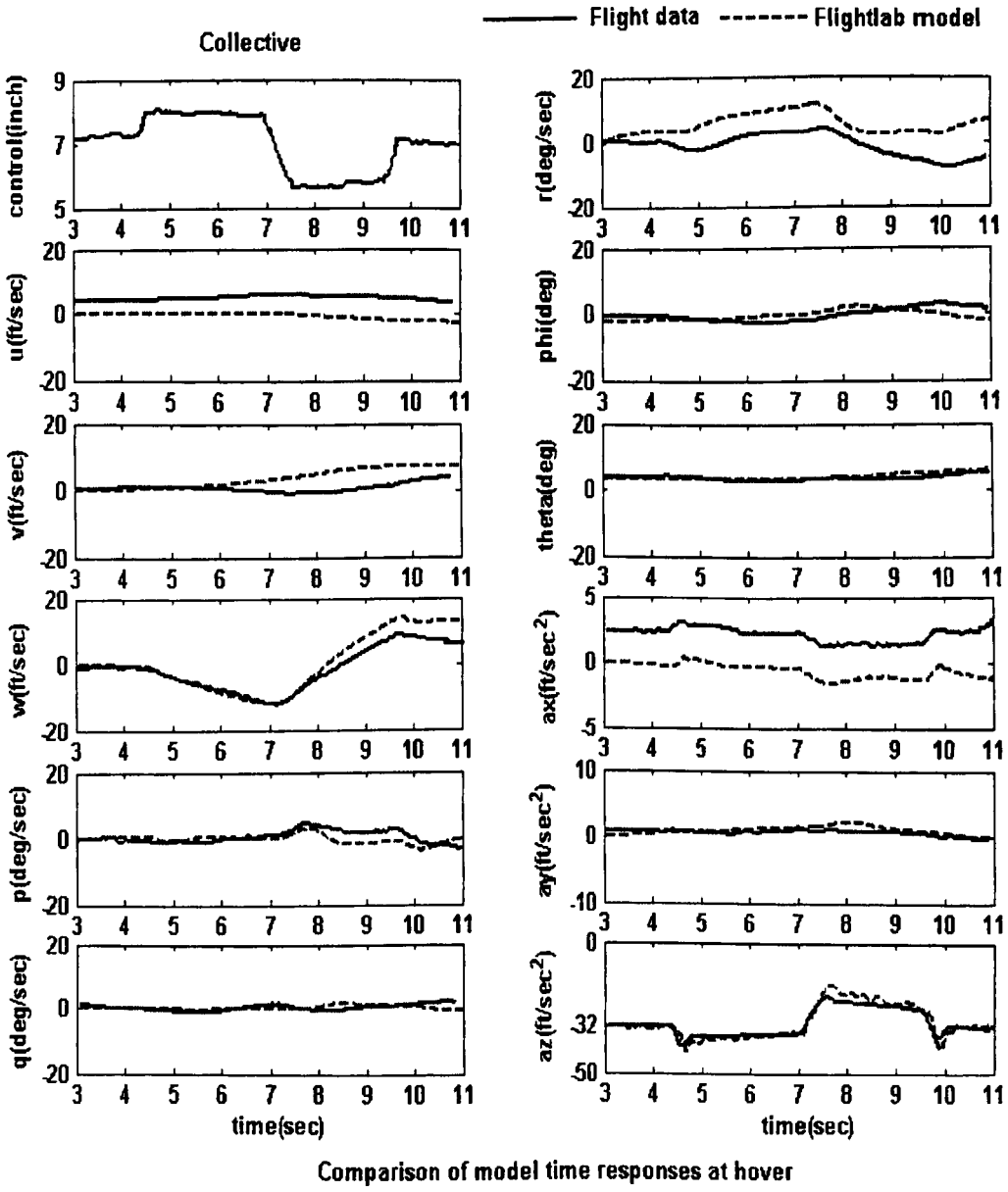

Figure 2.5 Comparison of helicopter dynamic responses at hover between flight test data and FGR model for collective input

Figure 2.5 shows the responses to a collective liver input. This input should influence the variations in vertical velocity w the most. In forward velocity (u) and acceleration (a_x) it can be seen that the initial condition is differ, this is due to the model has been set to the hover condition and hence the velocity and acceleration are zero but in real hover condition it is impossible to keep the aircraft in absolute zero velocity and acceleration, this is the case for the flight test data. From the figure, the results still give us confidence

about the flightlab model since the dynamic variation trends agreed well between the flight test and simulation results.

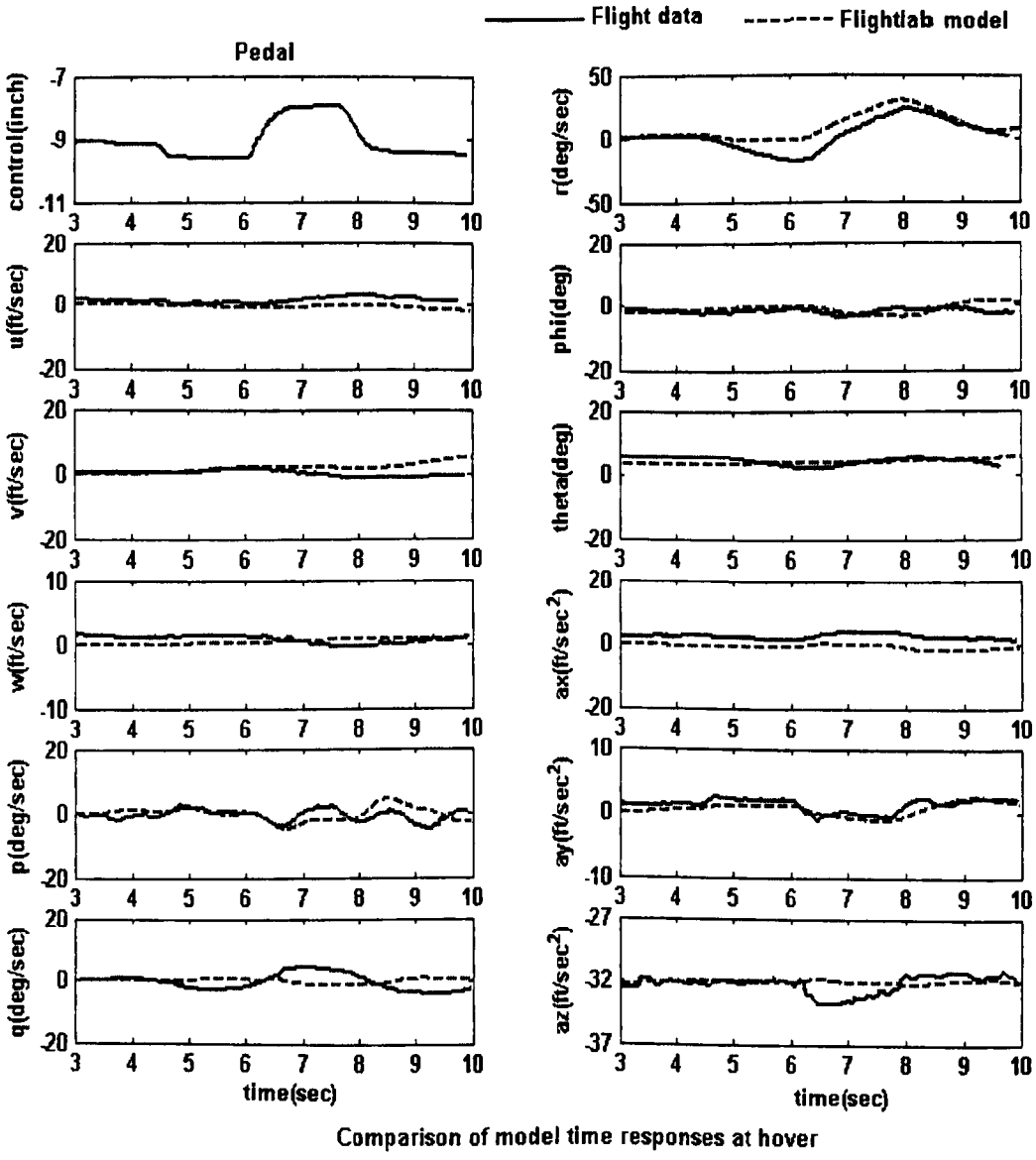

Figure 2.6 Comparison of helicopter dynamic responses at hover between flight test data and FGR model for pedal input

Finally Figure 2.6 shows the responses to a pedal input. The results do not give the good agreement as Figures 2.3 ~ 2.5. Further analysis about the flightlab model and the test conditions are carried out but it is difficult to find a good version to explain the discrepancies. Correlation with the hover dynamic manoeuvres is shown in Figures 2.3 ~ 2.5. The model response was computed using the actual flight measured control positions. Both the flight data and the simulation data ware plotted in same scale, which enables an easier comparison of the parameters of interest, such as translational velocities

(u, v, w), rotational velocities (p, q, r), Euler angles (ϕ, θ, ψ), and body axes accelerations (a_x, a_y, a_z).

In summary, comparison results show that there is a general agreement between the flight test data and the FGR model responses but discrepancies occurred. The differences may be caused by the following reasons: estimated parameters used in the model may be the causes of the differences; smallest error in initial condition will propagate to large divergences in the long term; and the environmental conditions the flight test conducted are not identical to ideal FGR model simulation environment.

Although the differences of simulation results between the flight test data and the FGR model responses appear, the model follows the same trend as the flight test data. Thus this FGR model can be considered as an acceptable helicopter model for the simulation study during hover in this thesis.

2.5 Summary

A study of general models of a helicopter is presented in this chapter, which started from a nonlinear dynamic model to a simplified linear model. The linear helicopter model is then introduced which is in the state space form, which enables the vehicle dynamic modes to be assessed by determining the eigenvalues of the state matrix. Finally a simulation model of a UH-60 alike helicopter is realised to be used to validate flight test data for the UH-60 helicopter at hover. This FGR model can be use to investigate the influences of an underslung load on flight handling performance and stability of the system. Modelling study of a helicopter allowed gaining insight knowledge of dynamics of helicopters, its leads to further study on dynamics of a helicopter with an underslung load. Simulation study of a UH-60 alike helicopter offered the opportunity to get familiar with FLIGHTLAB software, which is used as a tool in the next Chapter to study how the load influences the helicopter dynamics.

Chapter 3

Study on the influences of underslung load dynamics to the stability of helicopter

3.1 Introduction

The mechanics of helicopter flight can be described in terms of three aspects- trim, stability and response. The trim problem concerns the control positions required to hold the helicopter in equilibrium. The aircraft may be climbing, turning and at large angles of incidence and sideslip, but if the three translational velocity components are constant with the controls fixed, then the aircraft is in trim. Strictly speaking, climbing and diving flight cannot be described as trim conditions, because the changing air density will require continual corrections to the controls. Provided the rates of climb or descent are relatively small, the helicopter will be, practically speaking, in trim. Stability is concerned with the behaviour of the aircraft following a disturbance from trim. Classically, static stability is determined by the initial tendency (i.e. will the aircraft tend to return to, or depart from, the initial trim), while dynamic stability concerns longer-term effects. Responses refer to the helicopter's dynamic changes pilot control inputs and to atmospheric disturbances which is essentially a nonlinear problem [Padfield, 1996].

In the case of that an underslung load is attached to a helicopter, the helicopter dynamics will be seriously affected by the addition of further rigid body modes and aerodynamic forces, which, in turn can seriously degrade the helicopter's flight handling performance and reduce the operating envelop and the stability of the system [Cicolani *et al,* 1998].

In this chapter, the influence of the load to the stability of helicopter is investigated via simulation studies. A simulation model of an underslung load is developed in FLIGHTLAB simulation software and attached to the FGR model. The model is then used to perform simulation studies to reveal how the stability of the helicopter is degraded by the influences of the load.

3.2 Simulation model formulation for an underslung load in FLIGHTLAB

To investigate the influences of the underslung load on the flight handling performance of the helicopter, an underslung load was included into the FGR model using a single suspension point. FLIGHTLAB software provides a tool to perform the task of system analysis and to build extra component blocks to be added to the system, whereby a library of predefined modelling components are incorporated in the software and can be used to alter the design. An underslung load block is created using hinge, cable, and mass etc. which is then attached to the FGR model using a single suspension point located beneath the fuselage with a distance of 4.35ft below the centre of gravity of the helicopter. With this configuration, the load is connected to a non-linear helicopter system. The schematic diagram of the underslung load block is shown in Figure 3.1

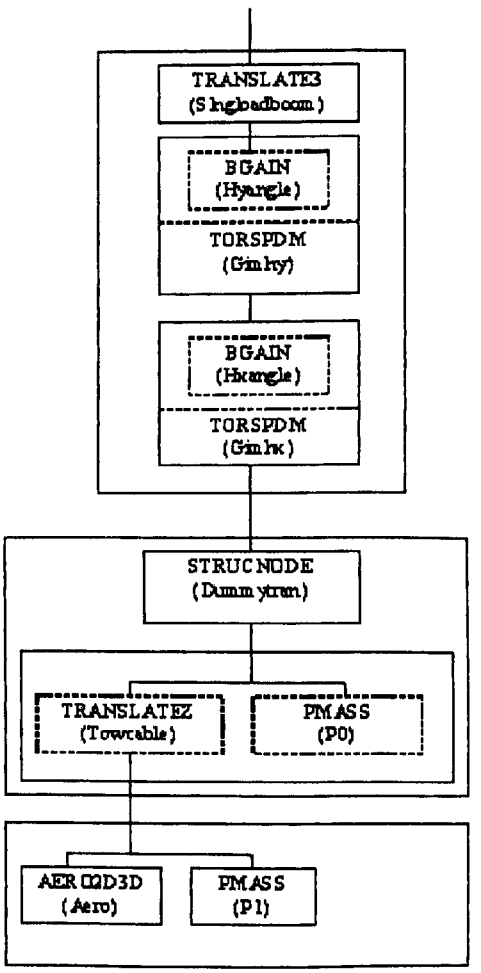

Figure 3.1: Schematic diagram for implementation of an underslung load block

The TRANSLATE3 a component in Figure 3.1 models a general linear translation. It is used to model the link between the subsystems. In this case, it is used to connect the underslung load (subsystem) to the helicopter (suspension point). TORSPDM is a component that models a hinge with both a torsional spring and damper about a single axis. It is used with a simplified control block BGAIN which handle the inputs and outputs to produce the suspension angles. For the second block, PMASS models the effective forces produced by a mass due to gravitational acceleration and inertial translational motion and TRANSLATEZ component models a static translation along Z axis. Using these two components by bringing them together with the use of STRUCNODE a sling (or cable) is modelled. At the other end, STRUCNODE is connected to the previous block developed to ensure the degree of freedom to the cable. Finally, the load is connected to the cable which is modelled by using PMASS together with AERO2D3D component which models a two dimensional aerodynamic panel (that produces airloads as a nonlinear function of dynamic pressure, angle of attack, and mach number) with three dimensional resolution of the forces and moments. It computes the lift, drag, and pitching moments. Details explanations of each of the block components can be found in the FLIGHTLAB user manuals [FLIGHTLAB user manuals, 2000].

For the simulation studies, the UH-60 helicopter parameters which were presented in Chapter 2 in Tables 2.1 ~ 2.4 are used to configure the helicopter system in FLIGHTLAB. Table 3.1 shows the load-sling parameters used for the underslung load subsystem.

Table 3.1: Load-sling parameters

Descriptions	Values	Units
sling hook attachment point	(354.0, 0.0, 199.8)	*inch*
hook / rigger device mass	50	*lbm*
sling / tow cable damping coefficient	10.0	*lbf* – sec / *ft*
sling / tow cable spring coefficient	10.0	*lbf / ft*
sling / tow cable offset	(0.0, 0.0, -48.0)	*inch*
airload offset	(0, 0, 0)	*ft*
airload reference area	1.0	ft^2
airload reference length	1.0	*ft*
sling / tow cable length	15 (20)	*ft*
sling / tow load mass	500 (1000 / 2000)	*lbm*

3.3 Simulation study and results

Simulation model of a helicopter with an underslung load described in Section 3.2 is employed to conduct the simulation studies to investigate the stability of the combined system. The behaviour of the system in hover as control deflection varies (hover performances) is investigated by applying a step control input. The output responses are obtained for different control inputs and parameters. Simulation results are obtained for all four control inputs (longitudinal, lateral, collective and pedal) without and with underslung load at hover by applying a step control input (1 inch). Two cases have been considered, that is, the system dynamic responses with a constant sling length and different load weights and a constant load weight with different sling lengths.

Case I: The underslung load with a constant sling length and different load weights

The dynamic responses of the helicopter with an underslung load to different inputs are shown in Figures 3.2 ~ 3.5.

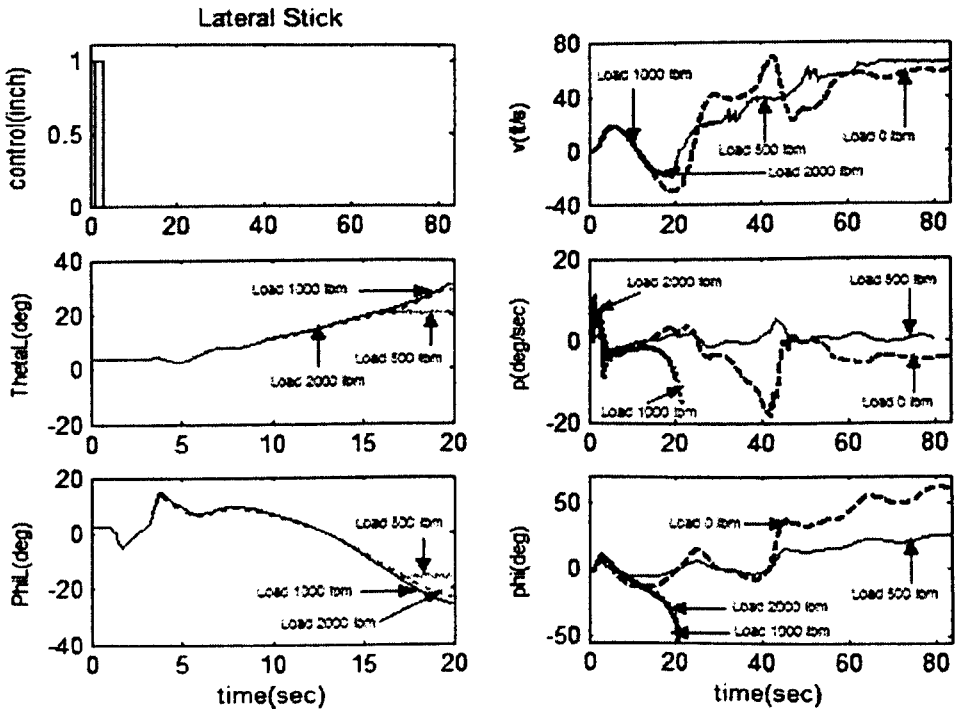

Figure 3.2 Helicopter dynamic responses for lateral input with a constant sling length (15ft) and three different load weights

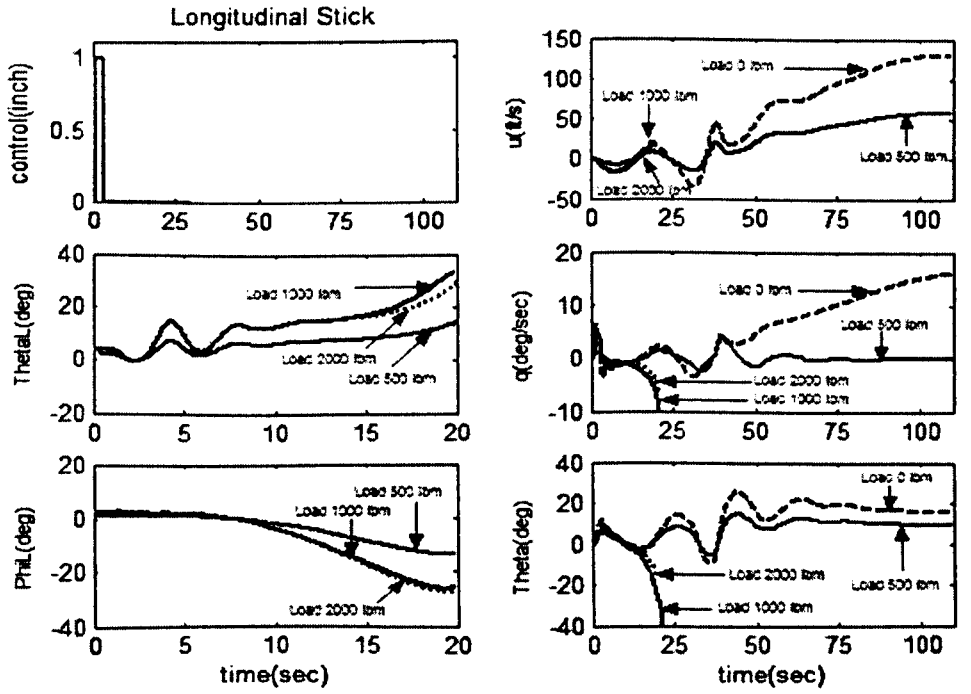

Figure 3.3 Helicopter dynamic responses for longitudinal input with a constant sling length (15ft) and three different load weights

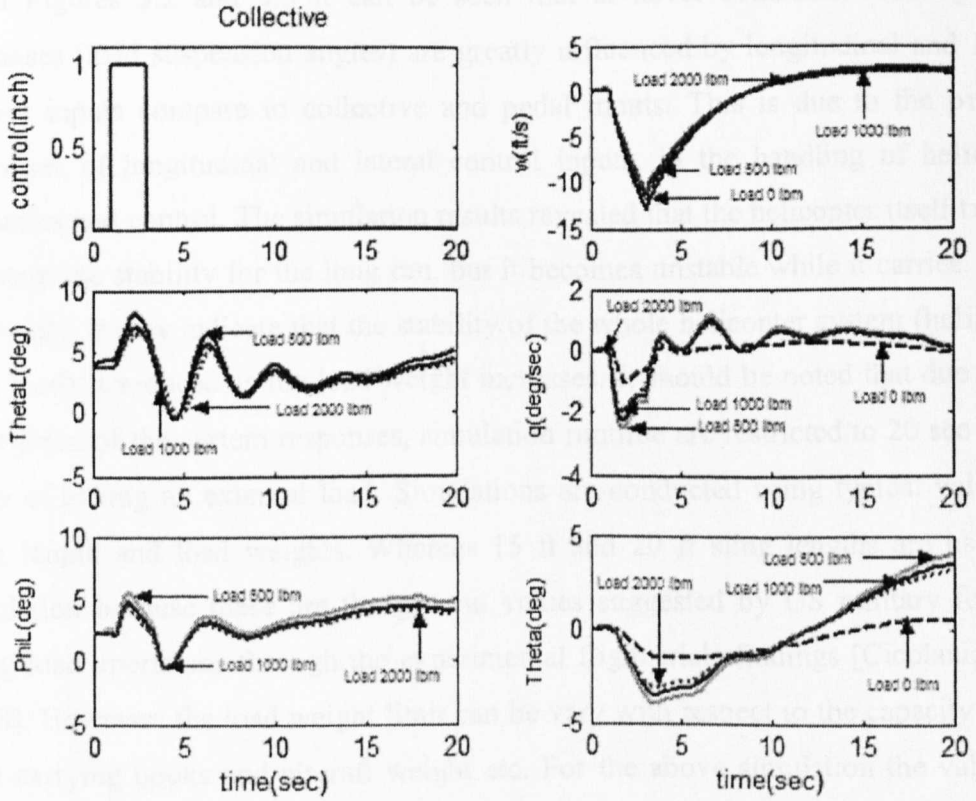

Figure 3.4 Helicopter dynamic responses for collective with a constant sling length (15ft) and three different load weights

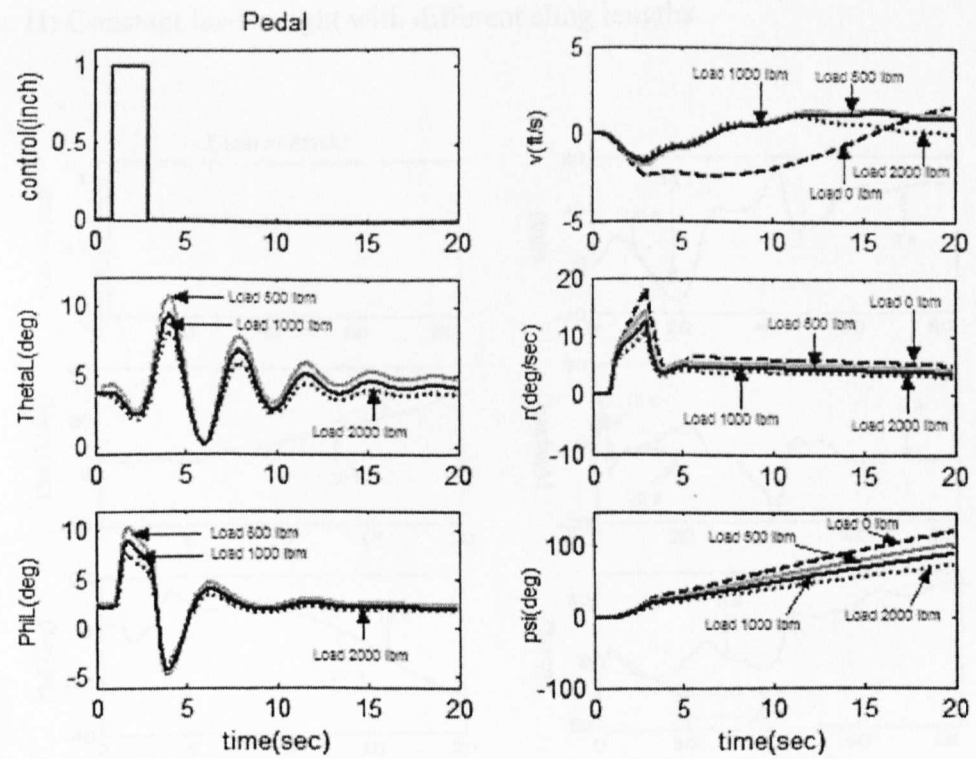

Figure 3.5 Helicopter dynamic responses for pedal with a constant sling length (15ft) and three different load weights

From Figures 3.2 and 3.3 it can be seen that at hover condition, load dynamic responses (load suspension angles) are greatly influenced by longitudinal and lateral control inputs compare to collective and pedal inputs. This is due to the primary responses of longitudinal and lateral control inputs, in the handling of helicopter dynamics and control. The simulation results revealed that the helicopter itself tried to maintain the stability for the long run, but it becomes unstable while it carries a load externally. It may indicate that the stability of the whole helicopter system (helicopter with load) is reduced as the load weight increases. It should be noted that due to the divergence of the system responses, simulation runtime are restricted to 20 sec in the cases of having an external load. Simulations are conducted using typical values of sling length and load weights. Whereas 15 ft and 20 ft sling lengths are used for simulation because these are the general values suggested by US military for safe slung load operations through the experimental flight trials findings [Cicolani, *et al,* 1998]. However, the load weight limit can be vary with respect to the capacity of the load carrying hooks and aircraft weight etc. For the above simulation the values of 500 lbm, 1000 lbm, and 2000 lbm are used as load weights.

Case II: Constant load weight with different sling lengths.

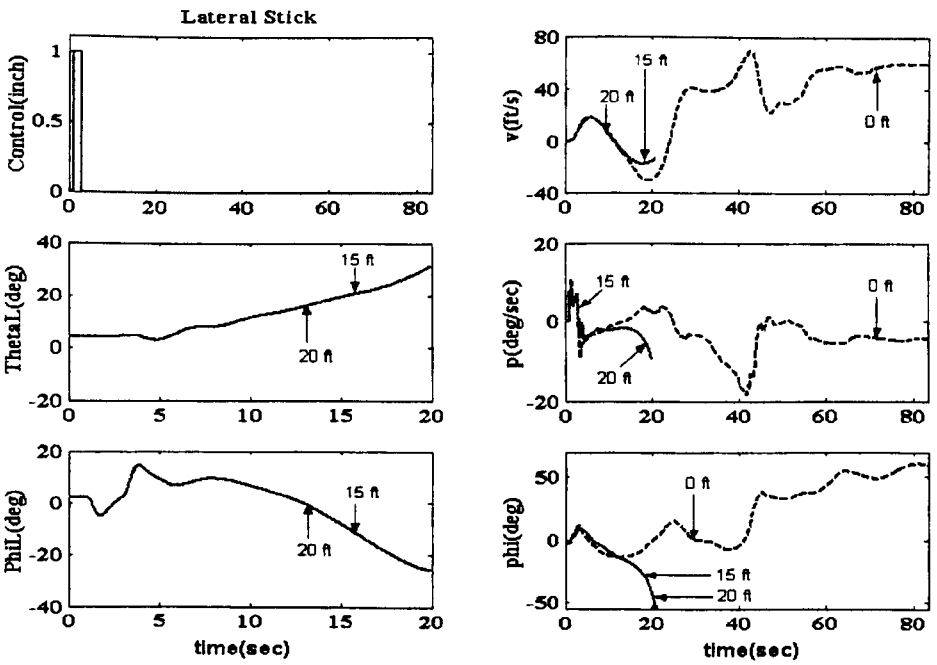

Figure 3.6 Helicopter dynamic responses for lateral input with constant load weight (1000 lbm) and two different sling lengths

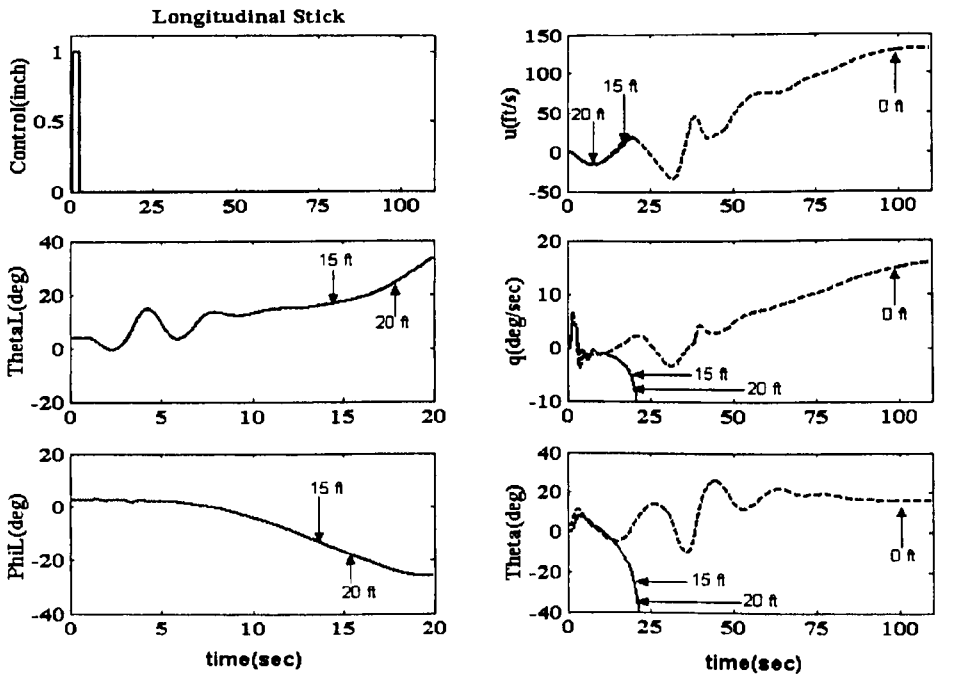

Figure 3.7 Helicopter dynamic responses for longitudinal input with constant load weight (1000 lbm) and two different sling lengths

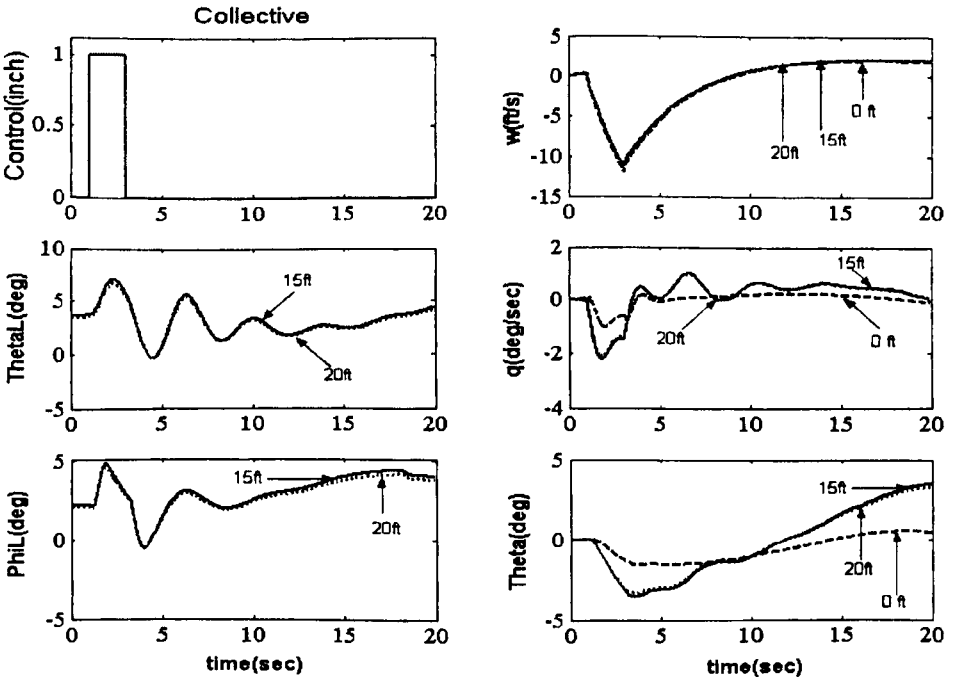

Figure 3.8 Helicopter dynamic responses for collective with constant load weight (1000 lbm) and two different sling lengths

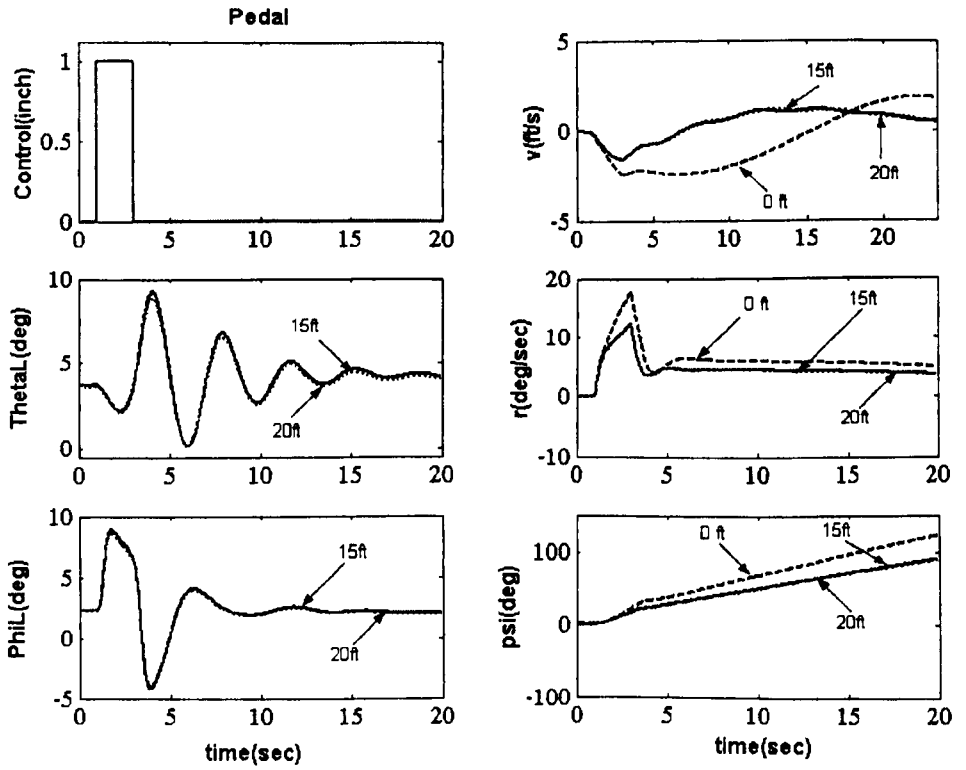

Figure 3.9 Helicopter dynamic responses for pedal with constant load weight (1000 lbm) and two different sling lengths

Again from the simulation results, it is revealed that the helicopter is less stable when it carries an underslung load. The increasing load weight has greater influence of the stability of the system then the sling length does. Again it can be noted that at hover condition helicopter dynamic responses with sling load are greatly influenced by longitudinal and lateral control inputs comparing with the collective and pedal inputs.

3.4 Stability analysis using a linearised model

Linearisation of a nonlinear system and a linear model of helicopter are discussed in Chapter 2. In this section, the helicopter model is linearised with reference to a standard nine state linear helicopter mathematical model [Fletcher, 1995]. FLIGHTLAB software provides a tool to perform the task of system linearization. This is achieved by applying small perturbation to the state of the system, executing the simulation model, and then averaging the resulting partial derivatives over one revolution of the helicopter rotor. This procedure was performed for the cases both with and without an underslung load. The linearised system is expressed in the state

space description form, $\dot{x} = Ax + Bu$ and the system stability was assessed by examining the location of the system poles on a root-locus diagram [Prouty, 1986]. Using FLIGHTLAB, the linearised model is obtained with the following state and input matrices.

$$A = \begin{bmatrix} -0.0000 & 0.0003 & -0.0000 & -0.0000 & 0.0000 & -0.0000 & 1.0000 & -0.0023 & 0.0503 \\ -0.0003 & -0.0000 & -0.0000 & -0.0000 & -0.0000 & -0.0000 & -0.0000 & 0.9989 & 0.0463 \\ -0.0001 & 0.0000 & -0.0000 & -0.0000 & 0.0000 & 0.0000 & -0.0000 & -0.0464 & 1.0002 \\ -1.9386 & -28.593 & -0.0030 & -0.0195 & -0.0126 & 0.0168 & -1.2000 & 5.7076 & 0.2683 \\ 32.8694 & -0.3640 & 0.0027 & 0.0126 & -0.0311 & -0.0013 & -4.1348 & -2.2350 & 0.3713 \\ 0.3138 & -1.4034 & 0.0004 & 0.0150 & 0.0034 & -0.3340 & 0.2866 & 0.6307 & 2.3410 \\ -0.9144 & -0.4783 & 0.0017 & 0.0226 & -0.0246 & 0.0007 & -6.5893 & -2.1301 & -0.0598 \\ 0.0631 & -0.6744 & 0.0008 & 0.0029 & 0.0046 & 0.0025 & 0.2059 & -1.4255 & -0.1636 \\ -0.7549 & -0.0119 & -0.0002 & 0.0009 & 0.0028 & 0.0006 & -0.0749 & -0.1032 & -0.2214 \end{bmatrix}$$

$$B = \begin{bmatrix} -0.0000 & 0.0000 & -0.0000 & 0.0000 \\ 0.0000 & 0.0000 & -0.0000 & -0.0000 \\ -0.0000 & 0.0000 & -0.0000 & -0.0000 \\ -2.2190 & 0.5734 & 0.3170 & -0.0019 \\ 3.5381 & -0.0453 & -0.0963 & 0.2007 \\ -1.5629 & 0.0237 & -6.0740 & -0.1014 \\ 1.9943 & -0.0714 & -0.0541 & 0.0731 \\ 0.0446 & -0.1097 & 0.0553 & -0.0281 \\ -0.8197 & -0.0082 & 0.1573 & -0.0635 \end{bmatrix}$$

In the case of with an underslung load, the simulation model contains four more state variables which are, the longitudinal and lateral suspension angle position and the movement of angle position due to the two degree of freedom of suspension angles. The numerical values vary with respect to the sling- load configuration. It may represent the system dynamic variations. To investigate the stability characteristics of dynamic variations two series of simulation studies were carried out. Firstly, the sling length was kept at a constant and the load varied between the limits 500~2000lb. The resulted system poles are listed in Table 3.2 ~ 3.6. The corresponding root loci are sketched in Figure 3.10. Secondly, the load was kept at a constant and the sling length varied between the limits 10~20ft. to see the effect of varying the sling length.

Case I: The underslung load with a constant sling length and different load weights

Five sets of parameters are tested and the system poles are tabulated in the following tables for different weights.

Table 3.2: System pole locations as sling length l =10 ft

Helicopter	500 lbm	750 lbm	1000 lbm	1500 lbm	2000 lbm
-1.0919	-1.1191	-1.1261	-1.0560	-1.1054	-1.1341
-6.3938	-6.4194	-6.4123	-9.9252	-6.7207	-6.3224
-0.0032	-0.0100	-0.0106	-0.0061	-0.0135	-0.0314
-0.0977	-0.0751	-0.0728	-0.2012	-0.0804	-0.0497
-0.3045	-0.3016	-0.2990	-0.2606	-0.3867	-0.3426
-0.3159 ± 0.4363i	-0.3220 ± 0.4621i	-0.3200 ± 0.4694i	-0.1809 ± 0.6219i	-0.3541 ± 0.4532i	-0.3102 ± 0.4695i
-0.0489 ± 0.3898i	-0.0180 ± 0.3955i	-0.0157 ± 0.3981i	0.0643 ± 0.4577i	0.0369 ± 0.3821i	0.0172 ± 0.4073i
-	-0.0393 ± 1.8376i	-0.0527 ± 1.8574i	-0.1055 ± 1.9883i	0.0833 ± 2.4535i	0.1282 ± 1.9577i
-	-0.0148 ± 1.8407i	-0.0170 ± 1.8615i	-0.8847 ± 1.2464i	0.0263 ± 1.9215i	0.0324 ± 1.9660i

Table 3.3: System pole locations as sling length l =12 ft

Helicopter	500 lbm	750 lbm	1000 lbm	1500 lbm	2000 lbm
-1.0919	-1.1179	-1.1201	-0.8852	-1.0997	-1.1297
-6.3938	-6.4212	-6.4201	-9.5586	-6.7151	-6.3301
-0.0032	-0.0100	-0.0106	-0.0108	-0.0136	-0.0314
-0.0977	-0.0751	-0.0728	-0.1194	-0.0800	-0.0497
-0.3045	-0.3016	-0.2990	-0.2895	-0.3867	-0.3425
-0.3159 ± 0.4363i	-0.3214 ± 0.4624i	-0.3161 ± 0.4715i	-0.1941 ± 0.6167i	-0.3532 ± 0.4545i	-0.3079 ± 0.4703i
-0.0489 ± 0.3898i	-0.0178 ± 0.3955i	-0.0145 ± 0.3983i	0.0723 ± 0.4599i	0.0366 ± 0.3821i	0.0165 ± 0.4074i
-	-0.0378 ± 1.6766i	-0.0488 ± 1.3827i	-0.1043 ± 1.8663i	0.0809 ± 2.3077i	0.1242 ± 1.7852i
-	-0.0157 ± 1.6809i	-0.0246 ± 1.3906i	-0.9112 ± 1.2077i	0.0297 ± 1.7567i	0.0374 ± 1.7993i

Table 3.4: System pole locations as sling length l =15 ft

Helicopter	500 lbm	750 lbm	1000 lbm	1500 lbm	2000 lbm
-1.0919	-1.1159	-1.1216	-0.7848	-0.6221	-0.9369
-6.3938	-6.4301	-6.4181	-9.2203	-7.9848	-7.5613
-0.0032	-0.0048	-0.0107	-0.0034	-0.0052	-0.0052
-0.0977	-0.0818	-0.0723	-0.0888	-0.0972	-0.0694
-0.3045	-0.3036	-0.2994	-0.3394	-0.3318	-0.3333
-0.3159 ± 0.4363i	-0.3199 ± 0.4628i	-0.3177 ± 0.4701i	-0.2295 ± 0.5050i	-0.2366 ± 0.5974i	-0.1834 ± 0.4968i
-0.0489 ± 0.3898i	-0.0211 ± 0.3868i	-0.0150 ± 0.3986i	0.0074 ± 0.3445i	0.0119 ± 0.4406i	0.0264 ± 0.3199i
-	-0.0316 ± 1.5043i	-0.0217 ± 1.5224i	-0.1020 ± 1.7380i	-0.0368 ± 1.8753i	-0.1160 ± 2.0003i
-	-0.0736 ± 1.5019i	-0.0494 ± 1.5150i	-0.7662 ± 1.1680i	-0.7349 ± 1.9064i	-1.2367 ± 0.8995i

Table 3.5: System pole locations as sling length l =18 ft

Helicopter	500 lbm	750 lbm	1000 lbm	1500 lbm	2000 lbm
-1.0919	-1.1159	-1.1201	-0.7715	-0.9645	-0.9300
-6.3938	-6.4301	-6.4201	-8.8828	-7.8716	-7.4020
-0.0032	-0.0048	-0.0106	-0.0036	-0.0355	-0.0049
-0.0977	-0.0818	-0.0728	-0.0869	-0.0556	-0.0753
-0.3045	-0.3036	-0.2990	-0.3400	-0.2968	-0.3326
-0.3159 ± 0.4363i	-0.3199 ± 0.4628i	-0.3161 ± 0.4715i	-0.2262 ± 0.5041i	-0.1481 ± 0.6810i	-0.1779 ± 0.4921i
-0.0489 ± 0.3898i	-0.0211 ± 0.3868i	-0.0145 ± 0.3983i	0.0065 ± 0.3422i	0.0998 ± 0.4702i	0.0294 ± 0.3190i
-	-0.0316 ± 1.5043i	-0.0246 ± 1.3906i	-0.1101 ± 1.5992i	-0.1171 ± 1.7848i	-0.1238 ± 1.8539i
-	-0.0736 ± 1.5019i	-0.0488 ± 1.3827i	-0.6747 ± 1.1132i	-1.0833 ± 0.9037i	-1.0826 ± 0.8996i

Table 3.6: System pole locations as sling length l =20 ft

Helicopter	500 lbm	750 lbm	1000 lbm	1500 lbm	2000 lbm
-1.0919	-1.1140	-1.1189	-0.8687	-1.1820	-0.8234
-6.3938	-6.4251	-6.4212	-8.5565	-7.4519	-7.2841
-0.0032	-0.0100	-0.0106	-0.0114	-0.0075	-0.0036
-0.0977	-0.0751	-0.0728	-0.0953	-0.2120	-0.0182
-0.3045	-0.3016	-0.2990	-0.3479	-0.3313	-0.3590
-0.3159 ± 0.4363i	-0.3189 ± 0.4640i	-0.3152 ± 0.4722i	-0.1636 ± 0.6092i	-0.2146 ± 0.5892i	-0.0306 ± 0.8253i
-0.0489 ± 0.3898i	-0.0169 ± 0.3956i	-0.0141 ± 0.3984i	0.0799 ± 0.4594i	0.1613 ± 0.4096i	0.2158 ± 0.2819i
-	-0.0369 ± 1.2974i	-0.0266 ± 1.3194i	-0.1247 ± 1.4470i	-0.1103 ± 1.6710i	-0.0993 ± 1.0002i
-	-0.0213 ± 1.3031i	-0.0487 ± 1.3117i	-0.6352 ± 1.0384i	-1.1169 ± 1.3222i	-1.5168 ± 1.0002i

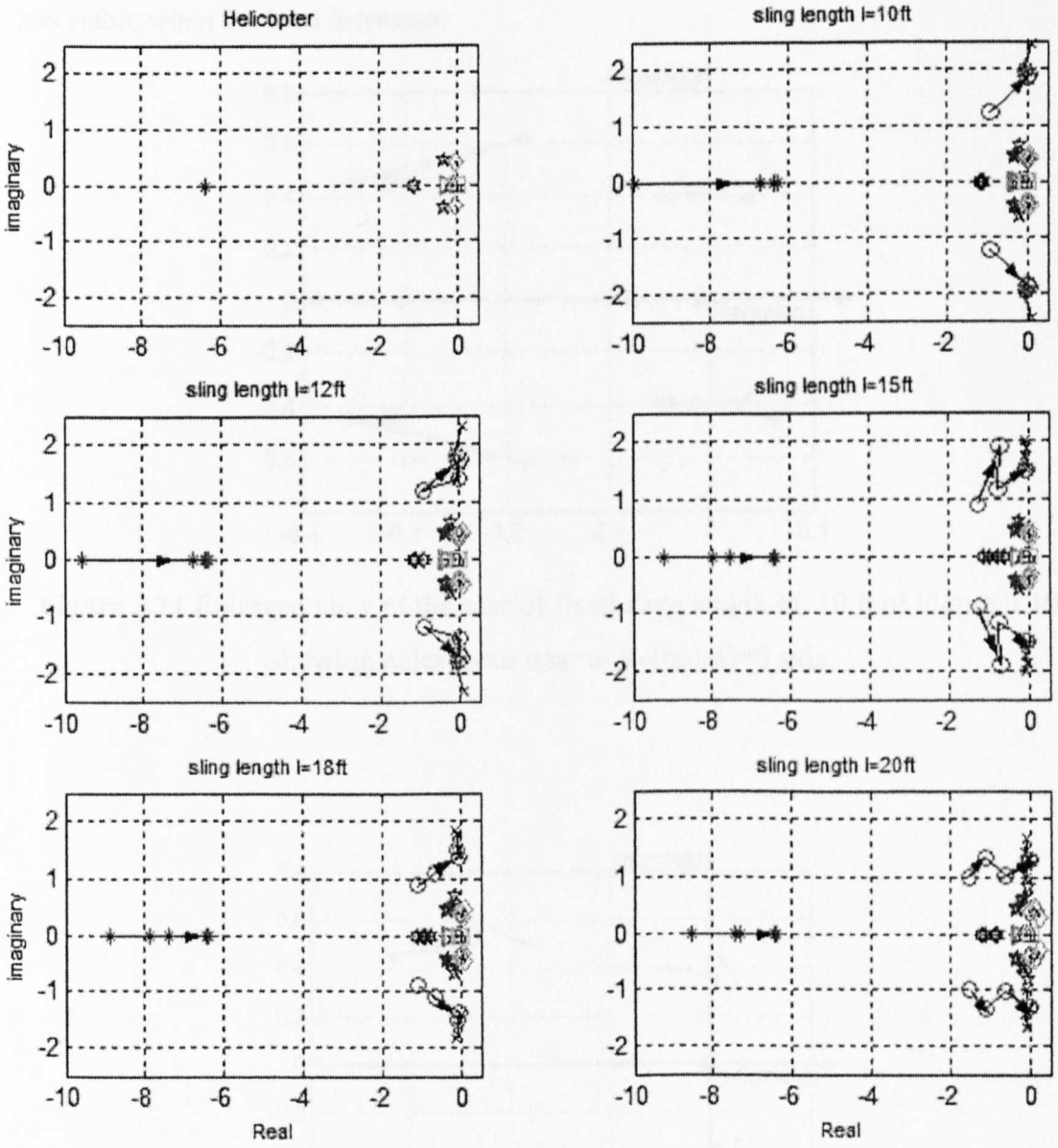

Figure 3.10 System root-locus diagram showing pole locus for constant sling length as load weight is increased.

Each of the diagrams shown in the Figure 3.10 can be enlarged to view the pole locus near to Re(pole)=0 axis to demonstrate the variation of the system poles and to show that the positions of the system poles crossed the imaginary axis as the load weight increased and the whole helicopter system becomes less stable. For example considering the case of fixed sling length of 10 ft and 15ft with different load weights, the enlarged view of poles locus near to Re(pole)=0 axis are shown as in Figure 3.11

and Figure 3.12. It is clear from the figures that the whole helicopter system becomes less stable when the load increases.

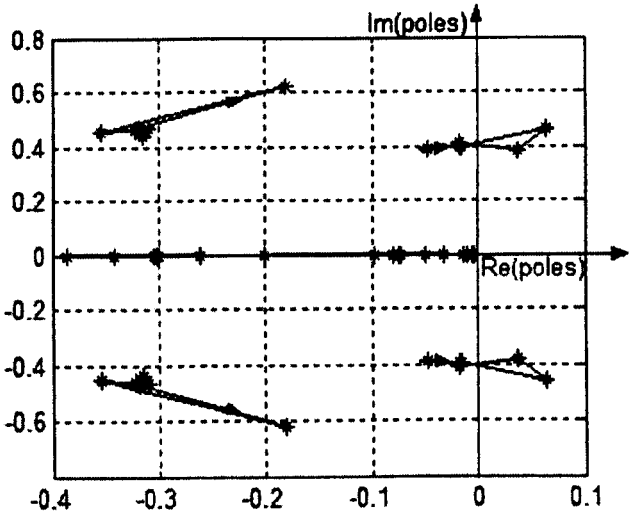

Figure 3.11 Enlarged view of the case of fixed sling length of 10 ft of Figure 3.10 showing poles locus near to Re(poles)=0 axis

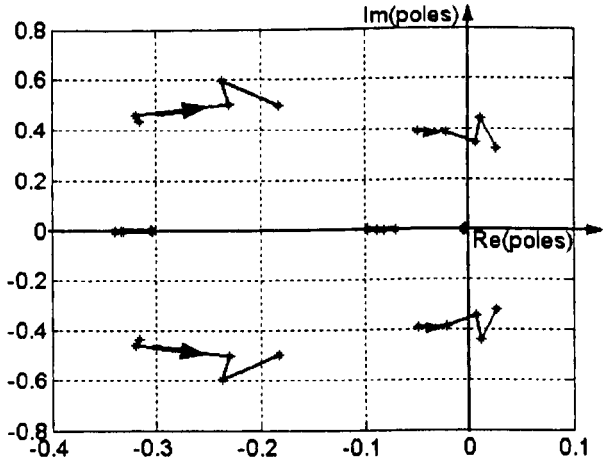

Figure 3.12 Enlarged view of the case of fixed sling length of 15 ft of Figure 3.10 showing poles locus near to Re(poles)=0 axis

The linearised helicopter model without carrying a load has system poles located on the left hand side of s-plane but near to the imaginary axis, which indicates that the system is stable but it may have strong oscillations in its dynamic responses and it is not very robust. The pole locus also indicates that the system (helicopter with load)

poles have the variation trends of moving further towards to right direction on the s-plane with increase of load weights.

For Case II the load weight was kept at a constant and the sling length varied between the limit of 10 ~ 20 ft. Five cases are tested and Tables 3.7 ~ 3.11 summarise the results of variation of the system poles and the corresponding root loci are illustrated in Figure 3.13.

Case I: The underslung load with a constant weight and different sling lengths

Five sets of different parameters are adopted for the simulation tests and the system pole locations are tabulated in the following tables.

Table 3.7: System pole locations as load weight M_L = 500 lbm

Helicopter	10 ft	12 ft	15 ft	18 ft	20 ft
-1.0919	-1.1191	-1.1179	-1.1159	-1.1159	-1.1140
-6.3938	-6.4194	-6.4212	-6.4301	-6.4301	-6.4251
-0.0032	-0.0100	-0.0100	-0.0048	-0.0048	-0.0100
-0.0977	-0.0751	-0.0751	-0.0818	-0.0818	-0.0751
-0.3045	-0.3016	-0.3016	-0.3036	-0.3036	-0.3016
-0.3159 ± 0.4363i	-0.3220 ± 0.4621i	-0.3214 ± 0.4624i	-0.3199 ± 0.4628i	-0.3199 ± 0.4628i	-0.3189 ± 0.4640i
-0.0489 ± 0.3898i	-0.0180 ± 0.3955i	-0.0178 ± 0.3955i	-0.0211 ± 0.3868i	-0.0211 ± 0.3868i	-0.0169 ± 0.3956i
-	-0.0393 ± 1.8376i	-0.0378 ± 1.6766i	-0.0316 ± 1.5043i	-0.0316 ± 1.5043i	-0.0369 ± 1.2974i
-	-0.0148 ± 1.8407i	-0.0157 ± 1.6809i	-0.0736 ± 1.5019i	-0.0736 ± 1.5019i	-0.0213 ± 1.3031i

Table 3.8: System pole locations as load weight M_L = 750 lbm

Helicopter	10 ft	12 ft	15 ft	18 ft	20 ft
-1.0919	-1.1261	-1.1201	-1.1216	-1.1201	-1.1189
-6.3938	-6.4123	-6.4201	-6.4181	-6.4201	-6.4212
-0.0032	-0.0106	-0.0106	-0.0107	-0.0106	-0.0106
-0.0977	-0.0728	-0.0728	-0.0723	-0.0728	-0.0728
-0.3045	-0.2990	-0.2990	-0.2994	-0.2990	-0.2990
-0.3159 ± 0.4363i	-0.3200 ± 0.4694i	-0.3161 ± 0.4715i	-0.3177 ± 0.4701i	-0.3161 ± 0.4715i	-0.3152 ± 0.4722i
-0.0489 ± 0.3898i	-0.0157 ± 0.3981i	-0.0145 ± 0.3983i	-0.0150 ± 0.3986i	-0.0145 ± 0.3983i	-0.0141 ± 0.3984i
-	-0.0527 ± 1.8574i	-0.0488 ± 1.3827i	-0.0217 ± 1.5224i	-0.0246 ± 1.3906i	-0.0266 ± 1.3194i
-	-0.0170 ± 1.8615i	-0.0246 ± 1.3906i	-0.0494 ± 1.5150i	-0.0488 ± 1.3827i	-0.0487 ± 1.3117i

Table 3.9: System pole locations as load weight M_L = 1000 lbm

Helicopter	10 ft	12 ft	15 ft	18 ft	20 ft
-1.0919	-1.0560	-0.8852	-0.7848	-0.7715	-0.8687
-6.3938	-9.9252	-9.5586	-9.2203	-8.8828	-8.5565
-0.0032	-0.0061	-0.0108	-0.0034	-0.0036	-0.0114
-0.0977	-0.2012	-0.1194	-0.0888	-0.0869	-0.0953
-0.3045	-0.2606	-0.2895	-0.3394	-0.3400	-0.3479
-0.3159 ± 0.4363i	-0.1809 ± 0.6219i	-0.1941 ± 0.6167i	-0.2295 ± 0.5050i	-0.2262 ± 0.5041i	-0.1636 ± 0.6092i
-0.0489 ± 0.3898i	0.0643 ± 0.4577i	0.0723 ± 0.4599i	0.0074 ± 0.3445i	0.0065 ± 0.3422i	0.0799 ± 0.4594i
-	-0.1055 ± 1.9883i	-0.1043 ± 1.8663i	-0.1020 ± 1.7380i	-0.1101 ± 1.5992i	-0.1247 ± 1.4470i
-	-0.8847 ± 1.2464i	-0.9112 ± 1.2077i	-0.7662 ± 1.1680i	-0.6747 ± 1.1132i	-0.6352 ± 1.0384i

Table 3.10: System pole locations as load weight M_L = 1500 lbm

Helicopter	10 ft	12 ft	15 ft	18 ft	20 ft
-1.0919	-1.1054	-1.0997	-0.6221	-0.9645	-1.1820
-6.3938	-6.7207	-6.7151	-7.9848	-7.8716	-7.4519
-0.0032	-0.0135	-0.0136	-0.0052	-0.0355	-0.0075
-0.0977	-0.0804	-0.0800	-0.0972	-0.0556	-0.2120
-0.3045	-0.3867	-0.3867	-0.3318	-0.2968	-0.3313
-0.3159 ± 0.4363i	-0.3541 ± 0.4532i	-0.3532 ± 0.4545i	-0.2366 ± 0.5974i	-0.1481 ± 0.6810i	-0.2146 ± 0.5892i
-0.0489 ± 0.3898i	0.0369 ± 0.3821i	0.0366 ± 0.3821i	0.0119 ± 0.4406i	0.0998 ± 0.4702i	0.1613 ± 0.4096i
-	0.0833 ± 2.4535i	0.0809 ± 2.3077i	-0.0368 ± 1.8753i	-0.1171 ± 1.7848i	-0.1103 ± 1.6710i
-	0.0263 ± 1.9215i	0.0297 ± 1.7567i	-0.7349 ± 1.9064i	-1.0833 ± 0.9037i	-1.1169 ± 1.3222i

Table 3.11: System pole locations as load weight M_L = 2000 lbm

Helicopter	10 ft	12 ft	15 ft	18 ft	20 ft
-1.0919	-1.1341	-1.1297	-0.9369	-0.9300	-0.8234
-6.3938	-6.3224	-6.3301	-7.5613	-7.4020	-7.2841
-0.0032	-0.0314	-0.0314	-0.0052	-0.0049	-0.0036
-0.0977	-0.0497	-0.0497	-0.0694	-0.0753	-0.0182
-0.3045	-0.3426	-0.3425	-0.3333	-0.3326	-0.3590
-0.3159 ± 0.4363i	-0.3102 ± 0.4695i	-0.3079 ± 0.4703i	-0.1834 ± 0.4968i	-0.1779 ± 0.4921i	-0.0306 ± 0.8253i
-0.0489 ± 0.3898i	-0.0172 ± 0.4073i	-0.0165 ± 0.4074i	0.0264 ± 0.3199i	0.0294 ± 0.3190i	0.2158 ± 0.2819i
-	-0.1282 ± 1.9577i	-0.1242 ± 1.7852i	-0.1160 ± 2.0003i	-0.1238 ± 1.8539i	-0.0993 ± 1.0002i
-	-0.0324 ± 1.9660i	-0.0374 ± 1.7993i	-1.2367 ± 0.8995i	-1.0826 ± 0.8996i	-1.5168 ± 1.0002i

In Case 2, each of the diagrams shown in Figure 3.13 can be enlarged to view the pole locus near to Re(pole)=0 axis to demonstrate the variation of the system poles and to show that the positions of the system poles crossed the imaginary axis as the sling length increased and the whole helicopter system becomes less stable. For example considering the case of fixed load weight of 500 lbm and 1000 lbm with different

sling lengths then the enlarged view of poles locus near to Re(pole)=0 axis can be shown as in Figure 3.14 and Figure 3.15.

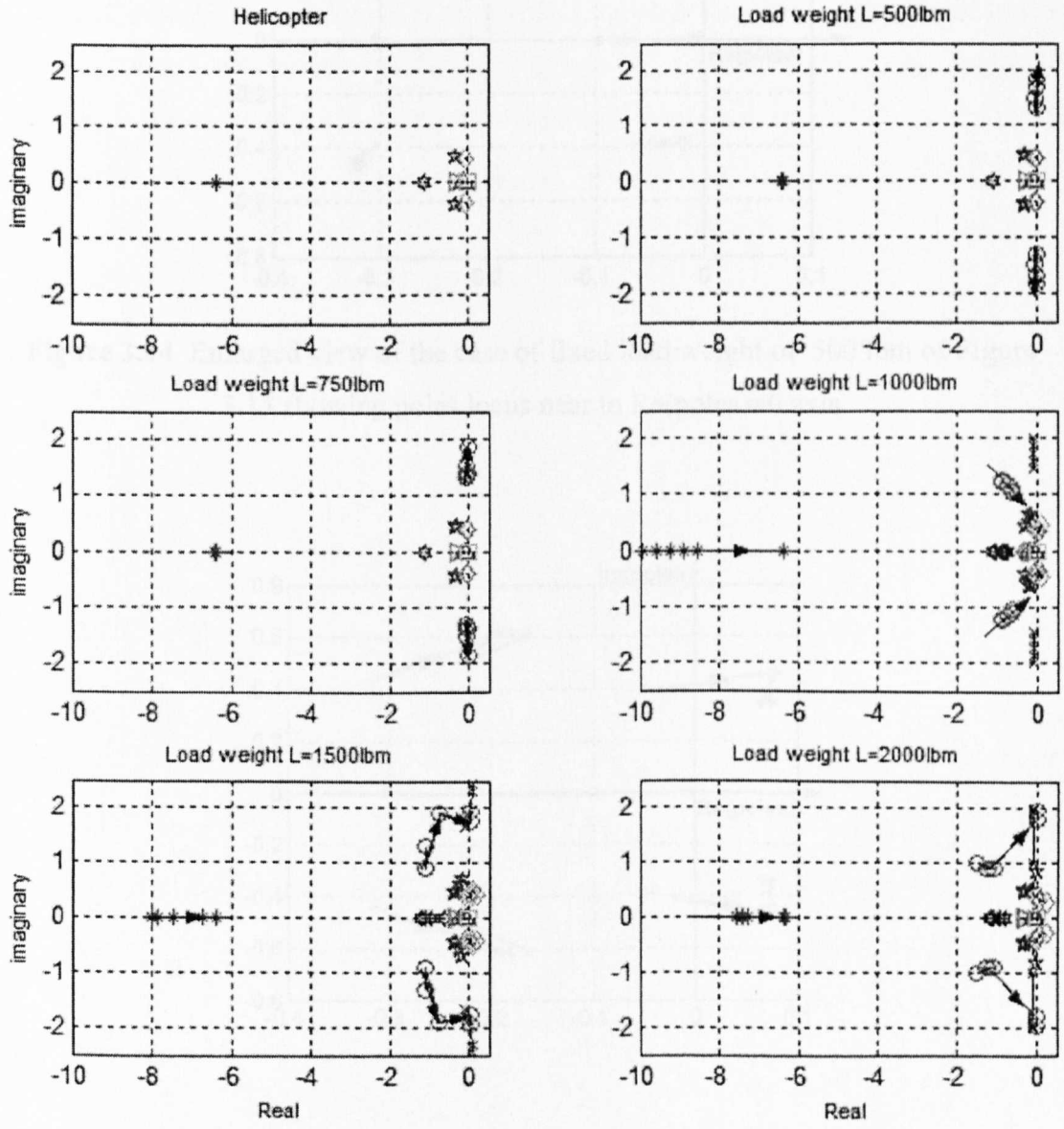

Figure 3.13 System root-locus diagram showing pole locus for constant load weight as sling length is increased.

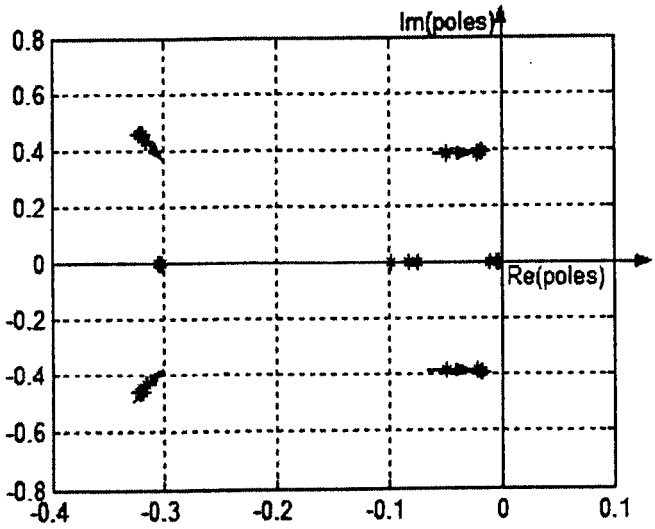

Figure 3.14 Enlarged view of the case of fixed load weight of 500 lbm of Figure 3.13 showing poles locus near to Re(poles)=0 axis

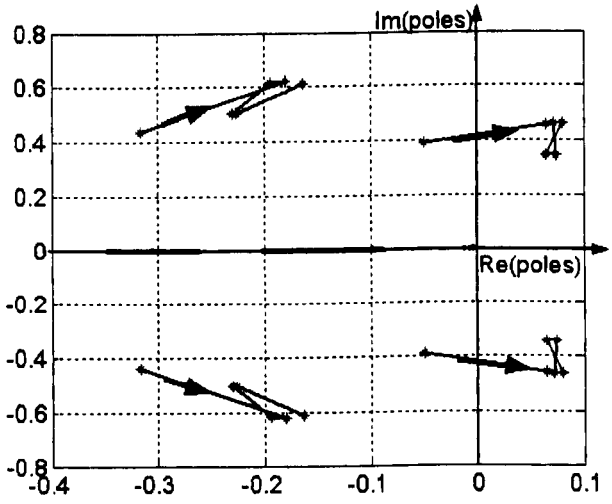

Figure 3.15 Enlarged view of the case of fixed load weight of 1000 lbm of Figure 3.13 showing poles locus near to Re(poles)=0 axis

3.5 Summary and discussion

From the simulation results, it is evident that the stability of the helicopter can be significantly affected due to the presence of an underslung load. Analysis using a linearised system model shows that the helicopter-load combination becomes

increasingly unstable as the load weight or sling length increases, which are revealed by the migration of the system poles towards to the right hand side of the complex s-plane. The analysis shows how the stability of helicopter is affected by the influences of the addition of the underslung load. However, It is important to point out that the linearised helicopter model is only an approximation to the true system, furthermore in the process of linearisation rotor dynamics are ignored and only the six degree of freedom ridged body dynamics are considered. These results could be improvable, if rotor dynamic and other factors affect the helicopter dynamic such as unsteady aerodynamic are taken into account. Thus, this analysis provides the basis for a further analysis of stability of the system.

Chapter 4

Influence of helicopter dynamics to the dynamics of the underslung load

To investigate the dynamic behaviour of a helicopter with an underslung external load, an underslung load mathematical model is developed and combined to the original helicopter model, which results in a complicated cascade connection nonlinear system description. The underslung load is attached to the helicopter by a single point and can swing freely. The load dynamic has no direct external control input. The external control input exerts the influences on the underslung load through manoeuvring the helicopter's dynamics. Thus the whole system can be considered as a cascade connection of two subsystems and the helicopter dynamics can be considered as the input to the underslung load subsystem.

The analysis begins with developing a mathematical model of the underslung load, accounting for two-dimensional motion of the suspension point. The model is then extended to three dimensions and applied to some example flight manoeuvres to study the resulting three-dimensional motion of the load.

4.1 Mathematical model of an underslung load

In this section, the underslung load is considered to be suspended from a single suspension point that is subject to motion and therefore modelled as a driven spherical pendulum. The equations that describe the load dynamics are obtained by first considering motion with reference to the longitudinal suspension angle θ_L in the x-z plane. This is then repeated for the lateral case involving φ_L and the y-z plane (Figure 4.1). These are then combined to simulate three-dimensional motion of the load. The underslung load system has six inputs, longitudinal, lateral, and vertical velocities together with the corresponding accelerations of the helicopter, whilst the outputs are the longitudinal and lateral directional suspension angles. The load is subject to an isotropic aerodynamic force (proportional to the square of its airspeed) such as would be experienced by a spherical shaped load. Aerodynamic interaction with the

helicopter that may occur for example due to rotor downwash has been ignored. Finally, the sling itself is assumed to be rigid and contribute zero aerodynamic force of its own. We use a co-ordinate system shown in Figure 4.1., whereas x, y, z are position axes, i.e., for example z represent the vertical axis in relation to the translation of earth axis. The rotational freedom of the load motion is ignored. With these assumptions, the equations governing the load motion can be derived as follows.

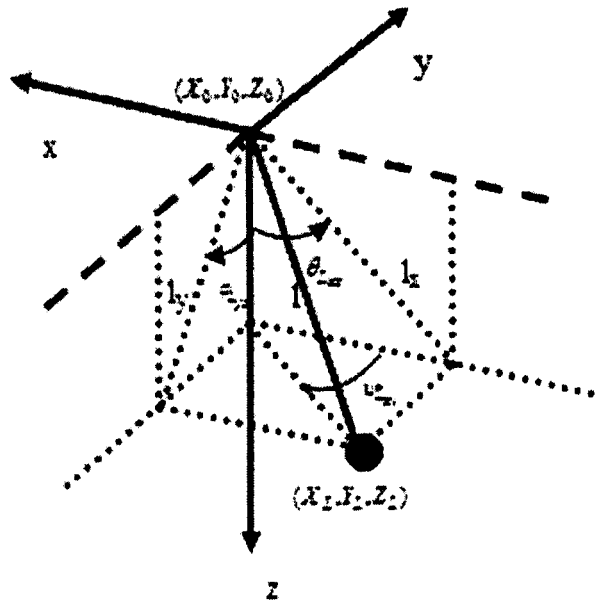

Figure 4.1 Geometry of a spherical pendulum with defined x, y, z position axes and load angles

Considering the motion in the x-z plane, the load position with respect to the coordinate system in Figure 4.1 can be written as follows.

$$X_L = X_0 - l_x \sin\theta_{Lxz} \tag{4.1a}$$

$$Z_L = Z_0 + l_x \cos\theta_{Lxz} \tag{4.1b}$$

where X_0 and Z_0 are the horizontal and vertical displacements of the suspension point and l_X, $\theta_{L_{xz}}$ represents the sling length and suspension angle in the x-z plane respectively. The resolved load velocities in the x-z plane are therefore given by:

$$\dot{X}_L = \dot{X}_0 - l_x\dot{\theta}_{Lxz} \cos\theta_{Lxz} \tag{4.2a}$$

$$\dot{Z}_L = \dot{Z}_0 - l_x\dot{\theta}_{Lxz} \sin\theta_{Lxz} \tag{4.2b}$$

and the resolved accelerations of the load are

$$\ddot{X}_L = \ddot{X}_0 + l_x\dot{\theta}_{Lxz}^2 \sin\theta_{Lxz} - l_x\ddot{\theta}_{Lxz}\cos\theta_{Lxz} \quad (4.3a)$$

$$\ddot{Z}_L = \ddot{Z}_0 - l_x\dot{\theta}_{Lxz}^2 \cos\theta_{Lxz} - l_x\ddot{\theta}_{Lxz}\sin\theta_{Lxz} \quad (4.3b)$$

The forces acting on the load in the horizontal direction can be described by

$$F_X = M_L\ddot{X}_L = T_L \sin\theta_{Lxz} - k_D sign(\dot{X}_L)\dot{X}_L^2$$

where F_X is the resultant force acting on the load in the horizontal direction of motion. T_L is the tension in the sling, so the horizontal directional tension component is represented by $T_L \sin\theta_{Lxz}$ and the last term represents the aerodynamic drag and always opposes motion. k_D represents the aerodynamic force darg constant.

Resolving forces in the vertical direction gives

$$F_Z = M_L\ddot{Z}_L = M_L g - T_L\cos\theta_{Lxz} - k_D sign(\dot{Z}_L)\dot{Z}_L^2$$

Similarly, where F_Z is the resultant force acting on the load in the vertical direction of motion. $M_L g$ is the load weight. The vertical directional tension component is represented by $T_L\cos\theta_{Lxz}$ and the last term represents the aerodynamic drag and always opposes motion. Substituting for $\dot{X}_L$ and $\dot{Z}_L$ from Equations (4.2a) and (4.2b), $\ddot{X}_L$ and $\ddot{Z}_L$ from (4.3a) and (4.3b) into F_X and F_Z to eliminate T_L and its gives:

$$\begin{aligned}\ddot{\theta}_{Lxz} = &-\frac{g}{l_x}\sin\theta_{Lxz} + \frac{\cos\theta_{Lxz}}{l_x}\ddot{X}_0 + \frac{\sin\theta_{Lxz}}{l_x}\ddot{Z}_0 \\ &+ \frac{k_D sign(\dot{X}_L)\cos\theta_{Lxz}}{M_L l_x}\dot{X}_0^2 + \frac{k_D sign(\dot{Z}_L)\sin\theta_{Lxz}}{M_L l_x}\dot{Z}_0^2 \\ &- \frac{2k_D}{M_L}\left[sign(\dot{X}_L)\cos^2\theta_{Lxz}\dot{X}_0 + sign(\dot{Z}_L)\sin^2\theta_{Lxz}\dot{Z}_0\right]\dot{\theta}_{Lxz} \\ &+ \frac{k_D l_x}{M_L}\left[sign(\dot{X}_L)\cos^3\theta_{Lxz} + sign(\dot{Z}_L)\sin^3\theta_{Lxz}\right]\dot{\theta}_{Lxz}^2 - K_\theta\dot{\theta}_{Lxz}\end{aligned} \quad (4.4a)$$

where M_L, and k_D are the mass of suspended load and aerodynamic drag force coefficient respectively. The aerodynamic drag force constant k_D is given by:

$$k_D = \frac{1}{2}\rho S C_D \quad (4.4b)$$

where ρ, S and C_D are the air density, the load area presented to the airflow and the drag coefficient for the load respectively. The term $K_\theta \dot{\theta}_{L_{xz}}$ in (4.4a) represents the friction of hinge which has an unknown value to be determined.

A similar procedure for motion in the y-z plane leads to an equation with the appropriate parameters:

$$\ddot{\varphi}_{L_{yz}} = -\frac{g}{l_y}\sin\varphi_{L_{yz}} + \frac{\cos\varphi_{L_{yz}}}{l_y}\ddot{Y}_0 + \frac{\sin\varphi_{L_{yz}}}{l_y}\ddot{Z}_0$$
$$+\frac{k_D sign(\dot{Y}_L)\cos\varphi_{L_{yz}}}{M_L l_y}\dot{Y}_0^2 + \frac{k_D sign(\dot{Z}_L)\sin\varphi_{L_{yz}}}{M_L l_y}\dot{Z}_0^2$$
$$-\frac{2k_D}{M_L}\left[sign(\dot{Y}_L)\cos^2\varphi_{L_{yz}}\dot{Y}_0 + sign(\dot{Z}_L)\sin^2\varphi_{L_{yz}}\dot{Z}_0\right]\dot{\varphi}_{L_{yz}}$$
$$+\frac{k_D l_y}{M_L}\left[sign(\dot{Y}_L)\cos^3\varphi_{L_{yz}} + sign(\dot{Z}_L)\sin^3\varphi_{L_{yz}}\right]\dot{\varphi}_{L_{yz}}^2 - K_\theta\dot{\varphi}_{L_{yz}} \qquad (4.4c)$$

where, similarly, $K_\theta\dot{\varphi}_{L_{yz}}$ describes the hinge friction force. Equations (4.4a) and (4.4c) may be used to derive the load angle $\psi_{L_{xy}}$ in the x-y plane, if required, from:

$$\psi_{L_{xy}} = \tan^{-1}\left(\frac{\tan\varphi_{L_{yz}}}{\tan\theta_{L_{xz}}}\right) \qquad (4.5)$$

and hence $\dot{\psi}_{L_{xy}}$ and $\ddot{\psi}_{L_{xy}}$.

4.2 Simulation studies of the load dynamics

In this section an investigation of the influences of helicopter dynamics to the dynamics of the underslung load is considered. Simulations were conducted to study the behavior of the suspended load in response to different flight maneuvering conditions. $\theta_{L_{xz}}$ is the longitudinal suspension angle, so the variation of load angle (longitudinal) depend upon the angle movement $\dot{\theta}_{L_{xz}}$. The angle movement $\dot{\theta}_{L_{xz}}$ is influenced by the value of frication force coefficient k_θ. Similarly, for lateral motion, $\varphi_{L_{yz}}$ represent the lateral directional suspension angle, so the variation of the lateral suspension angle movement $\dot{\varphi}_{L_{yz}}$ is influenced by the value of lateral frication force coefficient k_φ. The mathematical model is implemented in MATLAB-SIMULINK

software and the outline of schematic block diagram of the simulation model is shown in Figure 4.2.

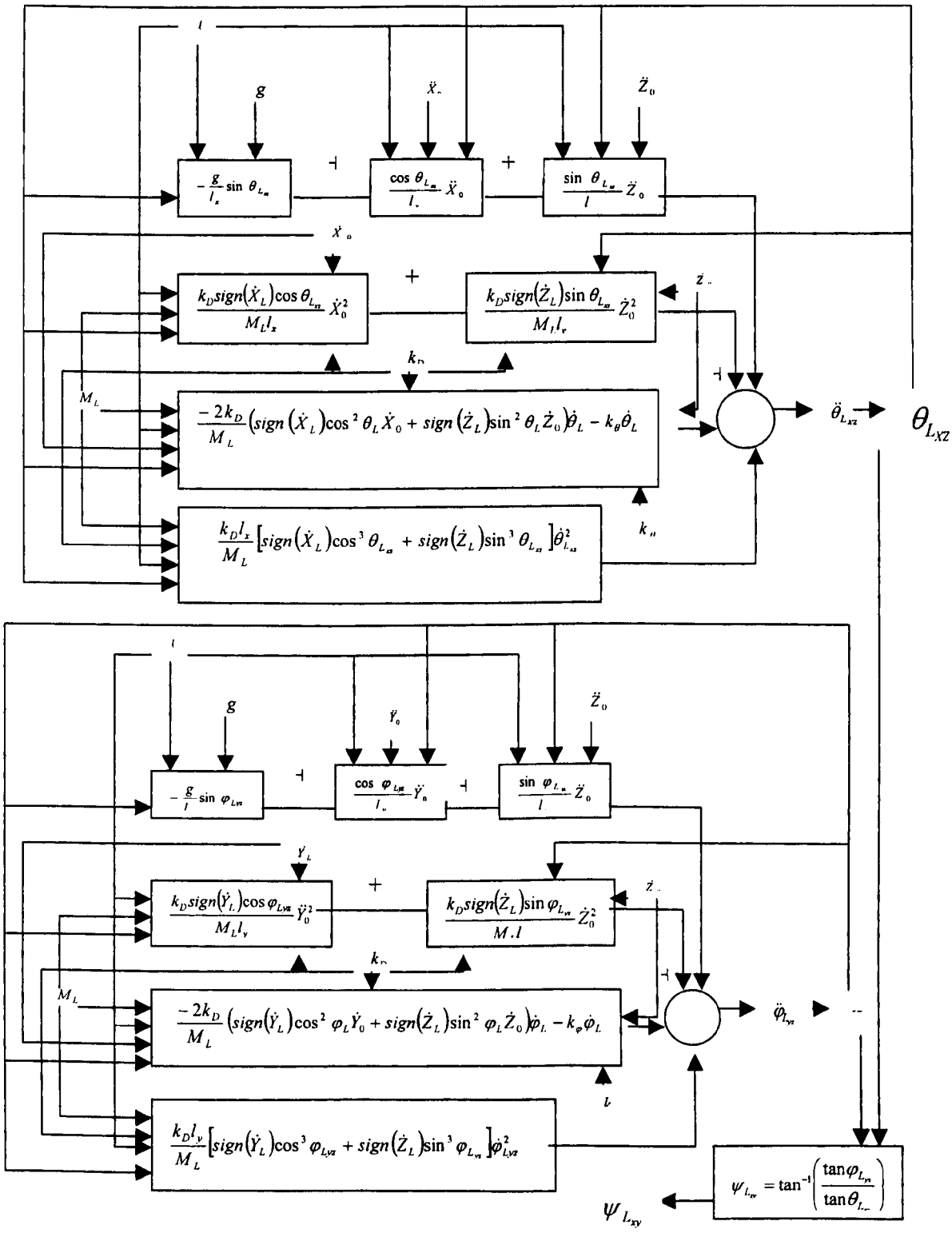

Figure 4.2: Schematic block diagram of an underslung load simulation model

4.2.1 Simulation study with a certain range imposed inputs

The mathematical model presented the previous section has been applied to investigate the effect of helicopter motion on the load behaviour. Three cases have been considered. Firstly, an idealised forward acceleration/deceleration profile is applied in which the helicopter accelerates at a constant rate from rest up to a constant speed. A brief sidestep is then performed, followed by a constant deceleration to rest (Figure 4.3). Three forward acceleration/deceleration rates have been considered, corresponding to three levels of aggressiveness, resulting in three different forward velocities - u1, u2, and u3. In each case the vertical speed w was kept at zero. Secondly, the effect of forward acceleration/deceleration is investigated in more detail (Figure 4.4). The underslung load in each of these tests was 500lbm suspended on a sling of length 15ft with the value of $k_D = 5\,lb/ft$. The values of forward velocities, forward acceleration/deceleration and the hinge friction used for these example simulation tests, are shown in Table 4.1 which are chosen with consideration of maximum safe operational values and typical flying speed. It is also important to point out that, if the hinge friction value is zero then the load movement (oscillation) continues for ever and it may not represent the real life situation.

Table 4.1: Simulation parameters for the designed motion profiles

Description	Symbol	value	Units
Forward velocity	u_1	65	ft/s
	u_2	40	ft/s
	u_3	25	ft/s
Forward accel./ decal.	du_1/dt	2.6	ft/s^2
	du_2/dt	1.6	ft/s^2
	du_3/dt	1.0	ft/s^2
Sideslip velocity	v	12.0	ft/s
Hinge friction coefficient	$k_\theta (k_\varphi)$	0.001	-

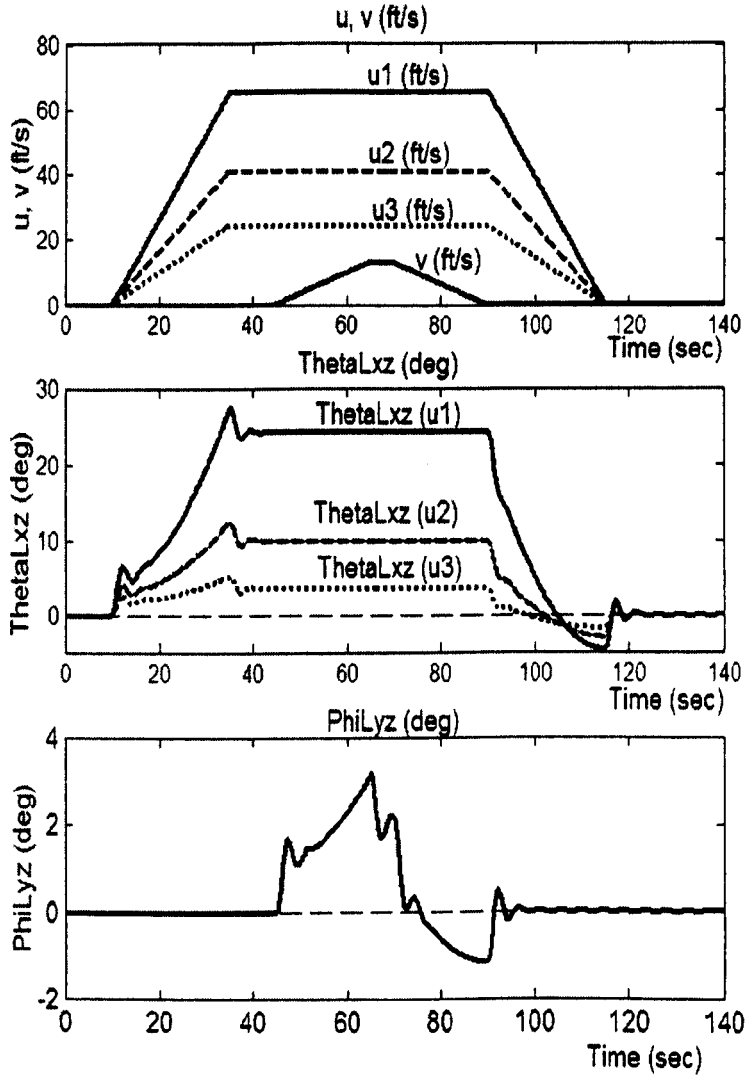

Figure 4.3 Underslung load suspension angle transients in response to the prescribed helicopter motion.

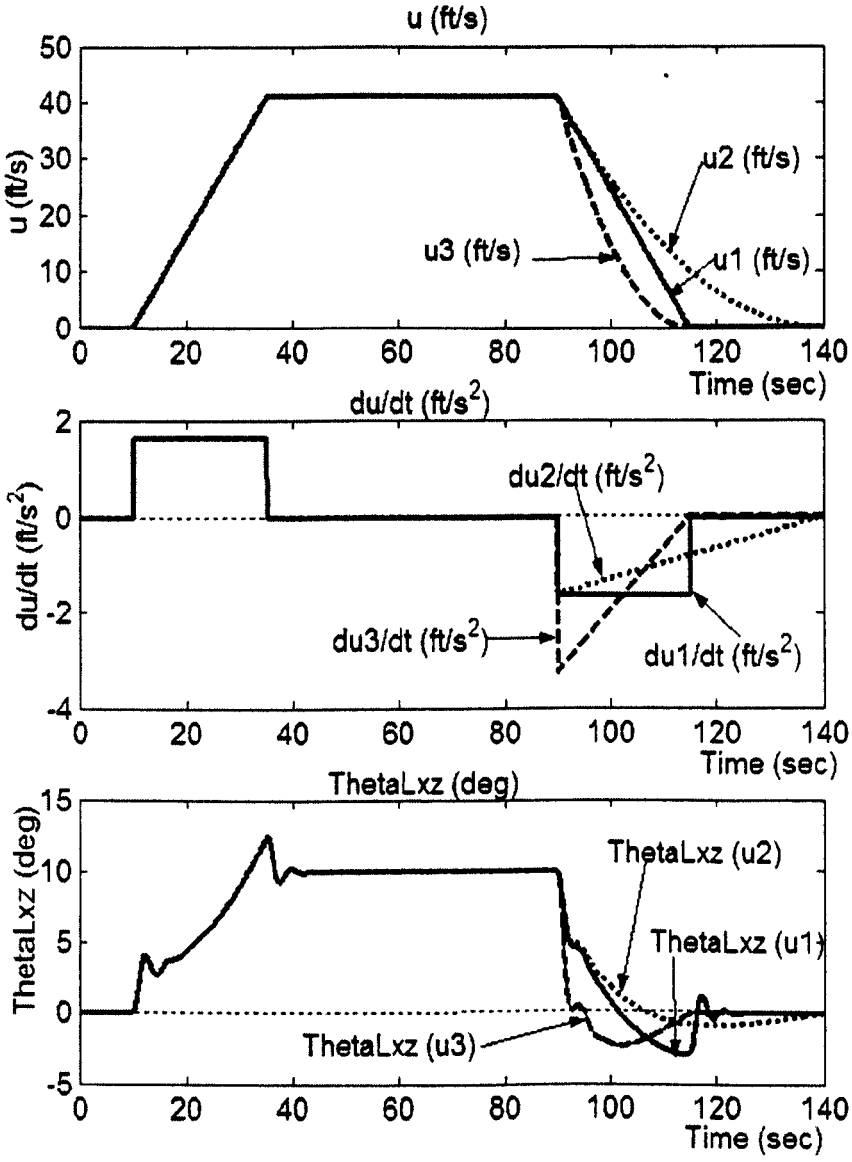

Figure 4.4 Underslung load suspension angle transient in the x-z plane in response to the prescribed helicopter motion.

From Figure 4.3, it can be seen that the levels of accelerations of helicopter motion do not affect the load oscillations very much. The simulation results also indicate that the different patterns of acceleration/deceleration of the helicopter motion result in different load dynamic behaviour. A typical example is shown in Figures 4.4. The deceleration profile shown as a dashed line in Figure 4.4 leads to more stable load dynamics, which shows that the pilot should apply appropriate velocity profiles for helicopter manoeuvring in positioning a load.

The dynamic response of the load depends on the value of k_D, load weight and sling length. From the simulation results obtained in Chapter 3, the effects of the load weight and sling length are addressed. To investigate the effects of the aerodynamic drag force constant k_D, tests were conducted for the underslung load suspension angle transient in the x-z plane in response to the prescribed helicopter motion with a constant sling length (15ft) and load weight (500 lb) for three different aerodynamic force drag constants (k_D) and the responses are shown in Figure 4.5.

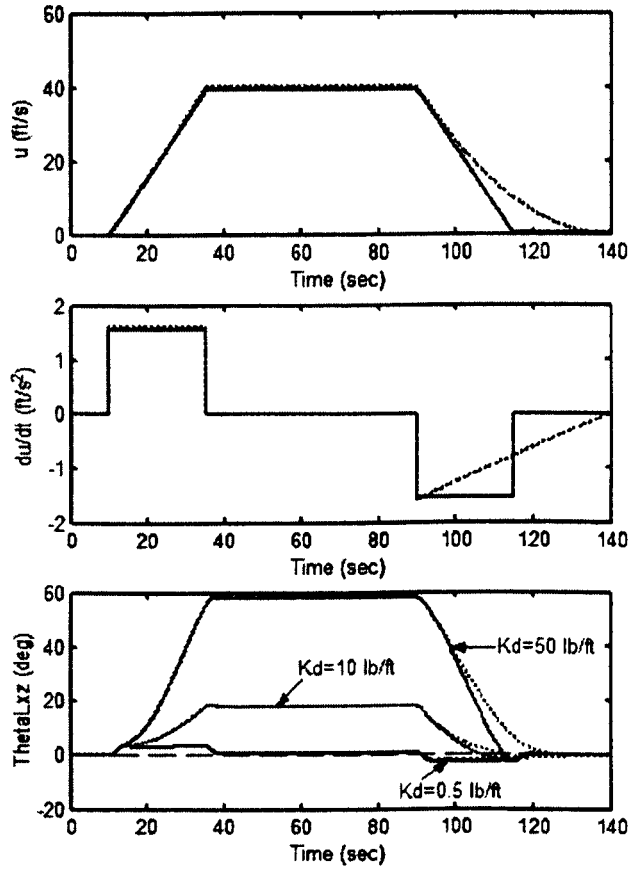

Figure 4.5 Underslung load suspension angle transient in the x-z plane in response to the prescribed helicopter motion with a constant sling length (15ft) and load weight (500 lb) for three different aerodynamic force drag constants (K_d).

From the simulation results (Figure 4.5) it is evident that the influence of the aerodynamic force drag constant change the system dynamic behaviour. It can be seen that the small value of k_D causes a periodic oscillation (see the response of the case k_D = 0.5 lb/ft) and smaller deflection from the initial position of the load. Increasing the value of k_D also increase the load angle deflection from its initial

position. Thus, its may suggest that bad operational weather condition such as high wind will enforcing difficulty in the process of positing a load.

4.2.2 Simulation study with the helicopter simulated inputs

In this case, an actual forward acceleration/deceleration data pattern obtained from the measurements recorded during a flight test conducted on a UH60 helicopter (without an under-slung load) [Fletcher, 1993] has been used as the load inputs to investigate the combined effect of u, v, and w velocities as the load may be experienced during the actual flight conditions. For this test, three load weights at a constant sling length and three different sling lengths at a constant load weight have been chosen as load parameters. Figures 4.6 and 4.7 show the simulation results for an actual forward acceleration/deceleration manoeuvre derived from measurements recorded during a flight test on a UH60 helicopter involving motion in all three dimensions.

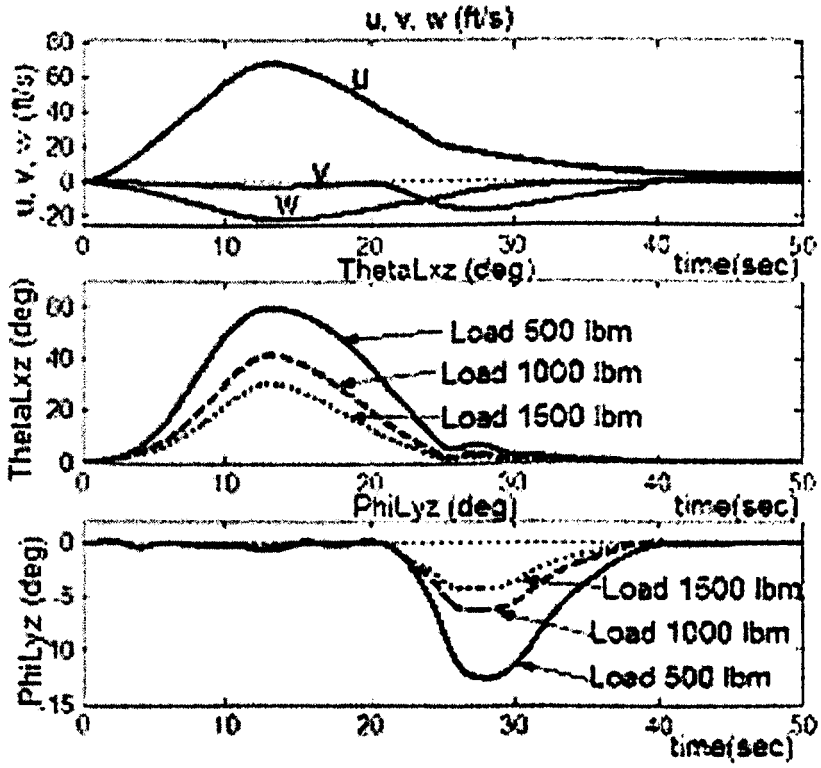

Figure 4.6 acceleration/deceleration manoeuvres with a constant sling length 15 ft and three different load weights.

NASA's underslung load experimental flight trials findings suggest that the limits of maximum external load can be carried by a UH-60 helicopter is about 8000 lbs with a

maximum sling length of 35 ft [Cicolani *et al,* 1998]. However, for safe slung load operation 20ft sling length is recommended by US military, but the load weight limit can vary within the allowable maximum load weight limit, which depends on the capacity of load carrying hooks. For operational safety, the underslung load weight is generally selected as up to 50% of the hook capacity and a hook with a capacity of 28% of helicopter weight is usually used for underslung load flight trials [Cicolani *et al,* 1998].

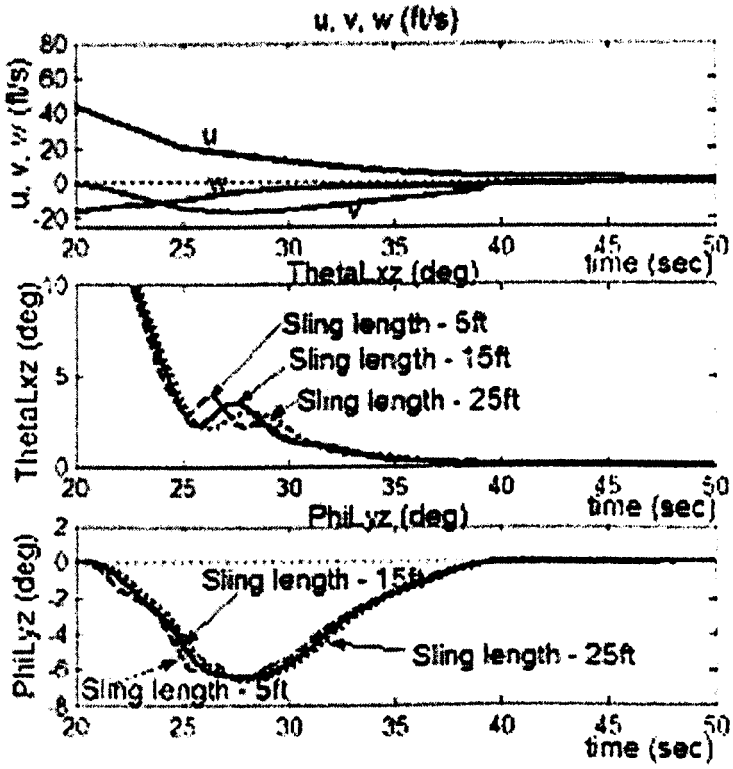

Figure 4.7 Expanded scale of the acceleration/deceleration manoeuvres shown in Figure 4.6 with a constant load weight of 500 lbm and three different sling lengths.

The results shown in Figure 4.6 reveal that heavier loads produce smaller deflections from the vertical as expected and that for this flight manoeuvre, relatively little oscillatory motion was apparent. From Figure 4.7, the sling length does not influence the load stability very much under the particular helicopter manoeuvre shown in Figures 4.6 and 4.7. However, it is clear that the frequency of load oscillation reduces as the sling length increases.

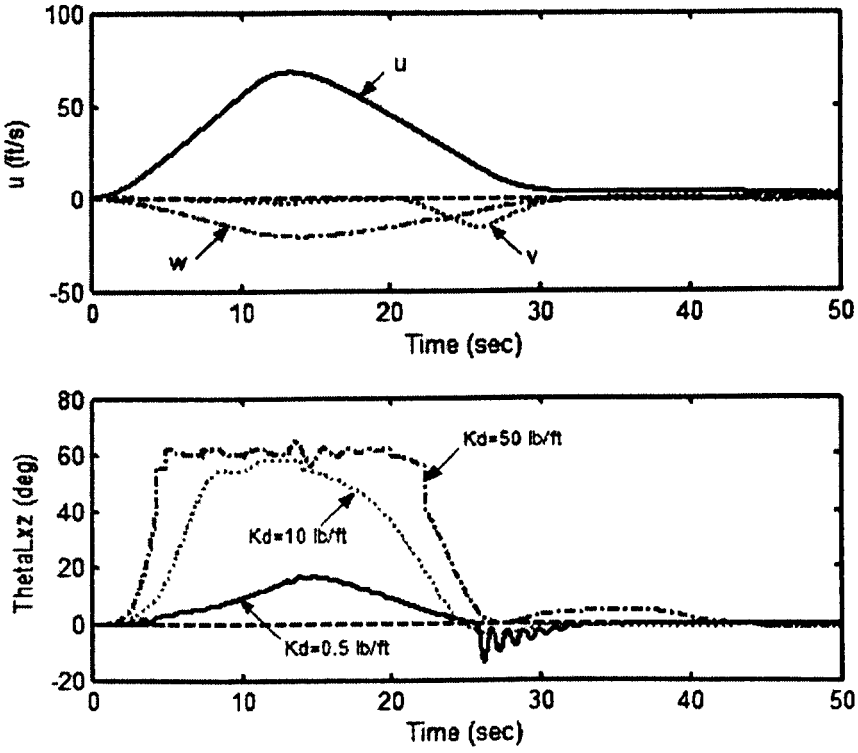

Figure 4.8 Underslung load suspension angle transient in the x-z plane in response to the helicopter motion with a constant sling length (15ft) and load weight (500 lb) for three different aerodynamic force drag constants (K_d).

Tests were conducted by varying the value of drag constant k_D to investigate the effect of aerodynamic drag forces that may involve in the load dynamic. However it should be noted that due to the symmetrical nature of the longitudinal and lateral motion in hover dynamic, the suspension angles relating to them have similar dynamic behaviour (see Figure 4.6). Thus, for this test only the longitudinal suspension angle dynamic behaviour is considered (Figure 4.8) and the value of 0.01 is used as a hinge frication coefficient. The simulation results suggest that the changing the value of k_D represents different air conditions and flying environment. For example, the large value of k_D case (k_D = 50 lb/ft) may represent the windy weather condition. It can be noted that the results from the prescribed motion also lead to the same conclusion (see Figure 4.5).

4.3 Summary and discussion

An investigation of the dynamic behaviour of a helicopter with an underslung external load is presented in this chapter. A mathematical model of an underslung load is developed and applied to study the behaviour of the suspended load in response to in-flight helicopter manoeuvres. The simulation studies for two different types of inputs from the helicopter dynamics were conducted. Firstly, different patterns of prescribed helicopter motion profiles were applied to the underslung load model. Secondly, an actual forward acceleration/deceleration manoeuvre derived from measurements recorded during a flight test conducted on a UH60 helicopter has been inputted to the load model. Simulation results reveal the importance of pilot control actions in positioning a load and the effect of system parameters such as aerodynamic drag force constant on the load dynamics.

Chapter 5

Helicopter control methods and application of Fuzzy Control

5.1 Introduction

The design of flight control systems for actively controlled helicopters is not an easy topic which is associated not only with the complex nature of the dynamics of the helicopter itself, but also with the range of design objectives which must be satisfied. Usually, the military rotorcraft handling qualities specification ADS-33D [Anonymous, 1996] is used to assess the capability of the control law. The requirement for the control law should be to stabilize the aircraft while controlling.

This chapter aims to get an overview of control design techniques applied to develop a control law for helicopters and an application example of fuzzy control is demonstrated via an experimental study for a twin rotor MIMO system.

5.2 Helicopter control methods

Variety of literature has been published concerning various aspects of helicopter controls. The content of this section is limited to the existing control methods to be successfully applied to helicopter control problems. Broader details of the subject can be found in various reports, which summarise the problems experienced in helicopter control design and suggest some technical solutions for those problems (see for example [Skogestad *et al,* 1996], [Prasad *et al,* 1988], [Mayajima, 1979]).

A review of reported methods for flight control law design shows that many approaches used to design the control law have involved the application of SISO techniques to each control loop individually [Manness *et al,* 1990]. The controller design methods such as linear quadratic regular (LQR) or linear quadratic gaussian (LQG) method (commonly referred to LQ methods [Gribble *et al,* 1990]), sliding

mode control (SMC) and eigenstructure assignment are used to evaluate multivariable control law design for helicopter flight [Garrard *et al,* 1987]. In the case of eigenstructure assignment method, the designer attempt to find optimum pole positions [Manness *et al,* 1990]. The main idea of SMC is to maintain the system sliding on a surface in the state space despite the uncertainties or perturbations. This is done by means of a discontinuous control law that switches between two structures, when the system passes through that surface [Shtessel *et al,* 1999], [Edwards *et al,* 1998]. Many researchers using the idea of SMC to develop flight control laws, for example see [Dorling *et al,* 1986], [Shkolnikov *et al,* 2001], [Shtessel *et al,* 2002], [Shtessel *et al,* 2003]. Sliding mode control is a technique for the design of nonlinear regulators [Dorling *et al,* 1986]. The first step in the two part synthesis procedure is to specify a desired sliding subspace. This involves using regulation techniques such as LQR or eigenstructure assignment to stabilise a reduced order system. A nonlinear controller is then developed in the second step to asymptotically drive the system towards the regulated subsystem so-called sliding subspace. However, designing the sliding subspace is very difficult job indeed, since there appears to be little guidance on how to design a sliding subspace, which may be limited this design method to helicopter control applications.

The method like H_∞ optimisation used to design a flight control law can be considered as a frequency domain method, since this technique is similar to that the design of the control law is based on a transfer function matrix representation of the system and it involves frequency domain performance specifications. For example, in the case of designing a control law for a helicopter, Yue [Yue *et al,* 1989] has described the application of H_∞ optimisation techniques to the determination of feedback control laws for improving the handling qualities of a combat helicopter. Quantitative feedback control technique is a control synthesis technique which involves shaping the loop transmission to meet bounds placed upon it by performance specifications in terms of desired system responses and disturbance rejection levels [Houpis, 1999]. A survey of quantitative feedback control technique can be found in Horowitz [Horowitz, 1991]. The possibility of applying Quantitative feedback control technique to helicopter flight control design is considered by several researches see for example [Thompson *et al,* 1999], [Snell *et al,* 1998], [Cheng, 1995]. However, due to the requirements of conservative and sequential design for each of the multivariable

sub-systems it is difficult to obtain best closed loop performance under practical constraints. Moreover, manual bound computation and trial and error loop shaping design procedures makes difficult to realise a stabilising feedback control law for helicopter system using quantitative feedback control technique.

Model reference techniques are those synthesis procedures which can be used to design feedforward controllers. For instance, integral inverse model following technique and controllers using nonlinear system inverses [Snell *et al,* 1992] are can be considered as model reference techniques [Ghosh *et al,* 2000]. In the case of integral inverse model following technique a regulator is designed to minimise the error transients between the responses of the system being controlled and a model which describes dynamics. The controller using nonlinear system inverses is essentially a procedure for the inversion of the system such that each input is linked with an output [Lane *et al,* 1988]. Jun [Jun *et al,* 1999] presented an investigation of state estimation of an autonomous flying helicopter. State estimator techniques such as Kalman filter and state observer and loop transfer techniques can be classified as output feedback methods. State estimator techniques provide a means of generating estimated state variables for feedback from available measurements [Saripalli *et al,* 2003]. However, the use of this method has a row back is that the use of estimated state feedback can create problems for the designer in that the resulting control laws are not, in most cases, robust to uncertainties or variations in the plant [Bryson, 1985]. The use of intelligent control methods for helicopter control system design such as fuzzy control and Neural Network (NN) has also been addressed by several researchers for example see [Kadmiry *et al,* 2001], [Steinberg, 1992].

Among all the design methods, PID control and linear feedback control are the most popularly accepted methods. A further discussion on PID control, LQ methods, nonlinear feedback linearization, eigenstructure assignment, classical SISO techniques, H_∞ optimisation and intelligent control methods for helicopter control system design is given in the following subsections.

5.2.1 PID control

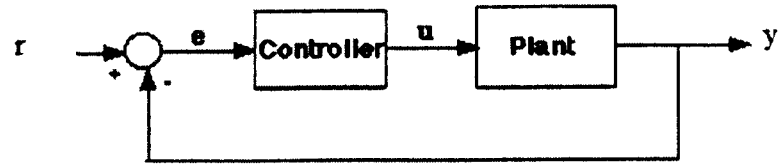

Figure 5.1 Closed loop system

PID (Proportional - Integral - Derivative) control is widely used in industry to control many different systems, including guidance, navigation and control system (GN-C). The PID controller works in the following manner, the variable (e) represents the tracking error, the difference between the desired input value (r) and the actual output (y) (see Figure 5.1). This error signal (e) will be sent to the PID controller, and the controller computes both the derivative and the integral of this error signal. The signal (u) just past the controller is now equal to the proportional gain (K_p) times the magnitude of the error plus the integral gain (K_I) times the integral of the error plus the derivative gain (K_D) times the derivative of the error. i.e., $u = K_p e + K_I \int e\,dt + K_D \frac{de}{dt}$ this signal (u) will be sent to the plant, and the new output (y) will be obtained. This new output (y) will be sent back to the sensor again to find the new error signal (e). The controller takes this new error signal and computes its derivative and it's integral again. This process goes on and on.

Ledin [Ledin *et al,* 2003] presents a PID controller to drive the helicopter to a specified point in a space by considering that the helicopter possesses a navigation system that tracks the vehicle's position, velocity and angular orientation without error [Ledin *et al,* 2003]. PID control is often used in applications where the plant is high order and its dynamic behaviour is not well understood. The PI type control is used to give high loop gain at low frequencies for good command tracking. Enns [Enns, *et al,* 1986] used the MIMO generalization PI technique and designed a MIMO PI control law for YAH-64 helicopter. Many researchers have applied PID or some form of PID control law to scaled size helicopter control (for example, see Sanders *et al,* 1998, Woodley, *et al,* 1997). But tuning the parameters of a PID controller is one

of the most common problems for a control engineer. Trial and error techniques (on-line tuning) are thus inadequate to derive a good compromise between controller performance and robustness. Chen [Chen *et al,* 1995] and Musch [Musch *et al,* 1997] presents some different approaches for better tuning of PID control. In particular, Musch [Musch *et al,* 1997] discusses the parameterization of PID control structures with a direct minimization of the H-infinity norm. In this work, the design of position controller for a model helicopter at hover via PID controller tuning is considered to address the tuning problems. PID control law design is still the most popular method in practices within the control community.

5.2.2 Linear Quadratic (LQ) control methods

The LQ methods, in particular, linear quadratic regulators (LQR) lead to a full state feedback law for the system and results excellent robustness properties and multivariable stability margins [Doyle, *et al* 1981]. However, in most applications, only part of the system states can be measured, so a state estimator is required in the feedback loop. For example, in the more realistic situation of output feedback a state estimator may be used or the design may be based on a reduced order model. In these cases, the original robustness properties do not apply and it may be appropriate to use loop transfer recovery (LTR) procedure, which can be used in conjunction with LQR design to recover the closed loop feedback properties of the LQR. The LQ methodology has provided an important tool for control law design [Gribble, 1993] and is commonly used in the design of flight control law, especially for fixed wing aircraft [Wendel *et al,* 1989]. The design freedoms in the LQR method are two matrices which penalise excursions of states and input vectors from the desired values. But it also generates the difficulties in determination of those two matrices. The LQR method has been considered as lacking visibility in the sense that it is not obvious how to choose these matrices to achieve desired loop properties [Manness *et al,* 1990]. In fact, LQR design can now be guided by eigenstructure assignment [Harvey, 1978, Garrard, *et al* 1989] or loop shaping [Doyle, 1981]. Although LQR theories guarantee stability robustness, these theories do not provide a direct means to obtain the desired responses types. Response types are obtained indirectly through choice of state and control weighting matrices. As indicated above the LQR method requires full state feedback, but which is usually not feasible. However stability

margins can be maintains without full state feedback but requires an estimator in the feedback loop. This estimator can seriously degrade the stability margins of the closed loop system [Rubio, *et al* 1997]. Recently the LQR based control design for commercial aircraft control application was studied by Blight [Blight *et al,* 1996] to redesign an autopilot control law in order to improve stability and reduce sensitivity to plant parameter variations. This controller was flight tested and implemented in the autopilot of Boeing 767 commercial transport airplane. In the autonomous flight control study of unmanned aerial vehicles (UAV), LQR is used as baseline inner loop controller [Boyle *et al,* 1999]. LQR has also been adopted for an autopilot design for a high-altitude, supersonic air-to-air bank-to-turn (BTT) missile [Bossi *et al* 1988]. One of the design requirements for such systems is a high level of robustness to parameter variations, which is difficult to meet with classical methods.

5.2.3 Nonlinear feedback linearization

The idea of nonlinear feedback linearization is that using feedback to cancel the nonlinear terms and then the design of the linearized system can be accomplished using standard linear controller synthesis procedures. For this method, the exact knowledge of the nonlinear terms is required for the exact cancellation and, linearization can not be obtained if any of the control actuators are saturated. So the method is not realistic in many cases. Smith [Smith *et al* 1987] states the success of the application of this control system concept to aircraft control. For example a controller using a nonlinear dynamic inversion controller has been flown by NASA on UH-1H helicopter [Meyer *et al,* 1983]. Despite these successes, there are some issues which can affect the use of this method to helicopter control. There are always some inaccuracies in mathematical models of a helicopter and the exact cancellation is very difficult to achieve.

5.2.4 Eigenstructure Assignment

This method uses feedback control to place a closed loop eigenvalues and shape closed loop eigenvectors to achieve performance specifications. The key to successful eigenstructure assignment is an appropriate manipulation of the closed-loop

eigenvectors [Manness *et al,* 1990]. The use of eigenstructure assignment for rotorcraft control system design has been considered by several researchers. An excellent review of the research in the area of eigenstructure assignment techniques applied to helicopter flight control system design is given in Garrard, *et al* 1989. This technique is useful when performance specifications can be expressed in terms of closed loop eigenvalues and eigenvectors. As far as the design of helicopter flight control system concerns, Garrard [Garrard, *et al* 1989] shows that eigenstructure assignment provides a straightforward methodology which results in control law. The control law is relatively simple for the implementation and do not require high order dynamic compensators in the feedback loops. However, even though this technique provides a direct simple method for achieving desired performance they do not provide guarantee to performance robustness. Generally, the eigenstructure assignment is always associated with a chosen design method in applications.

5.2.5 Classical SISO techniques

Classical single input single output (SISO) techniques concentrate on achieving a maximal loop gain over a specified frequency range consistent with specified gain and phase margins [Garrard, *et al* 1989]. Classical SISO techniques applied to each control loop individually. Review of publication of helicopter flight control law design, shows that SISO techniques are more widely used to design a helicopter flight control system. Innocenti [Innocenti *et al,* 1984] gives an example of classical SISO methods application to a flight control design. Enns [Enns, 1987] provides an interesting account of this classical type approach for the Apache AV05 YAH-64 flight control system.

Although classical SISO design methods are of very great practical value, and has proven to be a very reliable and successful technique, the row-back for the use of these methods is that, the classical SISO design techniques treat each control loop separately and do not explicitly include coupling between loops. Since this coupling can not be ignored in helicopters this method is not sufficient and a variety of other techniques need to be studied helicopter control systems.

5.2.6 H_∞ optimisation

This method can be considered as a multi input multi output (MIMO) generalization of classical SISO frequency response techniques [Skogestad *et al,* 1996]. This method is based on the use of H_∞ norm which is defined, for a transfer function matrix, as the maximum over all frequencies of the largest singular value of that matrix. Singular values provide information concerning guaranteed bounds on system performance and the H_∞ norm can place an upper bound on the uncertainty level in a given system which is to be controlled [Manness *et al,* 1990]. Problems of control system design can be formulated in terms of the minimisation of the H_∞ norm of an appropriately weighted closed loop transfer function matrix. Yue [Yue *et al,* 1990] has described the application of H_∞ method to the determination of feedback control law for improving the handling qualities of a helicopter. In that work a controller design is described which is able to give accurate control of pitch and roll attitude, yaw rate and heave velocity for a typical helicopter. Performance and robustness are achieved by the two-degree of freedom control system structure. A feedback compensator was designed to have suitable robustness properties against model uncertainty and disturbances and a pre-compensator was found to achieve desired performance objectives in terms of tracking accuracy and speed of responses. Since the desired response types for helicopters are given in terms of frequency response relationship between pilot inputs and helicopter outputs, the H_∞ approach appears to provide a suitable method for design of helicopter flight control laws [Skogestad *et al,* 1996]. Turner [Turner, 2000] gives an account of success of H_∞ method and shows the successful application of H_∞ approach to helicopter control. Furthermore, Postlethwaite [Postlethwaite *et al,* 2002] and Walker [Walker, 2003] show the applicability of H_∞ control law via means of flight test. These H_∞ controllers have been flight tested on Bell-205 helicopter at the NRC flight research lab, Ottawa. However, despite of these successes there is some row-back to this method such as, the underlying mathematical theory of H_∞ design is sophisticated. Dilemma of selecting the weighting function, which is critical to the success of the design, causes the repeated design iterations, and also, the order of the controller designed through H_∞ technique is very high which in turn increases the complexity of controllers.

5.2.7 Intelligent Control methods

The increasing demand of a controller design method, which is able to achieve high performance in uncertain and adverse conditions, has led to the development of intelligent control methods. The intelligent control systems are classically constituted by three basic levels. 1) the organisation level which organises sequences of complex actions in a long term memory, 2) the co-ordination level which coordinates decision making and learning in a short term memory to generate subtask sequences to execute simple commends on the basis of real time information of the world, 3) the execution level which performs the continuous-time control of the system [Antsakil *et al,* 1993].

The high degree of uncertainty and complex structure of the aircraft have leads to the intelligent flight control system development. Intelligent flight control systems learn knowledge of the aircraft and its mission and adapt to changes in the flight environment [Stengel 1994]. Usually the intelligent flight control laws are design to make the aircraft less dependent on proper pilot command for mission completion and enhance the mission capability of aircraft. Mission tasks performances are improved by learning from experience. Generally Intelligent flight control designs are low cost and reliably. Thus unmanned air vehicle (UAV) tests are usually carried out with the intelligent flight controller employed. The work described in Buskey [Buskey *et al,* 2001] emphasised the use of an artificial neural network (ANN) to have the helicopter achieve stable hover. Wan [Wan *et al,* 2001] present a control method for a MIMO nonlinear systems based on a combination of a neural network feedback controller and state-dependent Riccati equation controller. The resulting technique is applied to a six degree of freedom helicopter model. Recently an autonomous helicopter was flight tested with the learning control algorithm employed in the controller design [Bagnell *et al,* 2001]. The use of intelligent control methods for helicopter control system design has been considered by several researchers especially, some forms of fuzzy control development are widely considered. (for example, see [Kadmiry *et al,* 2001, Steinberg, 1992]). Fuzzy logic control has been applied to control, an intelligent unmanned helicopter [Sugeno *et al,* 1995]. Shim [Shim *et al,* 1998] compared the fuzzy logic controller performance with linear robust multi-variable control and non

linear tracking control methodologies for helicopter autopilot design and shows the fuzzy controller's capabilities of handling uncertainties and disturbances.

5.3 An application example of fuzzy control

To strengthen the discussion presented relating to intelligent control, in particular fuzzy control and its capabilities, this section is devoted to fuzzy controller development for a nonlinear twin rotor MIMO system, which is a helicopter alike experimental system that is available in the Control Engineering Laboratory at the University of Liverpool.

5.3.1 Introduction to the twin rotor MIMO system

The Twin Rotor MIMO System (TRMS) can be considered as a cut-down version of a helicopter system as shown in Figure 5.2. It consists of a beam pivoted on its base so it can rotate freely both in the horizontal and vertical planes [TRMS Reference manual 1997]. Two rotors, main and tail, are mounted at the two ends of the beam horizontally and vertically, which are controlled by a PC-based control system. The system has two inputs and multi-outputs so there exist coupling effects between the vertical and horizontal motions.

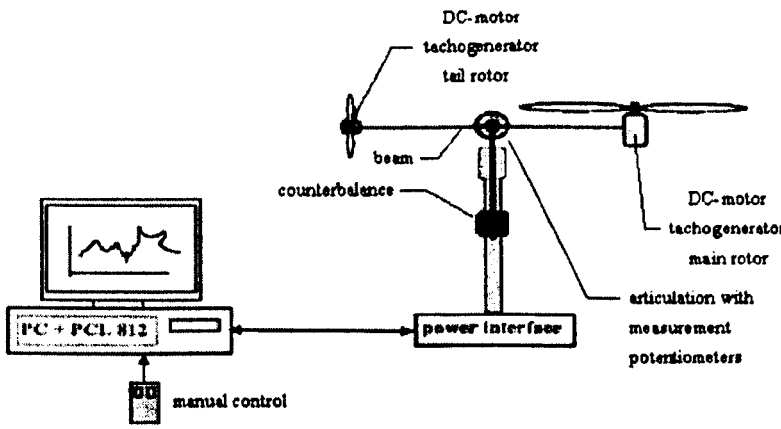

Figure 5.2. Twin Rotor MIMO system [Feedback Instruments Ltd, 1997]

The TRMS is intrinsically unstable and there is a time delay between the input and output operations. The current control algorithms provided by the manufacturer include PID and linear feedback controls. Those controllers were developed on the basis of the linear TRMS model so they may work well around the equilibrium point of the system but resulting in operational difficulties in the states that deviate far from the equilibrium [Khalil *et al,* 1996]. The experimental studies revealed that, under the current control strategy, the system is not robust enough and easily becomes unstable when it encounters the external disturbances. It is necessary to develop new control schemes to improve the system's robustness. Generally speaking, many possible directions could be explored for development of new control strategies. For this particular system, the new control strategy needs to be implemented in real-time. Therefore, it should have a simple structure and should not require any extra sensors to be added onto the system. The fuzzy logic control takes the factors of nonlinearities into account and can realise the human's knowledge in system stabilisation by only adding the 'if-then' rules to address the system environmental changes. Fuzzy logic control is customisable since the rules are easy to be understood and modified by the designers or users. All the above leads the fuzzy controller to have simple and flexible structure.

From the control point of view, the TRMS exemplifies a high order non-linear system with significant cross coupling terms. From Figure 5.2, there are two propellers driven by DC-motors at both ends of the beam. The propellers are perpendicularly positioned to each other such that only one propeller can affect the movement in the vertical plane (pitch angle α_v) or in the horizontal plane (azimuth angle α_h). There is a counter-weight fixed to the beam which determines the stable equilibrium position. By varying the supply voltages, the angular velocities of the motors are changed and will result in changes of the propulsive force on the beam perpendicular to the propellers, which in turn result in a movement of the beam.

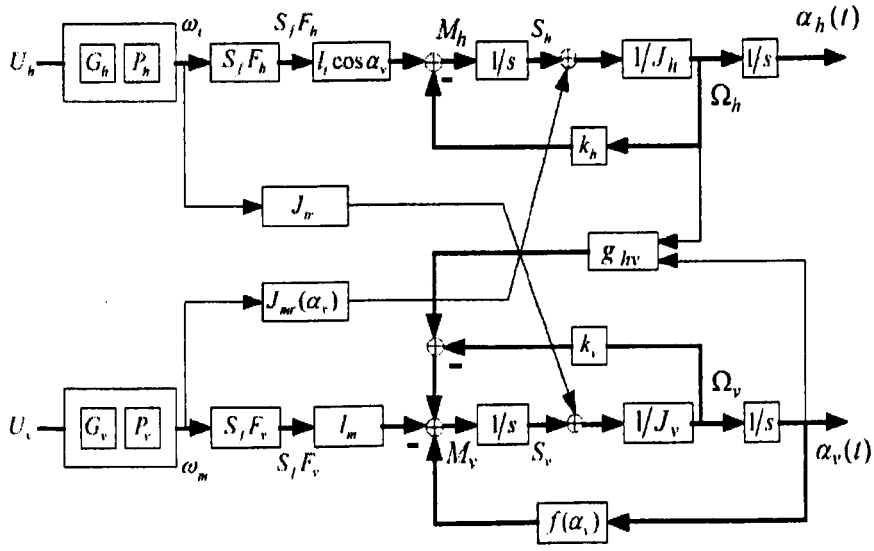

Figure 5.3. Block diagram of the TRMS model [Feedback Instruments Ltd, 1997]

The structure of the TRMS can be modelled by a block diagram shown in Figure 5.3. The control voltages U_h and U_v are inputs to the DC-motors, which drive the rotors. The model of the DC motor with the propeller is composed of a linear dynamic component. The linear part is in the form of the first order transfer functions:

$$G_h = 1/(T_h S + 1) \text{ and } G_v = 1/(T_v S + 1).$$

The non-linear functions P_h and P_v are static characteristics of the DC-motors with propellers. The input voltage is limited to the range +/- 10 volts. The nonlinear relations between the rotor's velocity and the resulting aerodynamic force can be approximated by the quadratic functions:

$$F_h = sign(\omega_h) k_h \omega_h^2 \text{ and } F_v = sign(\omega_v) k_v \omega_v^2$$

where k_h and k_v are positive constants.

It is important that the geometrical shape of the propellers is not symmetric, so that the behaviour in one direction is different from that in the other direction. Rotation of

a propeller produces an angular momentum, which, according to the law of conservation of angular momentum, must be compensated by the remaining body of the TRMS beam. This results in the interaction between two transfer functions represented by the moment of inertia of the motors with propellers which are represented by J_{hv} and J_{vh} as shown in Figure 5.3. This interaction directly influences the velocities of the beam in both planes. The forces F_h and F_v are multiplied by the arm length $l_h(\alpha_v)$ and l_v which are equal to the torques acting on the arm.

In order to simplify the design of the controller, if neglecting the coupling effect between the main rotor and tail rotor subsystems, the block diagrams can be simplified into two individual axis diagrams as shown in Figures 5.4 and 5.5.

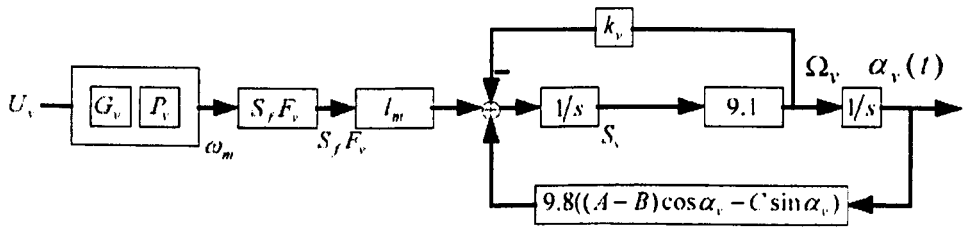

Figure 5.4. Block diagram of the main rotor subsystem [Xie *et al*, 2003]

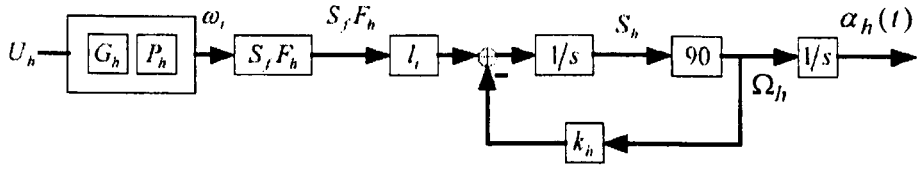

Figure 5.5. Block diagram of the tail rotor subsystem [Xie *et al*, 2003]

The components shown in the figure are described by

$$G_v = \frac{1}{1.432s+1}, \quad S_f = \frac{5}{2.895 \times 2048}, \quad l_m = 0.236,$$

$$K_v = 0.00545371 \ , \ A = 0.0217 , \ B = 0.0119 , \ C = 0.01678$$

$$P_v = 90.99u_{pv}^6 + 599.73u_{pv}^5 - 129.26u_{pv}^4 - 1238.64u_{pv}^3 + 63.45u_{pv}^2 + 1283.41u_{pv},'$$

$$F_v = -3.48\times10^{-12}u_{fv}^5 + 1.09\times10^{-9}u_{fv}^4 + 4.123\times10^{-6}u_{fv}^3 - 1.633\times10^{-4}u_{fv}^2 + 9.5455\times10^{-2}u_{fv}$$

$$G_h = \frac{1}{0.3842s+1}, \ S_f = \frac{5}{2.895\times2048}, \ l_t = 0.25,$$

$$K_v = 0.0095,$$

$$P_h = 2020\,u_{ph}^5 - 194.69u_{ph}^4 - 4283.15u_{ph}^3 + 262.27u_{ph}^2 + 3796.83u_{ph},$$

and

$$F_h = -3\times10^{-14}u_{fh}^5 + 1.595\times10^{-11}u_{fh}^4 + 2.511\times10^{-7}u_{fh}^3 - 1.808\times10^{-4}u_{fh}^2 + 0.801\times10^{-2}u_{fh} \ ,$$

where u_{pv} represents the input to the block of P_v, u_{fv} to F_v, u_{ph} to P_h, and u_{fh} to F_h.

5.3.2 Fuzzy control development

This section describes fuzzy set point weighting PID controller and its application to twin rotor MIMO system, which was partly reported in [Xie *et al* 2003]. It is always a problem in practice to determine a suitable set of parameters for a conventional PID controller. In general, it is not easy to satisfy different design specifications at the same time. A method to cope with this problem proposed by some researchers is to weight the set-point for the proportional action by a coefficient $0 < b < 1$ ([Astrom *et al* 1995], [Leva *et al* 1999]). In this way, the control law becomes:

$$u(t) = K_P e_b(t) + K_i \int_0^t e(\tau)d\tau + K_d \frac{de(t)}{dt}, \qquad (5.1)$$

where $e_b(t) = b \cdot y_d(t) - y(t)$. From previous study ([Aracil *et al*, 2000], [Driankov *et al*, 1998], [Driankov *et al*, 1996]), with this modification, the overshoot in system responses can be greatly reduced, but this increases the value of the rising time. It is desired to have a low overshoot and fast responses. So the fuzzy set-point weighting method is proposed and appears to be very effective. The method consists of two steps: 1) setting the PID control gains based on experiences of operators; 2) determining, through a fuzzy inference system, the value of the set-point weight. The expression of the modified PID controller can be written as:

$$u(t) = K_P(b(t)y_d(t) - y(t)) + K_d \frac{de(t)}{dt} + K_i \int_0^t e(\tau)d\tau \qquad (5.2)$$

$$b(t) = \omega + f(t) \qquad (5.3)$$

where ω is a positive constant less than or equal to one and $f(t)$ is the output of the fuzzy mechanism which consists of five triangular membership functions for the two inputs $e(t)$ (see Figure 5.6) and $\dot{e}(t)$ and nine triangular membership functions for the output (see Figure 5.7). Note that $e(t)$ and $\dot{e}(t)$ are normalized to the range of [-1, +1] using two constant parameters K_{in1} and K_{in2} respectively. Furthermore, the de-fuzzified output will be multiplied by another scalar constant K_{out}. There are different ways for assigning the values of the scaling coefficients and defining the shapes of the membership functions, such as, the Ziegler-Nichols method to tune the parameters [Visioli 2000].

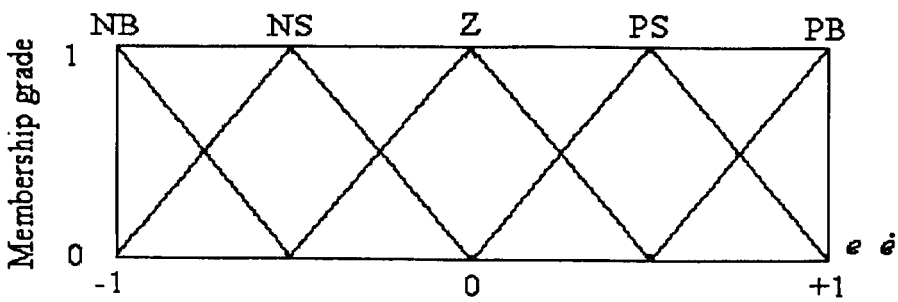

Figure 5.6. Membership functions for the two inputs e and $\dot{e}$

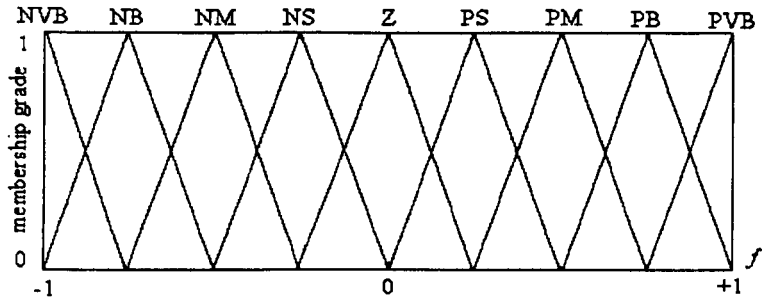

Figure 5.7. Membership functions for the output

The fuzzy rules are shown in Table 5.1 and the definitions of the linguistic variables are described in Table 5.2.

e \ ė	PB	PS	Z	NS	NB
PB	PVB	PB	PM	PS	Z
PS	PB	PM	PS	Z	NS
Z	PM	PS	Z	NS	NM
NS	PS	Z	NS	NM	NB
NB	Z	NS	NM	NB	NVB

Table 5.1. Basic rules table of the fuzzy inference

Linguistic variables	Linguistic meanings
NVB	Negative Very Big
NB	Negative Big
NM	Negative Medium
NS	Negative Small
Z	Zero
PS	Positive Small
PM	Positive Medium
PB	Positive Big
PVB	Positive Very Big

Table 5.2 Linguistic variables in the fuzzy inference system

The structure of the fuzzy controller is shown in Figure 5.8.

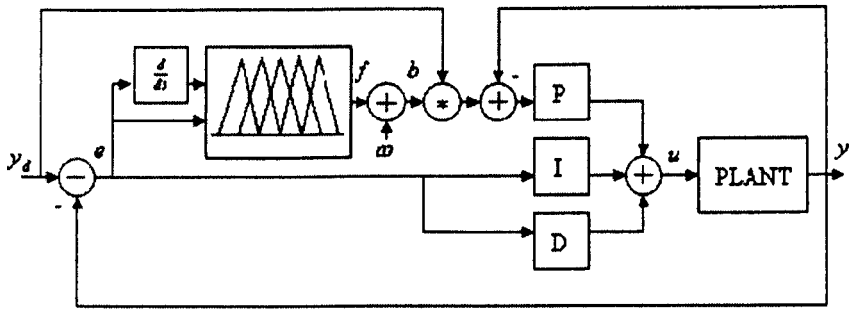

Figure 5.8. Control scheme with the fuzzy set point weighting (FSW) methodology

In the real process of the system, e and Δe can be positive or negative. A linguistic value of 'Zero' for e means that the measured current output is near to the set-point of system output. A 'Zero' for Δe means that the changes in output is very small, i.e. $\Delta e(t) = e(t) - e(t-1) \approx 0$. The sign and the magnitude for Δu constitute the value of the control signal. In Table 5.3, the top row of the table shows the change-of-error Δe and the left column is the error e. the cells of the table at the intersection of rows and columns contain the linguistic value for the output corresponding to the value of the first input written at the beginning of the row and to the value of the second input written on the top of the column.

e \ $\dot{e}$	PB	PS	Z	NS	NB
PB	PVB	PB	PM	PS	Z
PS	PB	PM	PS	Z	NS
Z	PM	PS	Z	NS	NM
NS	PS	Z	NS	NM	NB
NB	Z	NS	NM	NB	NVB

Table 5.3. Basic rules table of the fuzzy inference

Table 5.3 includes 25 rules, which take into account not only the errors but also the changes-of-errors as well. It describes the dynamics of the controller. The rules are organised into five groups:

- Group 0: For this group of rules, both e and Δe are (positive or negative) near to zero which indicates the steady-state behaviour of the process.

- Group 1: $e(t)$ is Positive Big or Small which implies that output $y(t)$ is significantly below the set-point. At the same time since $\Delta e(t)$ is negative, so $y(t)$ is moving towards the set-point.

- Group 2: y(t) is either close to the set-point ($e(t)$ is Zero and Negative Small) or significantly above it (Negative Big). At the same time, since $\Delta e(t)$ is negative, $y(t)$ is moving away from the set-point. The control here is intended to reverse this trend and make $y(t)$ start moving back to the set-point.

- Group 3: $y(t)$ is Negative Big or Negative Small, which means that $y(t)$ is below the set-point. At the same time, $y(t)$ is moving towards the set-point since $\Delta e(t)$ is positive.
- Group 4: For this group of rules, $e(t)$ is either close to the set-point (Positive Small, Zero) or significantly below it (Positive Big). At the same time since $\Delta e(t)$ is positive, $y(t)$ is moving away from the set-point.

5.3.3 Simulation and experimental results and analysis

The nonlinearities in the system is investigated via experimental studies. Through these studies, it has been found that the system is suffered many different forms of nonlinearities [Xie, 2002], for example the dead zone nonlinearity is observed and is shown in Figure 5.9.

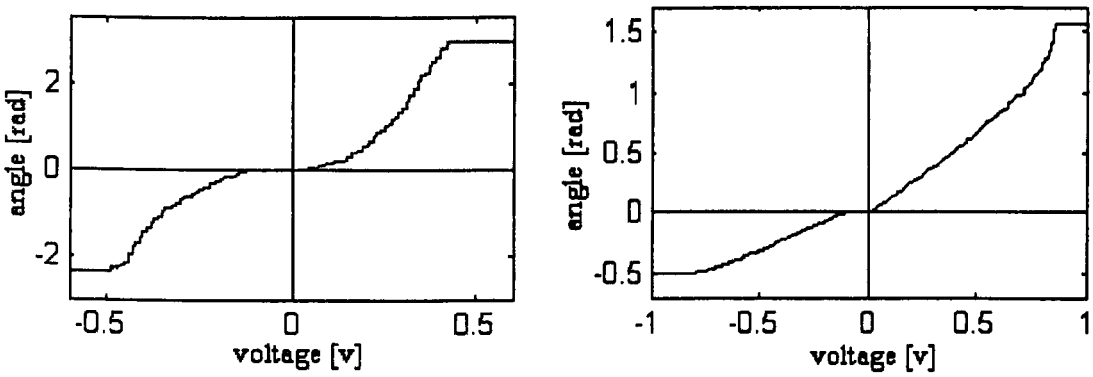

a) Horizontal direction (b) Vertical direction

Figure 5.9. Dead-zone nonlinearity of the system

The extensive experimental studies have been conducted to evaluate the effects of the FSPW PID controller. Test results have been compared with the results obtained using conventional PID controllers. The gains for FSPW PID controller are illustrated in Table 5.4. All of these studies reveal the fuzzy controller is more robust with respect to disturbances.

Table 5.4. Gains of FSPW PID controller

	K_P	K_i	K_d	K_{in1}	K_{in2}	K_{out}	ω
Vertical	0.85	0.75	0.65	1.2	1	1	0.85
Horizontal	0.85	0.2	1.45	1	1	1.303	1

Running the system online, the reference signal is a step input, the actual outputs of α_v is measured and shown in Figure 5.10 for using PID and FSPW PID controllers respectively. The performance features are summarized in Table 5.5. The actual outputs of α_h is measured and shown in Figure 5.11 for using PID controller FSPWPID controller respectively. The performance features are summarized in Table 5.6.

Table 5.5. The performances with PID and FSPW PID controllers (vertical dimension)

	Overshoot	Rising time	Settling time (sec)	IAE
PID controller	15.65%	2.52	9.51	2.063
FSPW PID controller	6.46%	1.74	3.6	1.332

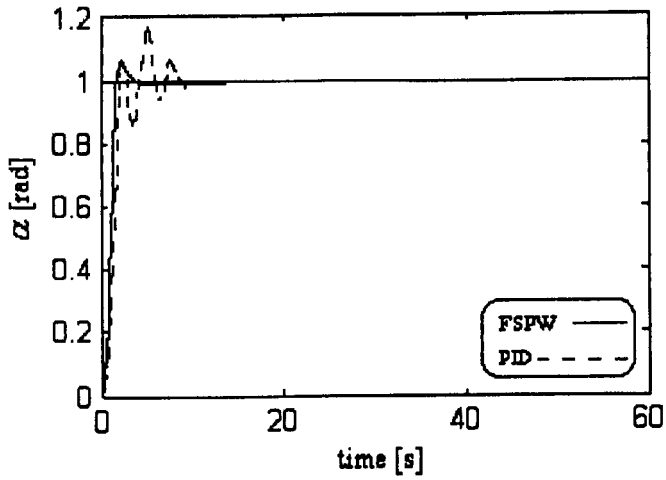

Figure 5.10. The step input response of pitch angle α_v using PID and FSPW PID

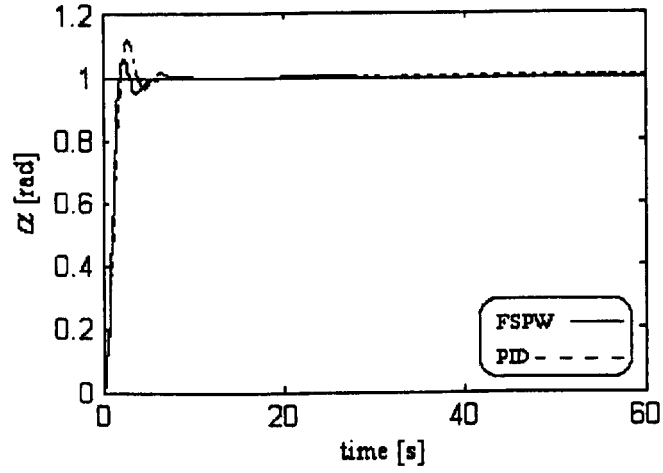

Figure 5.11 The step input response of azimuth angle α_h using PID and FSPW PID controller respectively.

Table 5.6. The performances with PID and FSPW PID controllers (horizontal dimension)

	Overshoot	Rising time (sec)	Settling time (sec)	IAE
PID controller	11.98%	2.07	7.11	2.0
FSPW PID controller	6.5%	1.89	4.89	1.582

Figures 5.10 & 5.11 and Tables 5.5 & 5.6 indicated that the system with a FSPW PID controller has smaller overshoot and taking a shorter period of time to settle down to the desired values. Similarly, external disturbances are exerted onto the system to

investigate the responses of the system to the disturbances using different controllers. The results are shown in Figures 5.12 and 5.13.

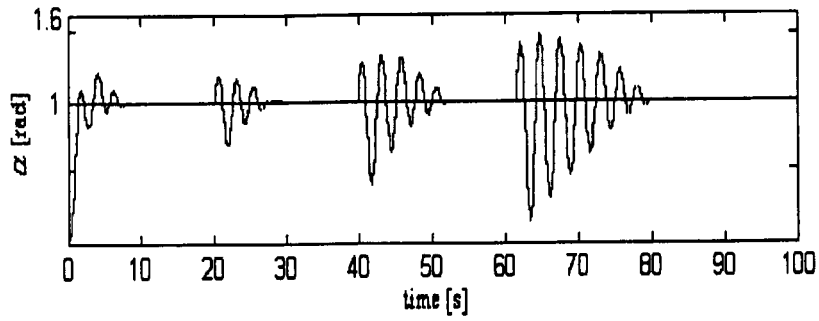

(a) Using the conventional PID controller

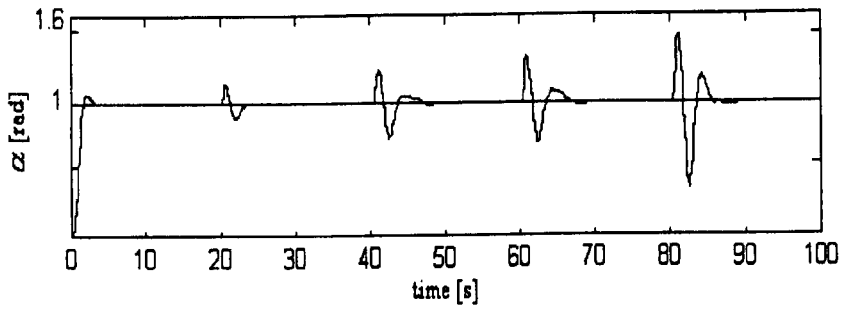

(b) Using FSPW PID controller

Figure 5.12. Dynamic responses of TRMS to the external disturbances in vertical direction

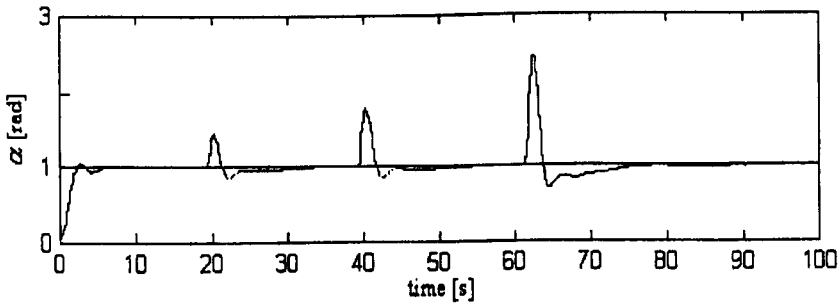

(a) Using the conventional PID controller

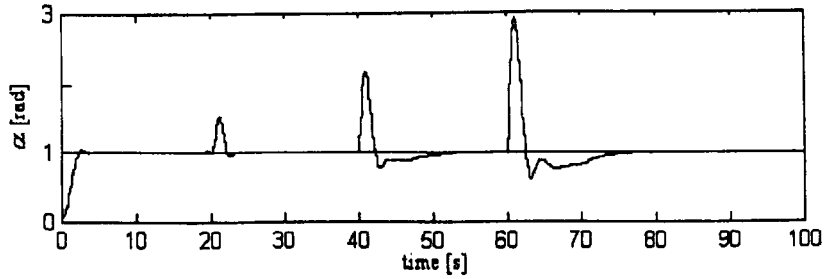

(b) Using FSPW PID controller

Figure 5.13. Dynamic responses of TRMS to the external disturbances in horizontal direction

From Figure 5.12, it can be seen that the system with FSPW PID controller takes much shorter time period to recover from the disturbances in comparing with the system with a PID controller. Figure 5.13 reveals that the system with FSPW PID controller takes a similar length of time period to recover when the system has suffered bigger external disturbances comparing with the system using a conventional PID controller only. Therefore, TRMS using the FSPW PID controllers are more robust with respect to disturbances. The more detailed description about FSPWPID controller can be found in Xie [Xie, 2002].

Further studies about Fuzzy control of the MIMO Twin Rotor system are still on-going at the University of Liverpool through an MSc project. To test the robustness propriety of the system extensively, different disturbances will be introduced to the system. If it is practically possible, then the underslung load will be considered which can be attached to the test system beam. The attached underslung load can be considered as an external disturbance to the helicopter system which can be used to study the helicopter dynamics with an underslung load.

5.4 Summary and discussion

Form the review of popular helicopter control methods, it is clear that in the past years, considerable attention has been paid to the design of controller to obtain a satisfactory helicopter handling quality. The control problem has been tackled using different approaches ranging from linear quadratic control, feedback linearization, eigenstructure assignment, classical SISO techniques and H_∞ robust control. Apart from the methods emphasised above there are many other techniques are reported for complex modern control system design ranging from sliding mode control, quantitative feedback theory and singular perturbation method. An experimental study conducted to development of a fuzzy set point weighting PID control for the twin rotor MIMO system is discussed.

The extensive studies of the reported controller design methods evidenced that the helicopter control and the control of a helicopter with an external underslung load is still a very active research area. The research in this area is mainly motivated by the

factor: current control methods can not provide the full satisfactory to the desired design requirements on flight handling quality, stability, robustness, etc. Lyapunov stability based deterministic control method used for helicopter control has been recently reported [Mahony *et al,* 1999]. The key advantage of Lyapunov control method is that the controller design takes the system uncertainty into account. The designed controller can give a guaranteed stability region for the systems considered. This method should have potential for solving some problems arising in helicopter control and is worth further investigation. The Next chapter will explore the possible application of the method to the control of a helicopter with an underslung load.

Chapter 6

Nonlinear deterministic control of a helicopter with an underslung load

6.1 Introduction

The interest of designing feedback controller for helicopter by means of nonlinear control strategy is nowadays gained a considerable attention by several researchers (see for example, Avila-Vilchis, *et al,* 2003, Isidori *et al,* 2003). Avila-Vilchis [Avila-Vilchis, *et al,* 2003] presents a nonlinear control strategy for a reduced order model of a helicopter. Due to the complexity of the helicopter model and dynamics, it is very difficult to develop a nonlinear control strategy if a complete nonlinear helicopter model is used. For instance, Isidori [Isidori *et al,* 2003] addressed the problem of controlling the motion of a helicopter described by a nonlinear mathematical model. To simplify the nonlinearity of the dynamics and the strong coupling effects in the model the unavoidability of the simplification of the system model is applied.

In general there are two main approaches for control of uncertain dynamical systems, that is, deterministic and stochastic control. If the uncertainty in the system model is assumed to have statistical characterization and the desired behaviour of the system is described in a statistical sense a stochastic approach is feasible; otherwise, if structural properties and bounding conditions relating to the uncertainties are known, a deterministic approach is appropriate [Wang, 1995]. Deterministic feedback control of uncertain dynamical systems proposes the use of determined linear or nonlinear feedback control functions, which operate effectively over a specified magnitude range of system parameter variations and disturbances, without any on-line identification of the system parameters. Benefit of such an approach is that no statistical information of the system variations is required to yield the desired dynamical behaviour and, hence, the controller may have a simple structure for implementation in practical systems. However the deterministic control design methodology requires the system state vector is available for measurements, and the

bounding knowledge of uncertainties are known, which may put restrictions on the applications of this method.

This chapter describes the work on the development of state feedback control, using deterministic control approach to ensure the stabilisation of the helicopter system and the positioning of the underslung load at hover.

6.2 Introduction to deterministic control of uncertain dynamical systems

In this section deterministic control of uncertain dynamical systems is introduced. The use of deterministic control approach based on Lyapunov techniques have been discussed by Rayn *et al,* 1984, Goodall *et al,* 1988, Qu, 1993, Wang, 1995 and among others. The basic notations and concepts required for the analysis are described in this section.

6.2.1 Basic notations

The state space is denoted by $X := \mathrm{P}^n$ and the control space by $\bar{u} := \mathrm{P}^m$, where $1 \le m \le n$. The Euclidean inner product (on X or $\bar{u}$ as appropriate) and induced norm are denoted by $<.,.>$ and $\|.\|$ respectively. Let $C(\mathrm{P}^p;\mathrm{P}^q)$ and $C^1(\mathrm{P}^p;\mathrm{P}^q)$ denote the space of all continuous functions and, the space of continuous functions with continuous first order partial derivatives respectively, and $C^\infty(\mathrm{P}^p;\mathrm{P}^q)$ denote the space of functions whose partial derivatives of any order exist and are continuous, mapping $\mathrm{P}^p \to \mathrm{P}^q$. For a real-valued continuous scalar function $x \to v(x)$, defined on P^n, $\nabla : \tilde{v} \to \nabla\tilde{v} \in \mathrm{P}^n$ denotes the gradient map. The Lie derivative of v along a vector field $f : \mathrm{P}^n \to \mathrm{P}^n$, is denoted by $L_f\tilde{v} : \mathrm{P}^n \to \mathrm{P}$ is defined by

$$(L_f\tilde{v})(x) = \langle \nabla\tilde{v}(x), f(x) \rangle$$

The Lie bracket of vector fields $f, g \in C^{\infty}(\mathrm{P}^{n}, \mathrm{P}^{n})$ is the vector field $[f, g] \in C^{\infty}(\mathrm{P}^{n}, \mathrm{P}^{n})$ defined by $[f, g] = (Dg)f - (Df)g$, where (Df) denotes the Jacobian matrix of f and (Dg) denotes the Jacobian matrix of g.

In this chapter, nonlinear systems with the following format are considered:

$$\dot{x}(t) = f(x(t)) + G(x(t))\tilde{u}(t) \tag{6.1}$$

where $x(t) \in \mathrm{P}^{n}$, $\tilde{u} \in \mathrm{P}^{m}$. In general mathematical models of dynamical systems are usually imprecise due to modelling errors and exogeneous disturbances [Goodall, 1994], [Goodall, *et al* 2001]. (6.1) can be considered as the nominal part of the system model and the uncertainty can be modelled by as an additive perturbation to the nominal system model, more specifically, the structure of the system has the form:

$$\dot{x}(t) = f(x(t)) + G(x(t))\tilde{u}(t) + \vartheta(x(t), u(t)) \tag{6.2}$$

where $\vartheta(x(t), u(t))$ models the uncertainty in the system.

The system (6.2) is globally asymptotically stable to the zero state if the system exhibits the following properties [e.g.,Goodall, 1994];

(1) Existence and Continuation of solutions:

For each $x \in \mathrm{P}^{n}$, there exists a local solution $x : [0, t_1) \to \mathrm{P}^{n}$ (i.e. an absolutely continuous function satisfying (6.2) almost everywhere (a.e) and $x(0) = x^{0}$) and every such solution can be extended into a solution on $[0, \infty)$.

(ii) Boundedness of solutions:

For each $\hbar > 0$, there exists $r(\hbar) > 0$ such that $x(t) \in r(\hbar)B_n$, for all $t \geq 0$ on every solution $x : [0, \infty) \to \mathrm{P}^{n}$ with $x^{0} \in \hbar B_n$, where B_n denote the open unit ball centred at the origin in P^{n}.

(iii) Stability of the state origin

For each $\delta > 0$, there exists $d(\delta) > 0$ such that $x(t) \in \delta B_n$ for all $t \geq 0$ on every solution $x : [0, \infty) \to \mathrm{P}^{n}$ with $x^{0} \in d(\delta)B_n$

(iv) Global attractivity of the state origin.

For each $\hbar > 0$ and $\varepsilon > 0$, there exists $T(\hbar, \varepsilon) \geq 0$ such that $x(t) \in B_n$ for all $t \geq T(\hbar, \varepsilon)$ on every solution $x : [0, \infty) \to \mathrm{P}^n$ with $x^0 \in \hbar B_n$.

6.2.2 Concept of invariant manifold

Consider a nonlinear system described by the ordinary differential equations below

$$\dot{x}(t) = f(t, x(t)), \tag{6.3}$$
$$x(t_0) = x^0,$$

where $f : \mathrm{P} \times X \to X$ and $f(t, 0) = 0$ for all t. To analyse the stability of (6.3), Lyapunov's second stability analysis method is applicable. The Lyapunov approach is to show that a candidate 'Lyapunov function' is nonincreasing along all solution to (6.3) by means that do not require explicit knowledge of solutions to (6.3). From this, appropriate conclusion can be drawn regarding stability concepts relating to solutions of the differentiate equation (6.3). An essential part of Lyapunov's method is the determination of the time derivative of the candidate 'Lyapunov function' along all solution of the dynamical system.

Consider a Lyapunov candidate $(t, x) \to \tilde{v}(t, x) : \mathrm{P} \times X \to \mathrm{P}$ which satisfies the condition $\tilde{v} \in C^1(\mathrm{P} \times X)$, in which case its time derivative along solutions to (6.3) is given by

$$\dot{v}(t, x(t)) = \frac{\partial \tilde{v}(t, x(t))}{\partial t} + \langle \nabla \tilde{v}(t, x(t)), f(t, x(t)) \rangle$$

for almost all $t \in \mathrm{P}$

Let $W(x(t))$ denote a positive definite function. If $\tilde{v}(t, x(t))$ satisfies

i) $\tilde{v}(t, 0) = 0$ for all $t \geq 0$;

ii) $W(x(t)) \leq \tilde{v}(t, x(t))$ for all $x(t) \in \Phi$, $\{0\} \subset \Phi \subset X$ and all $t \geq 0$;

iii) $\dot{v}(t, x(t)) < 0$ in Φ;

then $\tilde{v}(t, x(t))$ is said to be a Lyapunov function in Φ. If $\dot{\tilde{v}}(t, x(t)) \leq 0$ in Φ, then $\tilde{v}(t, x(t))$ is said to be a weak Lyapunov function.

A set E is said to be an invariant set with respect to the dynamical system $\dot{x} = f(x)$ if

$$x(0) \in \mathrm{E} \mapsto x(t) \in \mathrm{E} \text{ for all } t \in \mathrm{P}^{+}$$

In other words E is the set of points such that if a solution of $\dot{x} = f(x)$ belongs to E at some instant initialized points at $t = 0$, and then it belongs to E for all future time. Further details of the concept of invariant set can be found in Carr [Carr, 1981] and Marquez [Marquez, 2003].

Now, a set $\mathrm{E} \subset x$ is said to be a local invariant manifold for (6.3) if, for any $x^0 \in \mathrm{E}$, $x(t)$ with $x(0) = x^0$ is in E for $|t| < T$ where $T > 0$. If $T = \infty$, then E is said to be an invariant manifold.

6.3 Deterministic control of a helicopter with an underslung load

Considering the control of a helicopter with an underslung load, the dynamical models of both the helicopter and load have some terms which are uncertain. The uncertainties may arise from the helicopter to carry an unknown load or the immeasurable parameters in the dynamical models. The uncertainties may also arise from computational errors of the dynamical effects such as aerodynamics. Therefore for a realistic model uncertainties must be taken into account during the controller design.

6.3.1 Model of the helicopter system

A mathematical model of the helicopter has been described in Chapter 2 and Chapter 4 presented an underslung load model. Considering the two models, a mathematical model for a helicopter carrying an underslung load can be obtained. From Chapters 2 and 4, if the velocities and accelerations of the helicopter are considered as the inputs to the load, the combined system model will have a structure of cascade connection of two subsystems.

Recall the work described in Chapter 4, for the load model, the coordinate system used is described in Figure 6.1. For the case of the longitudinal motion in the X-Z plane, the mathematical model is described below.

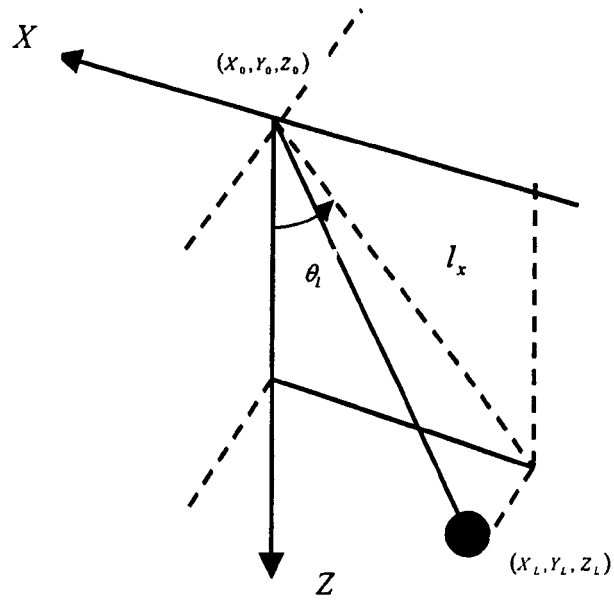

Figure 6.1: Coordinate system for the longitudinal motion in the X-Z plane.

$$\begin{aligned}\ddot{\theta}_L = &-\frac{g}{l_x}\sin\theta_L + \frac{\cos\theta_L}{l_x}\ddot{X}_0 + \frac{\sin\theta_L}{l_x}\ddot{Z}_0 \\ &+ \frac{k_D sign(\dot{X}_L)\cos\theta_L}{M_L l_x}\dot{X}_0^2 + \frac{k_D sign(\dot{Z}_L)\sin\theta_L}{M_L l_x}\dot{Z}_0^2 \\ &- \frac{2k_D}{M_L}\left(sign(\dot{X}_L)\cos^2\theta_L\dot{X}_0 + sign(\dot{Z}_L)\sin^2\theta_L\dot{Z}_0\right)\dot{\theta}_L - k_\theta\dot{\theta}_L \\ &+ \frac{k_D l_x}{M_L}\left[sign(\dot{X}_L)\cos^3\theta_L + sign(\dot{Z}_L)\sin^3\theta_L\right]\dot{\theta}_L^2\end{aligned}$$

Define $\tilde{\theta}_L = \begin{bmatrix}\theta_L & \dot{\theta}_L\end{bmatrix}^T = \begin{bmatrix}\theta_{L1} & \theta_{L2}\end{bmatrix}^T$ then the load model can be rewritten as follows:

$$\dot{\theta}_{L_1} = \theta_{L_2} \tag{6.4a}$$

$$\begin{aligned}\dot{\theta}_{L_2} = &\frac{-g}{l_x}\sin\theta_{L_1} + \frac{k_D l_x}{M_L}[sign(\dot{X}_L)\cos^3\theta_{L_1} + sign(\dot{Z}_L)\sin^3\theta_{L_1}]\theta_{L_2}^2 - k_\theta\theta_{L_2} \\ &+ \left(\frac{k_D sign(\dot{X}_L)\cos\theta_{L_1}}{M_L l_x}\right)\dot{X}_0^2 + \left(\frac{k_D sign(\dot{Z}_L)\sin\theta_{L_1}}{M_L l_x}\right)\dot{Z}_0^2 \\ &+ \frac{\cos\theta_{L_1}}{l_x}\ddot{X}_0 + \frac{\sin\theta_{L_1}}{l_x}\ddot{Z}_0 \\ &- \frac{2k_D}{M_L}\left(sign(\dot{X}_L)\cos^2\theta_{L_1}\dot{X}_0 + sign(\dot{Z}_L)\sin^2\theta_{L_1}\dot{Z}_0\right)\theta_{L_2}\end{aligned} \tag{6.4b}$$

The helicopter model is considered as the second subsystem. To simplify the analysis, we only consider the linear helicopter model which is expressed in the state space form $\dot{\tilde{x}}_H(t) = A\tilde{x}_H(t) + B\bar{u}(t)$. Recall the Equation (2.32) which describes the longitudinal helicopter motion. Whereas, the longitudinal rotational motion is described by the pitch angle θ and pitch rate q . Thus, the following equation represents the longitudinal rotational motion.

$$\dot{q} = \left(M_q q + M_u u + M_w w\right) + M_{\theta_{1s}}\theta_{1s} + M_{\theta_0}\theta_0 \tag{6.5}$$

Thus with the addition of the translation motion components u, w and rearranging the order of the states, the equation of longitudinal motion can be written as follows.

$$\begin{bmatrix} \dot{\theta} \\ \dot{q} \\ \dot{u} \\ \dot{w} \end{bmatrix} = \begin{bmatrix} 0 & 1 & 0 & 0 \\ 0 & M_q & M_u & M_w \\ -g\cos\theta_e & \left(X_q - w_e\right) & X_u & X_w \\ -g\sin\theta_e & \left(Z_q - u_e\right) & Z_u & Z_w \end{bmatrix} \begin{bmatrix} \theta \\ q \\ u \\ w \end{bmatrix} + \begin{bmatrix} 0 & 0 \\ M_{\theta_{1s}} & M_{\theta_0} \\ X_{\theta_{1s}} & X_{\theta_0} \\ Z_{\theta_{1s}} & Z_{\theta_0} \end{bmatrix} \begin{bmatrix} \theta_{1s} \\ \theta_0 \end{bmatrix} \tag{6.6}$$

The forces and moments that the load exerts on the helicopter are neglected. This situation corresponding to the case, where the load mass is much less then the helicopter mass. The moment due to the load is zero because of the assumption that the suspension point is the centre of gravity of the helicopter. This assumption is adopted for the simplicity of the application.

By applying a linear transformation $\bar{T}$ (see appendix B) and $\bar{T}$ is defined by

$$\bar{T} = \begin{bmatrix} 1 & 0 & 0 & 0 \\ 0 & 1 & a_{11} & a_{12} \\ 0 & 0 & 1 & 0 \\ 0 & 0 & 0 & 1 \end{bmatrix}$$

where $a_{11} = -\dfrac{Z_{\theta_{1s}} M_{\theta_0} - Z_{\theta_0} M_{\theta_{1s}}}{X_{\theta_{1s}} Z_{\theta_0} - Z_{\theta_{1s}} X_{\theta_0}}$, and $a_{12} = -\dfrac{X_{\theta_0} M_{\theta_{1s}} - X_{\theta_{1s}} M_{\theta_0}}{X_{\theta_{1s}} Z_{\theta_0} - Z_{\theta_{1s}} X_{\theta_0}}$: Applying the linear transformation $\bar{T}$ and let $\bar{q} = (q - a_{11}u - a_{12}w)$, then the system Equation (6.6) is transformed into the following form

$$\begin{bmatrix} \dot{\theta} \\ \dot{\bar{q}} \\ \dot{u} \\ \dot{w} \end{bmatrix} = \begin{bmatrix} X_{11} & X_{12} & X_{13} & X_{14} \\ X_{21} & X_{22} & X_{23} & X_{24} \\ X_{31} & X_{32} & X_{33} & X_{34} \\ X_{41} & X_{42} & X_{43} & X_{44} \end{bmatrix} \begin{bmatrix} \theta \\ \bar{q} \\ u \\ w \end{bmatrix} + \begin{bmatrix} 0 & 0 \\ B_{21} & B_{22} \\ X_{\theta_{1s}} & X_{\theta_0} \\ Z_{\theta_{1s}} & Z_{\theta_0} \end{bmatrix} \begin{bmatrix} \theta_{1s} \\ \theta_0 \end{bmatrix}, \tag{6.7}$$

where

$$X_{11} = 0, \qquad X_{12} = 1, \qquad X_{13} = a_{11}, \qquad X_{14} = a_{12}$$

$$X_{21} = (a_{11} g \cos\theta_e + a_{12} g \sin\theta_e), \qquad X_{22} = (M_q - a_{11}(X_q - w_e) - a_{12}(Z_q - u_e))$$

$$X_{23} = (M_q - a_{11}(X_q - w_e) - a_{12}(Z_q + u_e))a_{11} + (M_u - a_{11} X_u - a_{12} Z_u)$$

$$X_{24} = (M_q - a_{11}(X_q - w_e) - a_{12}(Z_q + u_e))a_{12} + (M_w - a_{11} X_w - a_{12} Z_w),$$

$$X_{31} = -g\cos\theta_e, \qquad X_{32} = (X_q - w_e), \qquad X_{33} = (X_q - w_e)a_{11} + X_u,$$

$$X_{34} = (X_q - w_e)a_{11} + X_w,$$

$$X_{41} = (-g\sin\theta_e), \qquad X_{42} = (Z_q + u_e), \qquad X_{43} = (Z_q + u_e)a_{11} + Z_u,$$

$$X_{44} = (Z_q + u_e)a_{12} + Z_w,$$

$$B_{21} = (M_{\theta_{1s}} - a_{11} X_{\theta_{1s}} - a_{12} Z_{\theta_{1s}}), \qquad B_{22} = (M_{\theta_0} - a_{11} X_{\theta_0} - a_{11} Z_{\theta_0}).$$

Using the equation (6.7) the system model can be rearranged to include the variables θ and $\bar{q}$ into the load model. For feedback control development purpose, an extra term is introduced into the system model, which is zero with the expression:

$$\frac{\kappa_1 k_D sign(\dot{X}_L)\cos\theta_{L_1} u}{M_L l_x} + \frac{\kappa_2 k_D sign(\dot{X}_L)\cos\theta_{L_1} w}{M_L l_x} - \frac{\kappa_1 k_D sign(\dot{X}_L)\cos\theta_{L_1} u}{M_L l_x} - \frac{\kappa_2 k_D sign(\dot{X}_L)\cos\theta_{L_1} w}{M_L l_x},$$

where $\kappa_i > 0$ $(i = 1, 2)$ are small positive constants.

With this rearrangement, the helicopter with underslung load combined system model can be rewritten as follows:

$$\dot{\bar{\theta}}_L(t) = f_1(\bar{\theta}_L(t)) + G_1(\bar{\theta}_L(t))[p(x_H(t)) + q(\bar{\theta}_L(t), x_H(t))] + H(t, \bar{\theta}_L, x_H(t)) \quad (6.8a)$$

$$\dot{x}_H(t) = f_2(\bar{\theta}_L(t),\ x_H(t)) + G_2\tilde{u}(t) \quad (6.8b)$$

where $\bar{\theta}_L(t) = [\theta_{L_1} \quad \theta_{L_2} \quad \theta \quad \bar{q}]^T$, $x_H = [u \quad w]^T$, $\tilde{u}(t) = [\theta_{1s} \quad \theta_0]^T$

and $p(x_H) = [u^2 + \kappa_1 u \quad w^2 + \kappa_2 w]^T$.

$$f_1(\bar{\theta}_L(t)) = \begin{bmatrix} \theta_{L_2} \\ \dfrac{-g}{l_x}\sin\theta_{L_1} + \dfrac{k_D l_x}{M_L}\left(sign(\dot{X}_L)\cos^3\theta_{L_1} + sign(\dot{Z}_L)\sin^3\theta_{L_1}\right)\theta_{L_2}^2 - k_\theta\theta_{L_2} \\ \bar{q} \\ (X_{21}\theta + X_{22}\bar{q}) \end{bmatrix}$$

$$G_1(\bar{\theta}_L(t)) = \begin{bmatrix} 0 & 0 \\ \dfrac{k_D sign(\dot{X}_L)\cos\theta_{L_1}}{M_L l_x} & \dfrac{k_D sign(\dot{Z}_L)\sin\theta_{L_1}}{M_L l_x} \\ 0 & 0 \\ 0 & 0 \end{bmatrix}$$

$$q\left(\bar{\theta}_L(t), x_H(t)\right)$$

$$= \begin{bmatrix} 0 \\ \frac{\cos\theta_{L_1}}{l_x}\dot{u} + \frac{\sin\theta_{L_1}}{l_x}\dot{w} - \frac{2k_D}{M_L}\left(sign\left(\dot{X}_L\right)\cos^2\theta_{L_1}u + sign\left(\dot{Z}_L\right)\sin^2\theta_{L_1}w\right)\theta_{L_2} - \frac{\kappa_1 k_D sign\left(\dot{X}_L\right)\cos\theta_{L_1}u}{M_L l_x} - \frac{\kappa_2 k_D sign\left(\dot{X}_L\right)\cos\theta_{L_1}w}{M_L l_x} \end{bmatrix}$$

$$H(t,\bar{\theta}_L(t),x_H(t)) = \begin{bmatrix} 0 \\ 0 \\ (a_{11}u + a_{12}w) \\ X_{23}u + X_{24}w \end{bmatrix},$$

$$f_2(\bar{\theta}_L(t),\, x_H(t)) = \begin{bmatrix} (X_{31}\theta + X_{32}\bar{q} + X_{33}u + X_{34}w) \\ (X_{41}\theta + X_{42}\bar{q} + X_{43}u + X_{44}w) \end{bmatrix}, \qquad G_2 = \begin{bmatrix} X_{\theta_{1_s}} & X_{\theta_0} \\ Z_{\theta_{1_s}} & Z_{\theta_0} \end{bmatrix}$$

It is assumed that the longitudinal motion is primarily controlled by longitudinal cyclic commands (θ_{1_s}) and main rotor collective θ_0.

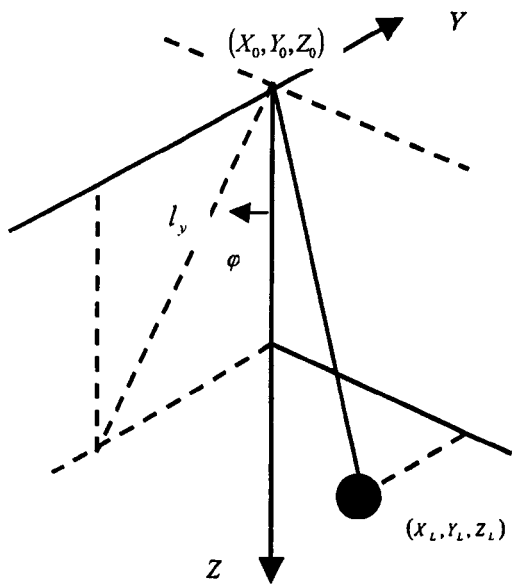

Figure 6.2: Coordinate system for the lateral motion in the Y-Z plane.

For the case of the lateral motion in the Y-Z plane, with the coordinate system described in Figure 6.3, the load model is:

$$\ddot{\varphi}_{L_{yz}} = -\frac{g}{l_y}\sin\varphi_{L_{yz}} + \frac{\cos\varphi_{L_{yz}}}{l_y}\ddot{Y}_0 + \frac{\sin\varphi_{L_{yz}}}{l_y}\ddot{Z}_0$$

$$+\frac{k_D sign(\dot{Y}_L)\cos\varphi_{L_{yz}}}{M_L l_y}\dot{Y}_0^2 + \frac{k_D sign(\dot{Z}_L)\sin\varphi_{L_{yz}}}{M_L l_y}\dot{Z}_0^2$$

$$-\frac{2k_D}{M_L}\left(sign(\dot{Y}_L)\cos^2\varphi_{L_{yz}}\dot{Y}_0 + sign(\dot{Z}_L)\sin^2\varphi_{L_{yz}}\dot{Z}_0\right)\dot{\varphi}_L - k_\varphi\dot{\varphi}_L$$

$$+\frac{k_D l_y}{M_L}\left[sign(\dot{Y}_L)\cos^3\varphi_{L_{yz}} + sign(\dot{Z}_L)\sin^3\varphi_{L_{yz}}\right]\dot{\varphi}_{L_{yz}}^2$$

Define $\tilde{\varphi}_L = [\varphi_L \quad \dot{\varphi}_L]^T = [\varphi_{L_1} \quad \varphi_{L_2}]^T$ then the model can be written as follows:

$$\dot{\varphi}_{L_1} = \varphi_{L_2} \tag{6.9a}$$

$$\dot{\varphi}_{L_2} = \frac{-g}{l_y}\sin\varphi_{L_1} + \frac{k_D l_y}{M_L}\left[sign(\dot{Y}_L)\cos^3\varphi_{L_1} + sign(\dot{Z}_L)\sin^3\varphi_{L_1}\right]\varphi_{L_2}^2 - k_\varphi\varphi_{L_2}$$

$$+\left(\frac{k_D sign(\dot{Y}_L)\cos\varphi_{L_1}}{M_L l_y}\right)\dot{Y}_0^2 + \left(\frac{k_D sign(\dot{Z}_L)\sin\varphi_{L_1}}{M_L l_y}\right)\dot{Z}_0^2$$

$$+\frac{\cos\varphi_{L_1}}{l_y}\ddot{Y}_0 + \frac{\sin\varphi_{L_1}}{l_y}\ddot{Z}_0$$

$$-\frac{2k_D}{M_L}\left(sign(\dot{Y}_L)\cos^2\varphi_{L_1}\dot{Y}_0 + sign(\dot{Z}_L)\sin^2\varphi_{L_1}\dot{Z}_0\right)\varphi_{L_2} \tag{6.9b}$$

For the lateral motion of helicopter model recall the equation (2.33) which describes the lateral helicopter motion. Whereas the lateral rotational motion can be describe by the following equation.

$$\dot{p} = \left(L_p p + L_v v + L_w w\right) + L_{\theta_{1c}}\theta_{1c} + L_{\theta_{0T}}\theta_{0T} \tag{6.10}$$

Thus the model for lateral motion can be rewritten as follows:

$$\begin{bmatrix}\dot{\phi}\\ \dot{p}\\ \dot{v}\\ \dot{w}\end{bmatrix} = \begin{bmatrix}0 & 1 & 0 & 0\\ 0 & L_p & L_v & L_w\\ g & (Y_p - w_e) & Y_v & Y_w\\ 0 & (Z_p - v_e) & Z_v & Z_w\end{bmatrix}\begin{bmatrix}\phi\\ p\\ v\\ w\end{bmatrix} + \begin{bmatrix}0 & 0\\ L_{\theta_{1c}} & L_{\theta_{0T}}\\ Y_{\theta_{1c}} & Y_{\theta_{0T}}\\ Z_{\theta_{1c}} & Z_{\theta_{0T}}\end{bmatrix}\begin{bmatrix}\theta_{1c}\\ \theta_{0T}\end{bmatrix} \tag{6.11}$$

now using a linear transformation $\bar{T}_1$ such that $x_H(t) = \bar{T}_1 z(t)$ and $\bar{T}_1$ is defined by

$$\bar{T}_1 = \begin{bmatrix} 1 & 0 & 0 & 0 \\ 0 & 1 & b_{11} & b_{12} \\ 0 & 0 & 1 & 0 \\ 0 & 0 & 0 & 1 \end{bmatrix},$$

where $b_{11} = -\dfrac{Z_{\theta_{1c}} L_{\theta_{0T}} - Z_{\theta_{0T}} L_{\theta_{1c}}}{Y_{\theta_{1c}} Z_{\theta_{0T}} - Z_{\theta_{1c}} Y_{\theta_{0T}}}$ and $b_{12} = -\dfrac{Y_{\theta_{0T}} L_{\theta_{1c}} - Y_{\theta_{1c}} L_{\theta_{0T}}}{Y_{\theta_{1c}} Z_{\theta_{0T}} - Z_{\theta_{1c}} Y_{\theta_{0T}}}$.

Let $\bar{p} = (p - b_{11}v - b_{12}w)$ then the equation (6.11) can be written in the following form

$$\begin{bmatrix} \dot{\phi} \\ \dot{\bar{p}} \\ \dot{v} \\ \dot{w} \end{bmatrix} = \begin{bmatrix} Y_{11} & Y_{12} & Y_{13} & Y_{14} \\ Y_{21} & Y_{22} & Y_{23} & Y_{24} \\ Y_{31} & Y_{32} & Y_{33} & Y_{34} \\ Y_{41} & Y_{42} & Y_{43} & Y_{44} \end{bmatrix} \begin{bmatrix} \phi \\ \bar{p} \\ v \\ w \end{bmatrix} + \begin{bmatrix} 0 & 0 \\ N_{21} & N_{22} \\ Y_{\theta_{1c}} & Y_{\theta_{0T}} \\ Z_{\theta_{1c}} & Z_{\theta_{0T}} \end{bmatrix} \begin{bmatrix} \theta_{1c} \\ \theta_{0T} \end{bmatrix} \tag{6.12}$$

where

$$Y_{11} = 0, \qquad Y_{12} = 1, \qquad Y_{13} = b_{11}, \qquad Y_{14} = b_{12},$$

$$Y_{21} = -(b_{11} g), \qquad Y_{22} = \left(L_p - b_{11}\left(Y_p + w_e\right) - b_{12}\left(Z_p - v_e\right)\right),$$
$$Y_{23} = \left(L_p - b_{11}\left(Y_p + w_e\right) - b_{12}\left(Z_p - v_e\right)\right)b_{11} + \left(L_p - b_{11} Y_v - b_{12} Z_v\right),$$
$$Y_{24} = \left(L_p - b_{11}\left(Y_p + w_e\right) - b_{12}\left(Z_p - v_e\right)\right)b_{12} + \left(L_p - b_{11} Y_w - b_{12} Z_w\right),$$

$$Y_{31} = g, \qquad Y_{32} = \left(Y_p + w_e\right), \qquad Y_{33} = \left(\left(Y_p + w_e\right)b_{11} + Y_v\right),$$
$$Y_{34} = \left(\left(Y_p + w_e\right)b_{12} + Y_w\right),$$

$$Y_{41} = 0, \qquad Y_{42} = \left(Z_p - v_e\right), \qquad Y_{43} = \left(\left(Z_p - v_e\right)b_{11} + Z_v\right),$$
$$Y_{44} = \left(\left(Z_p - v_e\right)b_{12} + Z_w\right),$$

$$N_{21} = \left(L_{\theta_{1c}} - b_{11} Y_{\theta_{1c}} - b_{12} Z_{\theta_{1c}}\right), \qquad N_{22} = \left(L_{\theta_{0T}} - b_{11} Y_{\theta_{0T}} - b_{12} Z_{\theta_{0T}}\right).$$

Using the equation (6.12) the helicopter with underslung load for lateral motion in the Y-Z plane can be described by

$$\dot{\bar{\varphi}}_L(t) = f_1(\bar{\varphi}_L(t)) + G_1(\bar{\varphi}_L(t))[p(x_H(t)) + q(\bar{\varphi}_L(t), x_H(t))] + H(t, \bar{\varphi}_L, x_H(t)) \quad (6.13a)$$

$$\dot{x}_H(t) = f_2(\bar{\varphi}_L(t), x_H(t)) + G_2\hat{u}(t) \quad (6.13b)$$

where

$$\dot{\bar{\varphi}}_L(t) = [\dot{\varphi}_{L_1} \;\; \dot{\varphi}_{L_2} \;\; \dot{\phi} \;\; \dot{\bar{p}}]^T, \qquad p(x_H(t)) = [v^2 \;\; w^2]^T$$

$$f_1(\bar{\varphi}_L(t)) = \begin{bmatrix} \varphi_{L_2} \\ \dfrac{-g}{l_y}\sin\varphi_{L_1} + \dfrac{k_D l_y}{M_L}\left(sign(\dot{Y}_L)\cos^3\varphi_{L_1} + \sin(\dot{Z}_L)\sin^3\varphi_{L_1}\right)\varphi_{L_2}^2 - k_\varphi\varphi_{L_2} \\ \bar{p} \\ \left(-b_{11}g\phi + (L_p - b_{11}(Y_p + w_e) - b_{12}(Z_p - v_e))\bar{p}\right) \end{bmatrix}$$

$$G_1(\bar{\varphi}_L(t)) = \begin{bmatrix} 0 & 0 \\ \left(\dfrac{k_D sign(\dot{Z}_L)\cos\varphi_{L_1}}{M_L l_y}\right) & \left(\dfrac{k_D sign(\dot{Z}_L)\sin\varphi_{L_1}}{M_L l_y}\right) \\ 0 & 0 \\ 0 & 0 \end{bmatrix}$$

$$q(\bar{\varphi}_L(t), x_H(t)) = \begin{bmatrix} 0 \\ \dfrac{\cos\varphi_{L_1}}{l_y}\dot{v} + \dfrac{\sin\varphi_{L_1}}{l_y}\dot{w} - \dfrac{2k_D}{M_L}\left(sign(\dot{Y}_L)\cos^2\varphi_{L_1}v + sign(\dot{Z}_L)\sin^2\varphi_{L_1}w\right)\varphi_{L_2} \end{bmatrix}$$

$$H(t, \bar{\varphi}_L(t), x_H(t)) = \begin{bmatrix} 0 \\ 0 \\ (\dot{\phi} - \bar{p}) \\ (Y_{23}v + Y_{24}w) \end{bmatrix}$$

and

$$, \qquad \hat{u}(t) = [\theta_{1c} \quad \theta_{0T}]^T$$

$$f_2(\bar{\varphi}_L(t), x_H(t)) = \begin{bmatrix} (Y_{31}\phi + Y_{32}\bar{p} + Y_{33}v + Y_{34}w) \\ (Y_{42}\bar{p} + Y_{43}v + Y_{44}w) \end{bmatrix}, \qquad G_2 = \begin{bmatrix} Y_{\theta_{1c}} & Y_{\theta_{0T}} \\ Z_{\theta_{1c}} & Z_{\theta_{0T}} \end{bmatrix}$$

It is assumed that the lateral motion is primarily controlled by lateral cyclic commands (θ_{1c}) and the tail rotor collective θ_{0T}.

6.3.2 Analysis of the first subsystem

The goal is to develop a nonlinear deterministic control law for the helicopter with underslung load modelled by equations (6.8) ~ (6.13). The analysis for the longitudinal motion is discussed first. The system equations can be considered to have two main parts, that is, known and unknown (or partly known). The known terms formed the nominal part of the system model. The unknown or partly known part can be considered as the uncertainty to the system. The whole system is then modelled by a nominal part with the addition of uncertainty. In fact, the known elements in the subsystem (6.8a) are characterised by the prescribed triple (f_1, G_1, p) and it is desired that the nominal part of the system is stable.

To analyse the nominal part of the system, Lyapunov Second method is applied. Choose a Lyapunov function candidate for the first subsystem v_1 as

$$v_1(\bar{\theta}_L) = \frac{1}{2}\left[\varsigma_1\theta_{L_1}^2 + \varsigma_2\theta_{L_2}^2 + (\varsigma_3\theta - \varsigma_4\bar{q})^2 + \varsigma_5\bar{q}^2\right], \tag{6.14}$$

where ς_i $(i = 1, 2, 3, 4, 5)$ are design parameters to be determined. Then

$$\begin{aligned} \dot{v}_1(\bar{\theta}_L) &= \left\langle \nabla v_1(\bar{\theta}_L),\ f_1(\bar{\theta}_L) + G_1(\bar{\theta}_L(t))\left[p(x_H(t)) + q(\bar{\theta}_L(t), x_H(t))\right] + H(t, \bar{\theta}_L, x_H(t)) \right\rangle \\ &= (L_{f_1}v_1)(\bar{\theta}_L) + \left\langle \nabla v_1(\bar{\theta}_L)\, G_1(\bar{\theta}_L(t))\left[p(x_H(t)) + q(\bar{\theta}_L(t), x_H(t))\right] + H(t, \bar{\theta}_L, x_H(t)) \right\rangle \end{aligned}$$

From (6.14), $\nabla v_1(\bar{\theta}_L)$ can be obtained as

$$\nabla v_1(\bar{\theta}_L) = \left[\varsigma_1\theta_{L_1} \quad \varsigma_2\theta_{L_2} \quad \varsigma_3(\varsigma_3\theta - \varsigma_4\bar{q}) \quad -\varsigma_4(\varsigma_3\theta - \varsigma_4\bar{q}) + \varsigma_5\bar{q}\right]^T.$$

Substituting $\nabla v_1(\bar{\theta}_L)$ and $f_1(\bar{\theta}_L)$ into the derivative of $(L_{f_1}v_1)(\bar{\theta}_L)$, we have

$$
\begin{aligned}
&(L_{f_1} v_1)(\bar{\theta}_L) \\
&= \varsigma_1 \theta_{L_1} \theta_{L_2} - k_\theta \varsigma_2 \theta_{L_2}^2 - \varsigma_2 \frac{g}{l_x} \sin \theta_{L_1} \theta_{L_2} + \frac{k_D l_x}{M_L} \varsigma_2 \left[sign(\dot{X}_L) \cos^3 \theta_{L_1} + sign(\dot{Z}_L) \sin^3 \theta_{L_1} \right] \theta_{L_2}^3 \\
&\quad + \varsigma_3 \left[\varsigma_3 \theta - \varsigma_4 \bar{q} \right] \bar{q} + \left(-\varsigma_3 \varsigma_4 \theta + (\varsigma_4^2 + \varsigma_5) \bar{q} \right) \left[X_{21} \theta + X_{22} \bar{q} \right]
\end{aligned}
$$

Checking the term of $-\sin(\theta_{L_1})\theta_{L_2}$, it can be seen that $-\sin(\theta_{L_1})\theta_{L_2} \le -\frac{2}{\pi}\theta_{L_1}\theta_{L_2}$ when θ_{L_1} and θ_{L2} are both positive or negative. The situation of θ_{L_1} and θ_{L2} having different signs will help with the system stability. Then,

$$
\begin{aligned}
&(L_{f_1} v_1)(\bar{\theta}_L) \\
&\le \varsigma_1 \theta_{L_1} \theta_{L_2} - k_\theta \varsigma_2 \theta_{L_2}^2 - \varsigma_2 \frac{g}{l_x} \frac{2}{\pi} \theta_{L_1} \theta_{L_2} + \frac{k_D l_x}{M_L} \varsigma_2 \left[sign(\dot{X}_L) \cos^3 \theta_{L_1} + sign(\dot{Z}_L) \sin^3 \theta_{L_1} \right] \theta_{L_2}^3 \\
&\quad + \varsigma_3 \left[\varsigma_3 \theta - \varsigma_4 \bar{q} \right] \bar{q} + \left(-\varsigma_3 \varsigma_4 \theta + (\varsigma_4^2 + \varsigma_5) \bar{q} \right) \left[X_{21} \theta + X_{22} \bar{q} \right]
\end{aligned}
$$

If the design parameter ς_1 is chosen as $\varsigma_1 = \frac{2g}{l_x \pi} \varsigma_2$, $(L_{f_1} v_1)(\bar{\theta}_L)$ satisfies the following

$$
\begin{aligned}
&(L_{f_1} v_1)(\bar{\theta}_L) \\
&\le -k_\theta \varsigma_2 \theta_{L_2}^2 + \frac{k_D l_x}{M_L} \varsigma_2 \left[sign(\dot{X}_L) \cos^3 \theta_{L_1} + sign(\dot{Z}_L) \sin^3 \theta_{L_1} \right] \theta_{L_2}^3 \\
&\quad + \varsigma_3 \left[\varsigma_3 \theta - \varsigma_4 \bar{q} \right] \bar{q} + \left(-\varsigma_3 \varsigma_4 \theta + (\varsigma_4^2 + \varsigma_5) \bar{q} \right) \left[X_{21} \theta + X_{22} \bar{q} \right]
\end{aligned} \tag{6.15}
$$

Further analysis on (6.15) will start from examining the first two terms. Rewrite these two terms, we have

$$
\begin{aligned}
&-k_\theta \varsigma_2 \theta_{L_2}^2 + \frac{k_D l_x}{M_L} \varsigma_2 \left[sign(\dot{X}_L) \cos^3 \theta_{L_1} + sign(\dot{Z}_L) \sin^3 \theta_{L_1} \right] \theta_{L_2}^3 \\
&= -k_\theta \varsigma_2 \theta_{L_2}^2 + \frac{k_D l_x}{M_L} \varsigma_2 \theta_{L_2} \left[sign(\dot{X}_L) \cos^3 \theta_{L_1} + sign(\dot{Z}_L) \sin^3 \theta_{L_1} \right] \theta_{L_2}^2 \\
&\le -k_\theta \varsigma_2 \theta_{L_2}^2 + \frac{k_D l_x}{M_L} \varsigma_2 \left| \max(\theta_{L_2}) \right| \left(sign(\dot{X}_L) \cos^3 \theta_{L_1} + sign(\dot{Z}_L) \sin^3 \theta_{L_1} \right) \theta_{L_2}^2 \\
&= -\varsigma_2 \theta_{L_2}^2 \left\{ k_\theta - \frac{k_D l_x}{M_L} \left| \max(\theta_{L_2}) \right| \left(sign(\dot{X}_L) \cos^3 \theta_{L_1} + sign(\dot{Z}_L) \sin^3 \theta_{L_1} \right) \right\}
\end{aligned}
$$

If the hinge friction is big enough to satisfy the following

$$k_\theta > \frac{k_D l_x}{M_L}\left|\max(\theta_{L_2})\left(sign(\dot{X}_L)\cos^3\theta_{L_1} + sign(\dot{Z}_L)\sin^3\theta_{L_1}\right)\right| \qquad (6.16)$$

then

$$\lambda_L = \left\{k_\theta - \frac{k_D l_x}{M_L}\left|\max(\theta_{L_2})\left(sign(\dot{X}_L)\cos^3\theta_{L_1} + sign(\dot{Z}_L)\sin^3\theta_{L_1}\right)\right|\right\} \geq 0$$

$$\text{and } -k_\theta \varsigma_2 \theta_{L_2}^2 + \frac{k_D l_x}{M_L}\varsigma_2\left[sign(\dot{X}_L)\cos^3\theta_{L_1} + sign(\dot{Z}_L)\sin^3\theta_{L_1}\right]\theta_{L_2}^3 \leq -\varsigma_2\theta_{L_2}^2\lambda_L,$$

On the other hand, the following analysis has been conducted for (6.15). form Chapter 4, the load movement for the longitudinal motion is described by

$$\dot{X}_L = \dot{X}_0 - l_x\theta_{L_2}\cos\theta_{L_1}$$

$$\dot{Z}_L = \dot{Z}_0 - l_x\theta_{L_2}\sin\theta_{L_1}$$

Around the hover condition $X_0 = 0$ and $Z_0 = 0$, then the signs for $\dot{X}_L$ and $\dot{Z}_L$ are opposite to the one of θ_{L_2} provided that θ_{L_1} is positive. Considering the term $\left(sign(\dot{X}_L)\cos^3\theta_{L_1} + sign(\dot{Z}_L)\sin^3\theta_{L_1}\right)\theta_{L_2}^3$ for all possible combinations of the signs of θ_{L_2} and θ_{L_1}, the analysis follows below:

(i) If $\theta_{L_1} > 0$ and $\theta_{L_2} > 0$ then $sign(\dot{X}_L) = -1$, $sign(\dot{Z}_L) = -1$, $\cos^3\theta_{L_1} > 0$, and $\sin^3\theta_{L_1} > 0$. Therefore, we have

$$\left(sign(\dot{X}_L)\cos^3\theta_{L_1} + sign(\dot{Z}_L)\sin^3\theta_{L_1}\right)\theta_{L_2}^3 < 0.$$

(ii) If $\theta_{L_1} < 0$ and $\theta_{L_2} > 0$ then $sign(\dot{X}_L) = -1$, $sign(\dot{Z}_L) = +1$, $\cos^3\theta_{L_1} > 0$ and $\sin^3\theta_{L_1} < 0$. So we have

$$\left(sign(\dot{X}_L)\cos^3\theta_{L_1} + sign(\dot{Z}_L)\sin^3\theta_{L_1}\right)\theta_{L_2}^3 < 0.$$

(iii) If $\theta_{L_1} > 0$ and $\theta_{L_2} < 0$ then $sign(\dot{X}_L) = +1$ and $sign(\dot{Z}_L) = +1$, $\cos^3\theta_{L_1} > 0$, and $\sin^3\theta_{L_1} > 0$. So the following is true

$$\left(sign(\dot{X}_L)\cos^3\theta_{L_1} + sign(\dot{Z}_L)\sin^3\theta_{L_1}\right)\theta_{L_2}^3 < 0.$$

(iv) If $\theta_{L_1} < 0$ and $\theta_{L_2} < 0$ then $sign(\dot{X}_L) = +1$ and $sign(\dot{Z}_L) = -1$, $\cos^3\theta_{L_1} > 0$, and $\sin^3\theta_{L_1} < 0$. So

$$\left(sign(\dot{X}_L)\cos^3\theta_{L_1} + sign(\dot{Z}_L)\sin^3\theta_{L_1}\right)\theta_{L_2}^3 < 0.$$

Therefore

$$-k_\theta \varsigma_2 \theta_{L_2}^2 + \frac{k_D l_x}{M_L}\varsigma_2\left[sign(\dot{X}_L)\cos^3\theta_{L_1} + sign(\dot{Z}_L)\sin^3\theta_{L_1}\right]\theta_{L_2}^3 \le -k_\theta \varsigma_2 \theta_{L_2}^2 .$$

Now examining the rest terms of $(L_{f_1} v_1)(\bar{\theta}_L)$ then

$$\varsigma_3[\varsigma_3\theta - \varsigma_4\bar{q}]\bar{q} + \left(-\varsigma_3\varsigma_4\theta + (\varsigma_4^2 + \varsigma_5)\bar{q}\right)[X_{21}\theta + X_{22}\bar{q}]$$

$$\begin{aligned} &= \varsigma_3^2\theta\bar{q} - \varsigma_3\varsigma_4\bar{q}^2 - \varsigma_3\varsigma_4 X_{21}\theta^2 - \varsigma_3\varsigma_4 X_{22}\theta\bar{q} \\ &\quad + (\varsigma_4^2 + \varsigma_5)X_{21}\theta\bar{q} + (\varsigma_4^2 + \varsigma_5)X_{22}\bar{q}^2 \\ &= -[\varsigma_3\varsigma_4 - (\varsigma_4^2 + \varsigma_5)X_{21}]\bar{q}^2 - \varsigma_3\varsigma_4 X_{21}\theta^2 + [\varsigma_3^2 - \varsigma_3\varsigma_4 X_{22} + (\varsigma_4^2 + \varsigma_5)X_{21}]\theta\bar{q} \end{aligned} \tag{6.17}$$

For the system, θ and θ_{L_1} always have different signs, θ and $\bar{q}$ always have different signs, and $\bar{q}$ and θ_{L_1} have the same signs. So

$$[\varsigma_3^2 - \varsigma_3\varsigma_4 X_{22} + (\varsigma_4^2 + \varsigma_5)X_{21}]\theta\bar{q} \le 0$$

if $$[\varsigma_3^2 - \varsigma_3\varsigma_4 X_{22} + (\varsigma_4^2 + \varsigma_5)X_{21}] \ge 0. \tag{6.18}$$

Therefore

$$\begin{aligned} &\varsigma_3[\varsigma_3\theta - \varsigma_4\bar{q}]\bar{q} + \left(-\varsigma_3\varsigma_4\theta + (\varsigma_4^2 + \varsigma_5)\bar{q}\right)[X_{21}\theta + X_{22}\bar{q}] \\ &\le -[\varsigma_3\varsigma_4 - (\varsigma_4^2 + \varsigma_5)X_{21}]\bar{q}^2 - \varsigma_3\varsigma_4 X_{21}\theta^2 \end{aligned}$$

Choose the design parameters to satisfy

$$[\varsigma_3\varsigma_4 - (\varsigma_4^2 + \varsigma_5)X_{21}] > 0. \tag{6.19}$$

If $X_{21} > 0$, then

$$-[\varsigma_3\varsigma_4 - (\varsigma_4^2 + \varsigma_5)X_{21}]\bar{q}^2 - \varsigma_3\varsigma_4 X_{21}\theta^2 < 0.$$

If $X_{21} < 0$, then

$$-[\varsigma_3\varsigma_4 - (\varsigma_4^2 + \varsigma_5)X_{21}]\bar{q}^2 - \varsigma_3\varsigma_4 X_{21}\theta^2 < 0 \tag{6.20}$$

in the region of $-[\varsigma_3\varsigma_4 - (\varsigma_4^2 + \varsigma_5)X_{21}]\bar{q}^2 < \varsigma_3\varsigma_4 X_{21}\theta^2$. Since θ is caused by the load motion here the value of θ should be much smaller than $\bar{q}$. The inequality (6.20) is easy to be satisfied.

In summary of the above analysis and by defining

$$\Psi_1(\bar{\theta}_L) = k_\theta \varsigma_2 \theta_{L_2}^2 + [\varsigma_3\varsigma_4 - (\varsigma_4^2 + \varsigma_5)X_{21}]\bar{q}^2 + \varsigma_3\varsigma_4 X_{21}\theta^2$$

and

$$\Psi_2(\bar{\theta}_L) = [\varsigma_3\varsigma_4 - (\varsigma_4^2 + \varsigma_5)X_{21}]\bar{q}^2 + \varsigma_3\varsigma_4 X_{21}\theta^2,$$

the following Lemma can be derived

Lemma 6.1. *Defining a Lyapunov function* (6.14) *and choosing the design parameters to satisfy* $\varsigma_1 = \dfrac{2g}{l_x\pi}\varsigma_2$, $[\varsigma_3\varsigma_4 - (\varsigma_4^2 + \varsigma_5)X_{21}] > 0$, *and*

$[\varsigma_3^2 - \varsigma_3\varsigma_4 X_{22} + (\varsigma_4^2 + \varsigma_5)X_{21}] \geq 0$, *then within the region specified by*

$-[\varsigma_3\varsigma_4 - (\varsigma_4^2 + \varsigma_5)X_{21}]\bar{q}^2 < \varsigma_3\varsigma_4 X_{21}\theta^2$

(i) $v_1(0) = 0$ *and* $v_1(\bar{\theta}_L) > 0$, $\forall \bar{\theta}_L \neq 0$

(ii) $v_1(\bar{\theta}_L) \to \infty$ *as* $\|\bar{\theta}_L\| \to \infty$

(iii) $(L_{f_1}v_1)(\bar{\theta}_L) \leq -\Psi_1(\bar{\theta}_L)$, $\forall \bar{\theta}_L$ *around the hover condition*

or $(L_{f_1}v_1)(\bar{\theta}_L) \leq -\Psi_2(\bar{\theta}_L)$, $\forall \bar{\theta}_L$ *if* (6.16) *holds.*

Both functions Ψ_1 and Ψ_2 are non-negative.

Recall the control term $p(x_H(t))$ in the first subsystem of (6.8), it can be seen that $[(Dp)(x_H)]^{-1}$ exists for all $x_H(t)$.

The unknown vector fields, $q(\bar{\theta}_L(t), x_H)$ and $H(t, \bar{\theta}_L(t), x_H)$, model the uncertainties imposed onto the system. Since $q(\bar{\theta}_L(t), x_H)$ is directly mapped into the "control" space of $x_H(t)$ it can be considered as a matched uncertainty [Goodall, *et al* 2001]. $H(t, \bar{\theta}_L(t), x_H)$ is unknown and it does belong to the control space of $x_H(t)$ so it represents the mismatched uncertainty in the system [Goodall, *et al* 2001].

Generally, the range of the (longitudinal) load suspension angle is within $-\frac{\pi}{2} < \theta_L < \frac{\pi}{2}$. The helicopter velocities and load suspension angle have maximum operational values, therefore the uncertainties in the system are bounded. With the Lyapunov function defined in (6.14),

$$(L_{g_1} v_1)(\bar{\theta}_L) = \langle \nabla v_1(\bar{\theta}_L)\, g_1 \rangle = \frac{k_D}{M_L l_x} \varsigma_2 \theta_{L_2}.$$

In $G_1(\bar{\theta}_L)$ the column g_1 and g_2 are same, therefore

$$(L_{g_2} v_1)(\bar{\theta}_L) = \frac{k_D}{M_L l_x} \varsigma_2 \theta_{L_2}.$$

By considering the maximum values of cos(.) and sin(.) functions, the bounding values relating to the uncertainty $q(\bar{\theta}_L(t), x_H)$ can be estimated as follows:

$$\begin{aligned}
\left\| q(\bar{\theta}_L, x_H) \right\| &\le \left| \frac{1}{l_x}(\dot{u} + \dot{w}) + \frac{1}{M_L}\left(-k_D(2 + \frac{\kappa}{l_x})(u + w) + \frac{k_\theta}{l_x} \right) \bar{\theta}_{L_2} \right| \\
&\le \left| \frac{k_\theta}{l_x} \theta_{L_2} \right| + \left| \frac{k_D}{M_L}(2 + \frac{\kappa}{l_x})(u + w) \right| + \left| \frac{1}{l_x}(\dot{u} + \dot{w}) \right| \\
&\le \frac{k_\theta}{l_x} \left\| \theta_{L_2} \right\| + \frac{k_D}{M_L}(2 + \frac{\kappa}{l_x}) \left\| p(x_H) \right\| + \alpha_2(t) \\
&\le \mu_1 \left| (L_{g_2} v_1)(\bar{\theta}_L) \right| + \alpha_1 \left\| p(x_H) \right\| + \alpha_2(t) \qquad (6.21)
\end{aligned}$$

where $\mu_1 = \frac{M_L k_\theta}{k_D}$, $\alpha_1 = \frac{k_D}{M_L}(2 + \frac{\kappa}{l_x})$ ($\kappa = \max[\kappa_1 \quad \kappa_2]$) and $\alpha_2(t)$ is defined by $\alpha_2(t) = \max \left| \frac{1}{l_x}(\dot{u} + \dot{w}) \right| > 0$.

For the mismatched uncertainty $H(t,\bar{\theta}_L(t),x_H)$ the following analysis are conducted to obtain its bounding function. The mismatched uncertainty can be rewritten as

$$H(t,\bar{\theta}_L(t),x_H)=\begin{bmatrix}0\\0\\(a_{11}u+a_{12}w)\\(X_{23}u+X_{24}w)\end{bmatrix}=\begin{bmatrix}0&0\\0&0\\a_{11}&a_{12}\\X_{23}&X_{24}\end{bmatrix}\begin{bmatrix}u\\w\end{bmatrix}.$$

Let $\bar{A}=\begin{bmatrix}a_{11}&a_{12}\\X_{23}&X_{24}\end{bmatrix}$ then

$$\|H(t,\bar{\theta}_L,x_H)\|\le\|\bar{A}\|\|x_H(t)\| \tag{6.22}$$

With the Lyapunov function defined in (6.14),

$$(L_{g_1}v_1)(\bar{\theta}_L)=\langle\nabla v_1(\bar{\theta}_L)\,g_1\rangle=\frac{k_D}{M_L l_x}\varsigma_2\theta_{L_2}$$

In $G_1(\bar{\theta}_L)$ the column g_1 and g_2 are same, therefore

$$(L_{g_2}v_1)(\bar{\theta}_L)=\frac{k_D}{M_L l_x}\varsigma_2\theta_{L_2}$$

Define a positive function as

$$\hat{\theta}(\bar{\theta}_L)=\sqrt{(\theta_{L_1}^2+\theta_{L_2}^2+\theta^2+\bar{q}^2+\bar{\varepsilon})}$$

where $\bar{\varepsilon}$ is a very small positive constant. Choosing $\beta_1=\frac{M_L l_x}{k_D\varsigma_2}\|\bar{A}\|$ then the mismatched uncertainty $H(t,\bar{\theta}_L(t),x_H)$ is bouneded by the following inequality:

$$\|H(t,\bar{\theta}_L,x_H)\|\le\hat{\theta}^{-1}(\bar{\theta}_L)\beta_1\sum_{i=1}^{2}(|(L_{g_i}v_1)(\bar{\theta}_L)|)|p_i(x_H)| \tag{6.23}$$

where g_i denotes the i th column of the matrix function $G_1(\bar{\theta}_L)$ and p_i is the i th component of $p(x_H)$ respectively. As β_1 has a design parameter ς_2 involved it is easy to have β_1 to lead (6.23) to be true. For the matched uncertainty, we have

$$\|q(\bar{\theta}_L,x_H)\|\le\frac{k_\theta}{l_x}|\theta_{L_2}|+\alpha_1\|p(x_H)\|+\alpha_2(t),$$

where $\mu_1 = \frac{k_\theta M_L}{k_D \varsigma_2}$. Following above analysis, the following lemma can be derived:

Lemma 6.2. *The uncertainties are bounded and satisfy*

$$\left\| q(\bar{\theta}_L, x_H) \right\| \le \frac{k_\theta}{l_x} \left| \theta_{L_2} \right| + \alpha_1 \left\| p(x_H) \right\| + \alpha_2(t) \tag{6.21}$$

and $\left\| H(t, \bar{\theta}_L, x_H) \right\| \le \hat{\theta}^{-1}(\bar{\theta}_L) \beta_1 \sum_{i=1}^{2} \left(\left| (L_{g_i} v_1) \bar{\theta}_L \right| \right) \left| p_i(x_H) \right|$. (6.23)

For the feedback control design in the later part of the section, it is expected that the constants satisfy $\alpha_1, \beta_1 \ge 0$ and $\alpha_1 + \beta_1 < 1$, for $\alpha_1 = \frac{k_D}{M_L}(2 + \frac{\kappa}{l_x})$ and $\beta_1 = \frac{M_L l_x}{k_D \varsigma_2} \left\| \bar{A} \right\|$. The desired condition $\alpha_1 + \beta_1 < 1$ can be verified by considering a typical case that the UH-60 helicopter carrying a load weight $1000\,lb$ by a $15\,ft$ sling length and let $k_D = 75\,lb/ft$. For the UH-60 helicopter model, with reference to the general mathematical model presented in Chapter 2, we have $X_{\theta_1} = 0.5734$, $X_{\theta_0} = 0.3170$, $Z_{\theta_{1s}} = 0.0237$, $Z_{\theta_0} = -6.0740$, $M_{\theta_{1s}} = -0.1097$, and $M_{\theta_0} = 0.0553$. So the following parameters can be calculated to have the values $a_{11} = -0.2$ and $a_{12} = -0.02$. For $X_u = -0.0195$, $Z_u = 0.0150$, $M_u = 0.0029$, $M_q = -1.4255$, $(X_q - w_e) = 5.7076$, $(Z_q + u_e) = 0.6307$, we have $X_{23} = 0.06$. And also, for $X_w = 0.0168$, $Z_w = -0.3340$, $M_w = 0.0025$, we have $X_{24} = 0.01$. Based on all the above parameters, $\sigma_{\max}(\bar{A}) = 0.0041$. In this case, let $\kappa = 0.01$, $\alpha_1 = \frac{k_D}{M_L}(2 + \frac{\kappa}{l_x}) = 0.15$. and $\beta_1 = \frac{M_L l_x}{k_D} \sigma_{\max}(\bar{A}) = 0.82$. Therefore, $\alpha_1 + \beta_1 = 0.15 + 0.82 = 0.97$ which satisfies $\alpha_1 + \beta_1 < 1$. Another example considers that the UH-60 helicopter carries a load weight $500\,lb$ by a $15\,ft$ sling length and let $k_D = 50\,lb/ft$ then $\alpha_1 = 0.2$ and $\beta_1 = 0.62$ therefore $(\alpha_1 + \beta_1) = 0.82$. Therefore, this assumption $\alpha_1 + \beta_1 < 1$ is realistic for the system discussed in the thesis.

6.3.3 Development of state feedback control

The purpose of controller design in this section is to position the load at or as close as to a specified location. A deterministic feedback control is developed which can be continuous and discontinuous.

Let $\bar{\theta}_L \to h(\bar{\theta}_L)$ where $h(\bar{\theta}_L) = [h_1(\bar{\theta}_L), h_2(\bar{\theta}_L)]^T$ be defined by

$$h_i(\bar{\theta}_L) = -(1-\alpha_1-\beta_1)^{-1}\gamma_1(L_{g_i}v_1)(\bar{\theta}_L), \quad (i=1,2) \tag{6.24}$$

where γ_1 is a positive design parameter.

Suppose $p(x_H(t)) = h(\bar{\theta}_L(t))$ (where $x_H(t) = (p^{-1}\circ h)(\bar{\theta}_L)$) to be considered as a feedback control for the first subsystem (6.8a) and apply Lemma 6.1 and 6.2, then

$$\begin{aligned}
\dot{v}_1(\bar{\theta}_L) &= \langle (\nabla v_1)(\bar{\theta}_L), \dot{\theta}_L \rangle \\
&= \left\langle (\nabla v_1)(\bar{\theta}_L)\ f_1(\bar{\theta}_L) + \sum_{i=1}^{2} g_i(\bar{\theta}_L)(h_i(\bar{\theta}_L) + q_i(p^{-1}\circ h)(\bar{\theta}_L)) + H(\cdot, \bar{\theta}_L, (p^{-1}\circ h)) \right\rangle \\
&\le -\bar{\Psi}(\bar{\theta}_L) - (\gamma_1 - \mu_1)|(L_{g_2}v_1)(\bar{\theta}_L)|^2 + \alpha_2(t)|(L_{g_2}v_1)(\bar{\theta}_L)| \\
&\le -\bar{\Psi}(\bar{\theta}_L) - \left[\sqrt{\gamma_1 - \mu_1}|(L_{g_2}v_1)(\bar{\theta}_L)| - \frac{\alpha_2(t)}{2\sqrt{\gamma_1 - \mu_1}}\right]^2 + \frac{\alpha_2^2(t)}{4(\gamma_1 - \mu_1)}
\end{aligned}$$

where $\bar{\Psi}$ represents either Ψ_1 or Ψ_2. That is, the solutions for the first subsystem will tend to a compact set if $p(x_H(t)) = h(\bar{\theta}_L(t))$. Therefore, the next step of the controller design is to find a control law which will drive the second subsystem state variables to lead $p(x_H(t)) \to h(\bar{\theta}_L(t))$ while t increases. To measure how close $p(x_H(t))$ and $h(\bar{\theta}_L(t))$, a new state variable vector is defined by

$$e(t) := ((p\circ x_H) - (h\circ\theta_L))(t) \tag{6.25}$$

So we have

$$\dot{e}(t) = (Dp)(x_H)\dot{x}_H(t) - (Dh)(\bar{\theta}_L)\dot{\theta}_L(t)$$

with the initial condition

$$e(0) = e^0 := p(x_H^0) - h(\theta_L^0).$$

Substituting the original system equations, we can obtain

$$\begin{aligned}\dot{e}(t) &= \Lambda(t,\bar{\theta}_L,e(t))\,\dot{e}(t)\\ &= (Dp)(\tilde{p})\big(f_2(\bar{\theta}_L,\tilde{p}) + G_2F(t,\bar{\theta}_L,\tilde{p})\big)\\ &\quad -(Dh)(\bar{\theta}_L)\big(f_1(\bar{\theta}_L) + G_1(\bar{\theta}_L)\big(e(t)+h(\bar{\theta}_L)+q(\bar{\theta}_L(t),\tilde{p})\big) + H(t,\bar{\theta}_L,\tilde{p})\big),\end{aligned}$$

where $\tilde{p} = p^{-1}\circ\big(e(t)+h(\bar{\theta}_L)\big)$.

Then the system with the newly defined state variable of ($\bar{\theta}_L$, e) can be modelled by

$$\begin{bmatrix}\dot{\bar{\theta}}_L\\ \dot{e}\end{bmatrix} = \begin{bmatrix} f_1(\bar{\theta}_L) + G_1(\bar{\theta}_L)\big(e+h(\bar{\theta}_L)+q(\bar{\theta}_L,\tilde{p})\big) + H(t,\tilde{\theta}_L,\tilde{p})\\ \Lambda(t,\bar{\theta}_L,e)\end{bmatrix} = \Gamma(t,\bar{\theta}_L,e) \qquad (6.26)$$

Choose A_2, Q_2 such that $\sigma(A_2)\subset C^-$ and Q_2 is a symmetric positive definite matrix, i.e., $Q_2 > 0$. Let $P_2 > 0$ denote the unique symmetric solution of the Lyapunov equation

$$P_2A_2 + A_2^TP_2 + Q_2 = 0 \qquad (6.27)$$

The continues state feedback control $F(t,\bar{\theta}_L,x_H)$ is designed to have the following structure:

$$(t,\bar{\theta}_L,x_H) \mapsto F(t,\bar{\theta}_L,x_H) = G_2^{-1}\big(u_f(\bar{\theta}_L,x_H) + u_{gain}(t,\bar{\theta}_L,x_H)\big), \qquad (6.28)$$

where

$$\begin{aligned}&u_f(\bar{\theta}_L,x_H)\\ &:= -f_2(\bar{\theta}_L,x_H) + [(Dp)(x_H)]^{-1}\big(A_2(p(x_H)-h(\bar{\theta}_L)) + (Dh)(\bar{\theta}_L)\big(f_1(\bar{\theta}_L)+G_1(\bar{\theta}_L)p(x_H)\big)\big)\end{aligned}$$

and

$$u_{gain}(t,\bar{\theta}_L,x_H) := -\rho_C(t,\bar{\theta}_L,x_H)\Pi\big(\rho_C(t,\bar{\theta}_L,x_H)[(Dp)(x_H)]^TP_2(p(x_H)-h(\bar{\theta}_L))\big)$$

In u_N , ρ_C is defined as any continuous function satisfying the following inequality

$$\rho_C(t,\bar{\theta}_L,x_H)$$

$$\geq \sum_{i=1}^{2}\left(\mu_1\left|\left(L_{g_i}v_1\right)(\bar{\theta}_L)\right|+\alpha_1|p_i(x_H)|+\alpha_2(t)\right)\left\|\left[(Dp)(x_H)\right]^{-1}(Dh)(\bar{\theta}_L)g_i\right\| \qquad (6.29)$$

$$+\max\left(\left\|\left[(Dp)(x_H)\right]^{-1}(Dh)(\bar{\theta}_L)\right\|\left\|H(\bar{\theta}_L,x_H)\right\|\right)$$

and

$$Z\to\Pi(Z)=:\begin{cases}\|Z\|^{-1}Z, & \text{if } \|Z\|>\eta\\ Z/\eta, & \text{otherwise}\end{cases} \qquad (6.30)$$

where η is a positive design parameter to be determined. The feedback control in (6.28) can be considered to have two parts. The first part is a nonlinear feedback which is to stabilise the known part of the system and the second part is a variable gain which is to address the uncertainty in the system.

For system (6.26), a Lyapunov function is chosen as

$$\tilde{v}\left(\begin{bmatrix}\bar{\theta}_L\\ e\end{bmatrix}\right)=v_1(\bar{\theta}_L)+\xi v_2(e) \qquad (6.31)$$

where $\xi>0$ is a design parameter to be specified and $v_2(e)=:\frac{1}{2}\langle e,\ P_2e\rangle$. Then

for $\left\|\rho_C(t,\bar{\theta}_L,x_H)\left[(Dp)(x_H)\right]^T P_2\left(p(x_H)-h(\bar{\theta}_L)\right)\right\|<\eta$, we have

$$\dot{\tilde{v}}=\left\langle\nabla v_1(\bar{\theta}_L),\ \dot{\bar{\theta}}_L\right\rangle+\xi\langle\nabla v_2(e),\ \dot{e}\rangle$$

$$\leq -\overline{\Psi}(\bar{\theta}_L)-(1+\alpha_1+\beta_1)\sum_{i=1}^{2}\left(\frac{1}{2}\left|\left(L_{g_i}v_1\right)(\bar{\theta}_L)\right|-|e_i|\right)^2$$

$$-[\mu_1(\gamma_1-1)-\frac{1}{4}(1+\alpha_1+\beta_1)]\sum_{i=1}^{2}\left(\left|\left(L_{g_i}v_1\right)(\bar{\theta}_L)\right|-\frac{2\alpha_2}{4\mu_1(\gamma_1-1)-(1+\alpha_1+\beta_1)}|e_i|\right)^2,$$

$$-[\frac{1}{2}\xi\sigma_{\min}(Q_2)-\frac{1}{4}(1+\alpha_1+\beta_1)]\|e\|^2+2\xi\eta+\frac{\alpha_2^2}{[4\mu_1(\gamma_1-1)-(1+\alpha_1+\beta_1)]}$$

for $\left\|\rho_C(t,\bar{\theta}_L,x_H)\left[(Dp)(x_H)\right]^T P_2\left(p(x_H)-h(\bar{\theta}_L)\right)\right\|\geq\eta$, we have

$$\tilde{v} \le -\overline{\Psi}(\bar{\theta}_L) - (1+\alpha_1+\beta_1)\sum_{i=1}^{2}\left(\frac{1}{2}\left|\left(L_{g_i}v_1\right)(\bar{\theta}_L)\right| - |e_i|\right)^2$$
$$-[\mu_1(\gamma_1-1) - \frac{1}{4}(1+\alpha_1+\beta_1)]\sum_{i=1}^{2}\left(\left|\left(L_{g_i}v_1\right)(\bar{\theta}_L)\right| - \frac{2\alpha_2}{4\mu_1(\gamma_1-1)-(1+\alpha_1+\beta_1)}|e_i|\right)^2$$
$$-[\frac{1}{2}\xi\sigma_{\min}(Q_2) - \frac{1}{4}(1+\alpha_1+\beta_1)]\|e\|^2 + \frac{\alpha_2^2}{[4\mu_1(\gamma_1-1)-(1+\alpha_1+\beta_1)]}$$

For both cases, the following is true:

$$\tilde{v} \le -\overline{\Psi}(\bar{\theta}_L) - (1+\alpha_1+\beta_1)\sum_{i=1}^{2}\left(\frac{1}{2}\left|\left(L_{g_i}v_1\right)(\bar{\theta}_L)\right| - |e_i|\right)^2$$
$$-[\mu_1(\gamma_1-1) - \frac{1}{4}(1+\alpha_1+\beta_1)]\sum_{i=1}^{2}\left(\left|\left(L_{g_i}v_1\right)(\bar{\theta}_L)\right| - \frac{2\alpha_2}{4\mu_1(\gamma_1-1)-(1+\alpha_1+\beta_1)}|e_i|\right)^2$$
$$-[\frac{1}{2}\xi\sigma_{\min}(Q_2) - \frac{1}{4}(1+\alpha_1+\beta_1)]\|e\|^2 + 2\xi\eta + \frac{\alpha_2^2}{[4\mu_1(\gamma_1-1)-(1+\alpha_1+\beta_1)]}$$

.

Therefore

$$\dot{\tilde{v}} \le -\left\langle \begin{bmatrix} \overline{\Psi}^{\frac{1}{2}}(\bar{\theta}_L) \\ \|e(t)\| \end{bmatrix}, T_1 \begin{bmatrix} \overline{\Psi}^{\frac{1}{2}}(\bar{\theta}_L) \\ \|e(t)\| \end{bmatrix} \right\rangle + \frac{\alpha_2^2}{[4\mu_1(\gamma_1-1)-(1+\alpha_1+\beta_1)]} + 2\eta\xi, \qquad (6.32)$$

where

$$T_1 := \begin{bmatrix} 1 & 0 \\ 0 & \left(\frac{1}{2}\xi\sigma_{\min}(Q_2) - \frac{1}{4}(1+\alpha_1+\beta_1)\right) \end{bmatrix}$$

Choosing $4\mu_1(\gamma_1-1) > (1+\alpha_1+\beta_1)$, $\gamma_1 > 1$ $\xi \ge \frac{(1+\alpha_1+\beta_1)}{2\sigma_{\min}(Q_2)}$ ensures that $\sigma_{\min}(T_1) = 1$

and guarantees that

$$\dot{\tilde{v}}\left(\begin{bmatrix} \bar{\theta}_L(t) \\ e(t) \end{bmatrix}\right) \le 0 \quad a.e., \quad \forall \begin{bmatrix} \bar{\theta}_L(t) \\ e(t) \end{bmatrix} \in P^4 \setminus \lambda(k^\eta)$$

where

$$\lambda(k^\eta) := \left\{ \begin{bmatrix} \bar{\theta}_L(t) \\ e(t) \end{bmatrix} : \left\| \begin{bmatrix} \bar{\Psi}^{\frac{1}{2}}(\bar{\theta}_L) \\ e(t) \end{bmatrix} \right\| \le k^\eta ; k^\eta := \frac{\alpha_2^2}{[4\mu_1(\gamma_1 - 1) - (1 + \alpha_1 + \beta_1)]} + 2\eta\xi \right\}$$

From the above analysis, the following theorem results:

Theorem 6.1. *Following Lemma 6.1 and 6.2 with the feedback control defined in (6.28), if the design parameters satisfy* $4\mu_1(\gamma_1 - 1) > (1 + \alpha_1 + \beta_1)$, $\gamma_1 > 1$, *and* $\xi \ge \frac{(1 + \alpha_1 + \beta_1)}{2\sigma_{\min}(Q_2)}$, *the compact set* $\lambda(k^\eta)$ *is globally asymptotically stable for the helicopter dynamic system.*

Theorem 6.1 indicates that the feedback control (6.28) can position the load at the specified location or to a small region around the specified location. The size of the region can be reduced by choosing proper design parameters.

The procedure for the development of a control law for the lateral motion is similar to the longitudinal motion. Therefore the stabilizing feedback control law for lateral motion can be written as with the appropriate parameter:

$$(t, \bar{\varphi}_L, x_H) \mapsto F(t, \bar{\varphi}_L, x_H) = G_2^{-1}(u_L(\bar{\varphi}_L, x_H) + u_N(t, \bar{\varphi}_L, x_H)) \qquad (6.33)$$

whereas,

$$u_L(\bar{\varphi}_L, x_H) := -f_2(\bar{\varphi}_L, x_H) + [(Dp)(x_H)]^{-1}(A_2(p(x_H) - h(\bar{\varphi}_L)) + (Dh)(\bar{\varphi}_L)(f_1(\bar{\varphi}_L) + G_1(\bar{\varphi}_L)p(x_H)))$$

$$u_N(t, \bar{\varphi}_L, x_H) = -\rho_C(t, \bar{\varphi}_L, x_H)\Pi\left(\rho_C(t, \bar{\varphi}_L, x_H)[(Dp)(x_H)]^T P_2(p(x_H) - h(\bar{\varphi}_L))\right)$$

ρ_c is a gain function which is introduced to address the uncertainties in the system.

6.4. Illustration example

In this section, the feedback control developed in Section 6.3 is applied to a helicopter model in its linearised model with an underslung load. Only longitudinal case is studied here. The load model adopted in this section is same as the model in Chapter 4

which has a weight $M_L = 1000lb$ with a $l_x = 15ft$ sling length, $k_D = 75$ and $k_\theta = 2.5$.

From the above analysis, the general format of the helicopter model is represented by

$$\dot{\bar{\theta}}_L(t) = f_1(\bar{\theta}_L(t)) + G_1(\bar{\theta}_L(t))[p(x_H(t)) + q(\bar{\theta}_L(t), x_H(t))] + H(t, \bar{\theta}_L, x_H(t)) \qquad (6.8a)$$

$$\dot{x}_H(t) = f_2(\bar{\theta}_L(t), x_H(t)) + G_2\tilde{u}(t) \qquad (6.8b)$$

System model:

In this example, a linear model of helicopter [Garrard 1989] is adopted, which has the system parameters below:

$$\begin{bmatrix} \dot{u} \\ \dot{v} \\ \dot{w} \\ \dot{p} \\ \dot{q} \\ \dot{r} \\ \dot{\phi} \\ \dot{\theta} \end{bmatrix} = \begin{bmatrix} -0.0199 & -0.0058 & -0.0058 & -0.0151 & 0.0232 & 0.0006 & 0 & -0.06652 \\ -0.0452 & -0.526 & -0.0061 & -0.026 & -0.0155 & 0.0148 & 0.6648 & -0.0003 \\ -0.0788 & -0.0747 & -0.3803 & 0.0008 & -0.0048 & 0.042 & 0.0228 & 0.0102 \\ 0.4557 & -2.5943 & -0.1787 & -2.9979 & -0.5943 & 0.4155 & 0 & 0 \\ 0.3688 & 0.1931 & -0.1753 & 0.071 & -0.5943 & 0.0013 & 0 & 0 \\ 1.0939 & 0.731 & -0.0358 & 0.4058 & 0.4069 & -0.4940 & 0 & 0 \\ 0 & 0 & 0 & 1 & 0.0005 & -0.0154 & 0 & 0 \\ 0 & 0 & 0 & 0 & 0.9994 & 0.0343 & 0 & 0 \end{bmatrix} \begin{bmatrix} u \\ v \\ w \\ p \\ q \\ r \\ \phi \\ \theta \end{bmatrix}$$

$$+ \begin{bmatrix} -0.0456 & -0.083 & 0.4735 & -0.0016 \\ -0.0369 & 0.2785 & 0.0086 & 0.3600 \\ -3.1126 & -0.0032 & 0.0076 & 0.0002 \\ -2.4241 & 20.8327 & 1.0196 & 9.1903 \\ -0.03205 & 0.02538 & -6.3329 & -0.0648 \\ 5.7889 & -2.6208 & 2.3832 & -11.0904 \\ 0 & 0 & 0 & 0 \\ 0 & 0 & 0 & 0 \end{bmatrix} \begin{bmatrix} \theta_o \\ \theta_{1s} \\ \theta_{1c} \\ \theta_{oT} \end{bmatrix}$$

If only the longitudinal motion is considered, then we have

$$\begin{bmatrix} \dot{\theta} \\ \dot{q} \\ \dot{u} \\ \dot{w} \end{bmatrix} = \begin{bmatrix} 0 & 0.9994 & 0 & 0 \\ 0 & -0.5943 & 0.3688 & -0.1753 \\ -0.06652 & 0.0232 & -0.0199 & -0.0058 \\ 0.0102 & -0.0048 & -0.0788 & -0.3803 \end{bmatrix} \begin{bmatrix} \theta \\ q \\ u \\ w \end{bmatrix} + \begin{bmatrix} 0 & 0 \\ 0.02538 & -0.03205 \\ -0.083 & -0.0456 \\ -0.0032 & -3.1126 \end{bmatrix} \begin{bmatrix} \theta_{1s} \\ \theta_o \end{bmatrix}$$

From the above system parameters, the following can be obtained:

$$a_{11} = -0.30635 \text{ and } a_{22} = 0.014785.$$

Let $\bar{T} = \begin{bmatrix} 1 & 0 & 0 & 0 \\ 0 & 1 & -0.30635 & 0.014785 \\ 0 & 0 & 1 & 0 \\ 0 & 0 & 0 & 1 \end{bmatrix}$, then $\bar{T}^{-1} = \begin{bmatrix} 1 & 0 & 0 & 0 \\ 0 & 1 & 0.30635 & -0.014785 \\ 0 & 0 & 1 & 0 \\ 0 & 0 & 0 & 1 \end{bmatrix}$

So the original system model can be transformed into the following format

$$\bar{T}^{-1}\begin{bmatrix} \dot{\theta} \\ \dot{q} \\ \dot{u} \\ \dot{w} \end{bmatrix} = \bar{T}^{-1}\begin{bmatrix} 0 & 0.9994 & 0 & 0 \\ 0 & -0.5943 & 0.3688 & -0.1753 \\ -0.06652 & 0.0232 & -0.0199 & -0.0058 \\ 0.0102 & -0.0048 & -0.0788 & -0.3803 \end{bmatrix}\bar{T}\bar{T}^{-1}\begin{bmatrix} \theta \\ q \\ u \\ w \end{bmatrix} + \bar{T}^{-1}\begin{bmatrix} 0 & 0 \\ 0.02538 & -0.03205 \\ -0.083 & -0.0456 \\ -0.0032 & -3.1126 \end{bmatrix}\begin{bmatrix} \theta_{1s} \\ \theta_0 \end{bmatrix}$$

That is,

$$\begin{bmatrix} \dot{\theta} \\ \dot{\bar{q}} \\ \dot{u} \\ \dot{w} \end{bmatrix} = \begin{bmatrix} 0 & 0.9994 & -0.3045119 & 0.014696 \\ -0.02053 & -0.58712 & 0.54373 & -0.18013 \\ -0.06652 & 0.0232 & -0.02701 & -0.0058 \\ 0.0102 & -0.0048 & -0.0788 & -0.3803 \end{bmatrix}\begin{bmatrix} \theta \\ \bar{q} \\ u \\ w \end{bmatrix} + \begin{bmatrix} 0 & 0 \\ 0 & 0 \\ -0.083 & -0.0456 \\ -0.0032 & -3.1126 \end{bmatrix}\begin{bmatrix} \theta_{1s} \\ \theta_0 \end{bmatrix}$$

The system transformed has the following structure:

$$f_1(\bar{\theta}_L(t)) = \begin{bmatrix} \theta_{L_2} \\ -2.133\ \sin\theta_{L_1} + 1.125\left(sign(\dot{X}_L)\cos^3\theta_{L_1} + sign(\dot{Z}_L)\sin^3\theta_{L_1}\right)\theta_{L_2}^2 - 2.5\theta_{L_2} \\ \bar{q} \\ -0.02053\,\theta + -0.58712\,\bar{q} \end{bmatrix}$$

$$G_1(\bar{\theta}_L(t)) = \begin{bmatrix} 0 & 0 \\ \dfrac{k_D sign(\dot{X}_L)\cos\theta_{L_1}}{M_L l_x} & \dfrac{k_D sign(\dot{X}_L)\sin\theta_{L_1}}{M_L l_x} \\ 0 & 0 \\ 0 & 0 \end{bmatrix} = \begin{bmatrix} 0 & 0 \\ 0.005 sign(\dot{X}_L)\cos\theta_{L_1} & 0.005 sign(\dot{Z}_L)\sin\theta_{L_1} \\ 0 & 0 \\ 0 & 0 \end{bmatrix}$$

$$q(\bar{\theta}_L(t), x_H(t)) = \begin{bmatrix} 0 \\ 0.0667\cos\theta_{L_1}\dot{u} + 0.0667\sin\theta_{L_1}\dot{w} - 0.15\left(sign(\dot{X}_L)\cos^2\theta_{L_1}u + sign(\dot{Z}_L)\sin^2\theta_{L_1}w\right)\theta_{L_2} \end{bmatrix}$$

$$H(t, \bar{\theta}_L(t), x_H(t)) = \begin{bmatrix} 0 \\ 0 \\ -0.3045119u + 0.014696w \\ 0.54373u - 0.18013w \end{bmatrix}, \quad G_2 = \begin{bmatrix} -0.083 & -0.0456 \\ -0.0032 & -3.1126 \end{bmatrix}$$

and $f_2(\bar{\theta}_L(t), x_H(t)) = \begin{bmatrix} (-0.06652\theta + 0.0232\bar{q} - 0.02801u - 0.0058w) \\ (0.0102\theta - 0.0048\bar{q} - 0.0788u - 0.3803w) \end{bmatrix}$.

Verification of the conditions required for feedback control design:

The next step is to check if the system satisfies all the conditions required for application of the method developed in Section 6.3. With the given system parameters, we can calculate the following:

$$\alpha_1 = \frac{k_D}{M_L}(2 + \frac{\kappa}{l_x}) = 0.15$$

$$\|\bar{A}\| = \max(\sigma(\bar{A}^T\bar{A})) = \max(\sigma\left(\begin{bmatrix} -0.3045119 & 0.0149629 \\ 0.54373 & -0.180135 \end{bmatrix}^T\begin{bmatrix} -0.3045119 & 0.0149629 \\ 0.54373 & -0.180135 \end{bmatrix}\right))$$

$$= \max(\sigma\left(\begin{bmatrix} 0.38837 & -0.10242 \\ -0.10242 & 0.03266 \end{bmatrix}\right)) = 0.6447$$

$$\beta_1 = \frac{M_L l_x}{k_D \varsigma_2}\|\bar{A}\| = 128.8/\varsigma_2$$

If ς_2 is chosen to be 200, then $\beta_1 = 128.8/\varsigma_2 = 0.644$. Hence, $\alpha_1 + \beta_1 = 0.794 < 1$ is true. And also, we can obtain $\mu_1 = \frac{k_\theta M_L}{k_D \varsigma_2} = 0.1667$. From Section 6.3, the design parameter ς_1 can be chosen as $\varsigma_1 = \frac{2g}{l_x \pi}\varsigma_2 = 271.62$.

The following is to check if (6.16) holds with the given parameters. For the given system parameters, we have

$$\frac{k_D l_x}{M_L}\left|\max(\theta_{L_2})\left(sign(\dot{X}_L)\cos^3\theta_{L_1} + sign(\dot{Z}_L)\sin^3\theta_{L_1}\right)\right| \le \frac{k_D l_x}{M_L}\left|\max(\theta_{L_2})\right| 2 \le 2.25\left|\max(\theta_{L_2})\right|$$

In general, it can not imagine that the load can swing over 45 degrees of angle within 1 second. Therefore, it is realistic to assume that $\left|\max(\theta_{L_2})\right| \le 1$, which leads to

$$\frac{k_D l_x}{M_L}\left|\max(\theta_{L_2})\left(sign(\dot{X}_L)\cos^3\theta_{L_1} + sign(\dot{Z}_L)\sin^3\theta_{L_1}\right)\right| \le 2.25\left|\max(\theta_{L_2})\right| < k_\theta ,$$

that is, (6.16) holds.

If the design parameters ς_3, ς_4, and ς_5 are chosen to be $\varsigma_3 = 1$, $\varsigma_4 = 0$, and $\varsigma_5 = 1$, the inequalities $[\varsigma_3\varsigma_4 - (\varsigma_4^2 + \varsigma_5)X_{21}] > 0$ and $[\varsigma_3^2 - \varsigma_3\varsigma_4 X_{22} + (\varsigma_4^2 + \varsigma_5)X_{21}] \ge 0$ hold. If γ_1 is chosen to be 3.8, $4\mu_1(\gamma_1 - 1) > (1 + \alpha_1 + \beta_1)$ and $\gamma_1 > 1$ are true. For the purpose of simplifying analysis, it is preferred to choose $A_2 = -3I$, $P_2 = \frac{1}{3}I$ so $Q_2 = 2I$. In this case, the design parameter ξ is given a value of 0.5 and $\xi \ge \frac{(1 + \alpha_1 + \beta_1)}{2\sigma_{min}(Q_2)}$ holds.

With all the above analysis, the suitable Lyapunov function for the system may be

$$\tilde{v}\left(\begin{bmatrix}\bar{\theta}_L \\ e\end{bmatrix}\right) = \frac{1}{2}\left[271.62\theta_{L_1}^2 + 200\theta_{L_2}^2 + \theta^2 + \bar{q}^2\right] + \frac{1}{6}\langle e,\ e\rangle$$

Remark: *Using the word "may" above is because the Lyapunov function is subject to changes with respect to the size of the compact set of* $\lambda(k^\eta)$.

For the chosen Lyapunov function, we have that $\Psi_1(\bar{\theta}_L) = 500\theta_{L_2}^2 + 0.3045\bar{q}^2$ and $-[\varsigma_3\varsigma_4 - (\varsigma_4^2 + \varsigma_5)X_{21}]\bar{q}^2 < \varsigma_3\varsigma_4 X_{21}\theta^2$ holds for all situations, which implies that the solution is applicable to the whole variable range.

Design of feedback control:

Based on the above system and design parameters,

$$h_1(\bar{\theta}_L) = -(1-\alpha_1-\beta_1)^{-1}\gamma_1(L_{g_1}v_1)(\bar{\theta}_L) = -18.447\theta_{L_2}$$

and $h_2(\bar{\theta}_L) = -(1-\alpha_1-\beta_1)^{-1}\gamma_1(L_{g_2}v_1)(\bar{\theta}_L) = -18.447\theta_{L_2}$ as well.

With $G_2 = \begin{bmatrix} -0.083 & -0.0456 \\ -0.0032 & -3.1126 \end{bmatrix}$, we have $G_2^{-1} = \begin{bmatrix} -12.055 & 0.1766 \\ 0.0124 & -0.3215 \end{bmatrix}$.

For the specified system, we can derive the following:

$$[(Dp)(x_H)]^{-1} = \begin{bmatrix} \frac{1}{2u+\kappa_1} & \\ & \frac{1}{2w+\kappa_2} \end{bmatrix}$$

and $A_2(p(x_H) - h(\bar{\theta}_L)) = -3\begin{bmatrix} u^2+\kappa_1 u + 18.447\theta_{L_2} \\ w^2+\kappa_2 w + 18.447\theta_{L_2} \end{bmatrix}$

With $(Dh)(\bar{\theta}_L) = \begin{bmatrix} 0 & -18.447 & 0 & 0 \\ 0 & -18.447 & 0 & 0 \end{bmatrix}$, we have

$$(Dh)(\bar{\theta}_L)(f_1(\bar{\theta}_L) + G_1(\bar{\theta}_L)p(x_H))$$

$$= \begin{bmatrix} 39.354\sin\theta_{L_1} + -20.753(sign(\dot{X}_L)\cos^3\theta_{L_1} + sign(\dot{Z}_L)\sin^3\theta_{L_1})\theta_{L_2}^2 - 2.5\theta_{L_2} \\ 39.354\sin\theta_{L_1} + -20.753(sign(\dot{X}_L)\cos^3\theta_{L_1} + sign(\dot{Z}_L)\sin^3\theta_{L_1})\theta_{L_2}^2 - 2.5\theta_{L_2} \end{bmatrix}$$

$$- \begin{bmatrix} -18.447[0.005sign(\dot{X}_L)\cos\theta_{L_1}(u^2+\kappa_1 u) + 0.005sign(\dot{Z}_L)\sin\theta_{L_1}(w^2+\kappa_2 w)] \\ -18.447[0.005sign(\dot{X}_L)\cos\theta_{L_1}(u^2+\kappa_1 u) + 0.005sign(\dot{Z}_L)\sin\theta_{L_1}(w^2+\kappa_2 w)] \end{bmatrix}$$

Therefore, we can obtain the first part of the feedback control by substituting all the above derived functions :

$$u_f(\bar{\theta}_L, x_H) := -f_2(\bar{\theta}_L, x_H) + [(Dp)(x_H)]^{-1}(A_2(p(x_H) - h(\bar{\theta}_L)) + (Dh)(\bar{\theta}_L)(f_1(\bar{\theta}_L) + G_1(\bar{\theta}_L)p(x_H))).$$

To derive the part addressing the uncertainties of the feedback control, the gain function needs to be examined, which is described below:

$$\sum_{i=1}^{2}\left(\mu_1\left|\left(L_{g_i}v_1\right)\left(\bar{\theta}_L\right)\right|+\alpha_1|p_i(x_H)|+\alpha_2(t)\right)\left\|\left[(Dp)(x_H)\right]^{-1}(Dh)\left(\bar{\theta}_L\right)g_i\right\|$$
$$+\max\left(\left\|\left[(Dp)(x_H)\right]^{-1}(Dh)\left(\bar{\theta}_L\right)\right\|H(\bar{\theta}_L,x_H)\right\|\right)$$

$$\leq \left|[0.3334\theta_{L_2}+0.15(u^2+\kappa_1 u)+0.15(w^2+\kappa_2 w)]0.092\right.$$
$$\left.+340.29\sqrt{(-0.3045u+0.0147w)^2+(-0.54373u-0.1803w)^2}\right|\sqrt{\frac{1}{(2u+\kappa_1)^2}+\frac{1}{(2w+\kappa_2)^2}}$$

$$\leq \{0.03334|\theta_{L_2}|+0.015(u^2+w^2)+64.06(|u|+|w|)\}\left|\frac{u+w+\kappa}{(2u+\kappa_1)(2w+\kappa_2)}\right|$$

So we can choose

$$\rho_C\left(t,\bar{\theta}_L,x_H\right)=\{0.03334|\theta_{L_2}|+0.015(u^2+w^2)+64.06(|u|+|w|)\}\left|\frac{u+w+\kappa}{(2u+\kappa_1)(2w+\kappa_2)}\right|$$

$\left[(Dp)(x_H)\right]^T P_2\left(p(x_H)-h\left(\bar{\theta}_L\right)\right)$ can be obtained as follows:

$$\left[(Dp)(x_H)\right]^T P_2\left(p(x_H)-h\left(\bar{\theta}_L\right)\right)=\frac{1}{3}\begin{bmatrix}(2u+\kappa_1)[u^2+\kappa_1 u+18.447\theta_{L_2}]\\(2w+\kappa_1)[w^2+\kappa_1 w+18.447\theta_{L_2}]\end{bmatrix}$$

From all the above analysis, $u_{gain}\left(t,\bar{\theta}_L,x_H\right)$ can be derived:

$$u_{gain}\left(t,\bar{\theta}_L,x_H\right)=-\rho_C\left(t,\bar{\theta}_L,x_H\right)\Pi\left(\rho_C\left(t,\bar{\theta}_L,x_H\right)\left[(Dp)(x_H)\right]^T P_2\left[p(x_H)-h\left(\bar{\theta}_L\right)\right]\right).$$

Therefore, all the terms in the feedback control are obtained and the feedback control is $F\left(t,\bar{\theta}_L,x_H\right)=G_2^{-1}\left[u_f\left(\bar{\theta}_L,x_H\right)+u_{gain}\left(t,\bar{\theta}_L,x_H\right)\right]$.

6.5 Discussion

In this chapter, a generalised state feedback control is introduced, which has been proved to be able to locate the load at the specified position or its neighbourhood. An illustration example is given in the chapter. The advantages of the method are 1) the system uncertainties are taken into account priory to the controller design which leads

to a robust feedback control; 2) the method results in a guaranteed load positioning accuracy which depends on the design parameters; 3) the controller can be further simplified with the analysis to individual helicopter system. The main disadvantage is that the controller requires the full state feedback which may leads to implementation difficulties.

Only the longitudinal case is discussed for the controller design but the lateral case can be followed easily. In the analysis, a linearised helicopter model is adopted which has simplified the design procedure but the quality of the feedback control is limited by the accuracy of the system model. Due to the complexity of nonlinear helicopter model, the compromise between the control quality and simplicity has to be made in most situations. The work described in this chapter is only an initial trial of using the deterministic Lyapunov control method to the problem of stability of helicopter and a lot of open challenging topics remained to be explored.

7. Concluding Remarks

A summary of the work is presented in this chapter and the main contributions are highlighted. The further study may be continued in a number of different areas and directions. Suggestions for some possible future research work are given at the end of this chapter.

7.1 Summary

The main objectives of the project are to study the dynamics of helicopter with an external underslung load and to develop a robust control strategy to ensure the stability of the combined system. The achievement of the thesis is summarised below.

The helicopter dynamics is studied with reference to general dynamical model of helicopter and then the general model is bridged to UH-60 helicopter model. Validation of the model is accounted by comparisons with flight test data for UH-60 helicopter at hover condition. Dynamics of helicopter with an underslung load is investigated by developing an underslung load mathematical model, by considering the helicopter dynamics as the input to the load model. The results are presented in Chapters 3 and 4. In Chapter 3, influence of the underslung load dynamics to the stability of helicopter is analysed using the UH-60 helicopter model. In Chapter 4, the influences of helicopter dynamics to the dynamics of the underslung load are investigated. The results obtained in Chapter 3 provides an insight knowledge of the stability of the combined system while the results in Chapter 4 revealed the importance of pilot control action in positioning a load and the effects of system parameters on the load dynamics. The control problem is addressed from an overview of flight control design techniques which are applied to develop control laws for helicopter. An experimental study is conducted to demonstrate the intelligent flight control methods, such as the fuzzy control. For the experimental study the twin rotor MIMO system is used, and the results are presented in Chapter 5. In Chapter 6, the control of helicopter with underslung load problem is addressed. In this chapter a generalised state feedback control is introduced and a nonlinear feedback control law

is developed using a deterministic control approach. For the control law development the helicopter with underslung load system is considered as a cascade connection of uncertain nonlinear system. Considering the control of a helicopter with an undreslung load, the dynamical models of both helicopter and load have some uncertainties. The uncertainties may arise from the helicopter to carry an unknown underslung load or the immeasurable parameters in the dynamical models. The uncertainties also arise from computational errors of the dynamical effects such as aerodynamics. Therefore, for a realistic model uncertainties must be taken into account during the controller design.

7.2 Recommendations for further study

The work developed in this thesis may be extended in many directions. Suggestions for some possible future investigations are given below.

i) Experimental study of flight simulation

Control system analysis confirmed that the applicability of the nonlinear stabilizing feedback control law for the helicopter with underslung load system. However, these analysis alone will not guarantee the practical implementation. Thus the use of flight simulator is recommended to gain an insight into the experimental difficulties of the underslung load operation. Comparison of online flight simulation result with the offline simulation results will allow further investigation and improvement of the control law. Once an agreement is achieved, the control law can be implementable or in the more realistic sense the controller employed is ready to use to conduct some flight trials.

ii) Nonlinear optimal control design

Recalling the design procedure for the nonlinear deterministic control law, one of the main requirements is a full state measurement which is difficult to realise. However, if all the states are not measurable, state observers for unmeasurable states can be constructed to obtain the control law. Therefore, for example in the case of all the

states are not measurable then a condition can be identified in which states observers can be constructed and investigated.

A Linear helicopter models

The linearised helicopter model is expressed in the state space description form,

$\dot{x}(t) = Ax(t) + B\overline{u}(t)$

A.1(a) UH-60 like FGR linear helicopter model.

The UH-60 like FGR model presented in Chapter 3 was obtained with the stability augmentation system (SAS) is turned on. Thus, the model is stable. An unstable model is also obtained by turning off the SAS and is presented below.

$$A = \begin{bmatrix} -0.0000 & 0.0000 & -0.0000 & 0.0000 & 0.0000 & 0.0000 & 1.000 & -0.0023 & 0.0503 \\ -0.0000 & -0.0000 & 0.0000 & -0.0000 & -0.0000 & -0.0000 & -0.0000 & 0.9989 & 0.0462 \\ -0.0000 & 0.0000 & -0.0000 & 0.0000 & 0.0000 & 0.0000 & -0.0000 & -0.0462 & 1.0002 \\ 0.0001 & -28.623 & -0.0018 & -0.0185 & 0.0122 & 0.0172 & -1.6650 & 3.0335 & -0.2607 \\ 32.1225 & -0.3207 & 0.0017 & 0.0124 & -0.0316 & -0.0003 & -1.7901 & -1.7648 & 0.3538 \\ 1.4863 & -1.4259 & 0.0007 & 0.0153 & -0.0024 & -0.3341 & -0.1352 & 0.3937 & 2.3529 \\ -0.0002 & -0.4553 & 0.0013 & 0.0223 & 0.0249 & 0.0006 & -4.2805 & -1.7132 & -0.0107 \\ -0.0001 & -0.6729 & 0.0007 & 0.0028 & 0.0045 & 0.0024 & 0.2113 & 0.9317 & -0.0473 \\ -0.0000 & -0.0222 & 0.0001 & 0.0010 & 0.0030 & 0.0007 & -0.1861 & -0.1337 & -0.1889 \end{bmatrix}$$

$$B = \begin{bmatrix} 0.0000 & 0.0000 & -0.0000 & -0.0000 \\ 0.0000 & 0.0000 & -0.0000 & 0.0000 \\ 0.0000 & 0.0000 & -0.0000 & -0.0000 \\ 0.0452 & 0.5795 & 0.3181 & -0.0010 \\ 0.5703 & -0.0621 & -0.1039 & 0.1974 \\ -0.0050 & 0.0315 & -6.0698 & -0.1001 \\ 0.7074 & -0.0747 & -0.0575 & 0.0721 \\ -0.0039 & -0.1100 & 0.0558 & -0.0277 \\ 0.0371 & -0.0036 & 0.1596 & -0.0624 \end{bmatrix}$$

Where definitions of the states input vectors are $x = [\phi\ \theta\ \psi\ u\ v\ w\ p\ q\ r]^T$ and $\overline{u}(t) = [\theta_{1c}\ \theta_{1s}\ \theta_0\ \theta_{0T}]^T$. The helicopter is trimmed at hover condition.

B Linear transformation

Consider the linear state space representation of a system

$$\dot{x}(t) = Ax(t) + B\bar{u}(t)$$

Apply to it a linear transformation $x(t) = T\,z(t)$

where T is a non-singular $(n \times n)$ constant matrix. This defines a new states vector $z(t)$.

Thus,

$$z(t) = T^{-1}x(t)$$

where the non-singularity of T guarantees the existence of T^{-1}, so the states variables $x_i(t)$ and $z_i(t)$ are linear combinations of each others.

Therefore,

$$x_i(t)\sum_{j=1}^{n} T_{ij}z_j(t) \text{ and } z_i(t) = \sum_{j=1}^{n} T_{ij}^{-1}x_j(t)$$

where T_{ij}^{-1} are the elements of the matrix of T^{-1}.

Substituting into the state equation the following can be obtained

$$\frac{d}{dt}(Tz) = ATz(t) + B\bar{u}(t)$$

$$\dot{z}(t) = T^{-1}ATz(t) + T^{-1}B\bar{u}(t)$$

the system (A, B) with state vector $x(t)$ has been transformed into the system $(T^{-1}AT,\ T^{-1}B)$

Appendix C

Notations

T	rotor thrust (N, lbf)
a_0	blade lift curve slope $(1/rad)$
c	blade chord (m, ft)
h_R	negative z co-ordinate of rotor hub (m, ft)
I_β	blade flapping moment of inertia $(kg\,m^2, slug\,ft^2)$
K_β	blade flapping stiffness-spring constant $(N\,m/rad, ft\,lb/rad)$
R	blade radius (m, ft)
s	rotor solidity $= \frac{bc}{\pi R}$
x_{cg}	centre of gravity location forward of fuselage reference point. (m, ft)
γ_s	rotor shaft forward tilt. $(positive\ forward, rad)$
δ_0	blade profile drag coefficient
δ_2	blade lift dependent drag coefficient
θ_{tw}	linear blade twist (rad)
b	number of main rotor blades
δ_3	blade pitch/cone coupling angle (rad)
ρ	air density $(kg/m^3, slug/ft^3)$
$\gamma\ (\gamma_0)$	blade Lock number $= \frac{\rho c a_0 R^4}{I_\beta}$
C_Q	main rotor torque coefficient
C_T	main rotor thrust coefficient
C_X, C_Y, C_Z	main rotor force coefficients in shaft axes
C_{XW}, C_{YW}, C_{ZW}	main rotor force coefficients in the hub-wind axes
$F_0^{(1)}, F_{1c}^{(1)}, F_{1s}^{(1)}, F_{2c}^{(1)}, F_{2s}^{(1)} F_{1c}^{(2)}, F_{1s}^{(2)}$	harmonic components of integrated blade aerodynamic loads
L_R, M_R, N_R	rotor moments in body references axes $(N\,m, ft\,lb)$
L_H, M_H, N_H	rotor moments in shaft references axes $(N\,m, ft\,lb)$
Q_R	main rotor torque $(N\,m, ft\,lb)$
s_β	stiffness number $= \frac{\left(\lambda_\beta^2 - 1\right)}{n_\beta}$
u_H, v_H, w_H	rotor hub velocity components $(m/s, ft/s)$
u_{wg}, v_{wg}, w_{wg}	wind velocity components $(m/s, ft/s)$

u_A, v_A, w_A	aircraft aerodynamic velocities at Centre of gravity $(m/s,\ ft/s)$
u, v, w	aircraft velocity components at Centre of gravity (CG) $(m/s,\ ft/s)$
X_R, Y_R, Z_R	rotor forces in body reference axes $(N,\ lbf)$
α_{sw}, α_{cw}	blade incidence functions (rad)
β	blade flapping angle (rad)
$\beta_0, \beta_{1c}, \beta_{1s}$	harmonics of flapping (rad)
β_{1cw}, β_{1sw}	cyclic flapping in hub-wind axes (rad)
Δ	transformation matrix from hub-wind system
Δn	aircraft normal acceleration increment
δ	main rotor blade drag coefficient
η_a	rotor loading parameter
θ, θ_p	blade pitch angles (rad)
θ_0	main rotor collective pitch at root (rad)
θ_{1c}, θ_{1s}	blade cyclic pitch components (rad)
$\theta_{1c}^*, \theta_{1s}^*$	blade cyclic pitch components before phasing (rad)
$\theta_{1cw}, \theta_{1sw}$	blade cyclic pitch components in hub-wind axes (rad)
λ_0	rotor downwash component
$\lambda_{1c}, \lambda_{1s}$	harmonic downwash components
$\lambda_{1cw}, \lambda_{1sw}$	harmonic downwash components in hub-wind axes
λ_β	rotor blade flap frequency ratio
μ	normalised rotor velocity in x-y plane $\left(\frac{V}{\Omega R}\right)$
μ_x, μ_y, μ_z	normalised rotor velocity components (normalised by ΩR)
x	wake angle (rad)
ψ	blade azimuth angle (rad)
Ψ_w	rotor sideslip angle (rad)
Ω	rotor speed (rad/s)
p_w, q_w, r_w	roll, pitch and yaw rates of rotor in hub-wind axes (rad/s)
a_{0T}	tail rotor blade lift curve slope $(1/rad)$
F_T	fin blockage factor
h_T	negative z co-ordinate of hub
k_3	pitch/flap coupling (δ_3 angle)
l_T	tail rotor location aft of fuselage reference point $(m,\ ft)$
$\left(\frac{n_\beta}{\lambda_\beta^2}\right)_T$	tail rotor $\frac{inertia\ number}{(flap\ frequency)^2}$

R_T	tail rotor blade radius $(m,\ ft)$
s_T	tail rotor solidity
δ_{0T}	blade profile drag coefficient
δ_{2T}	blade lift dependent drag coefficient
δ_T	tail rotor blade drag coefficient
C_{TT}	tail rotor thrust coefficient
C_{QT}	tail rotor torque coefficient
L_T, M_T, N_T	tail rotor moments $(N\,m,\ ft\,lb)$
Q_T	tail rotor torque $(N\,m,\ ft\,lb)$
X_T, Y_T, Z_T	tail rotor forces (N, lbf)
$\theta_{0T}(\theta^*_{0T})$	tail rotor pitch (with δ_3 correction) (rad)
λ_{0T}	tail rotor uniform downwash
μ_T, μ_{zT}	normalised tail rotor velocities
Ω_T	tail rotor speed (rad/s)
a_{0TP}	lift curve slop at zero incidences
C_{ZTP}	maximum normal force coefficient
$k_{\lambda T}$	main rotor downwash factor at tail rotor
S_{TP}	tail plane area $(m^2,\ ft^2)$
l_{TP}	location aft of fuselage reference point $(m,\ ft)$
θ_T	tail plane setting (positive nose up relative to fuselage x axis) (rad)
L_{TP}, M_{TP}, N_{TP}	tail plane moments $(N\,m\,,\ ft\,lb\ )$
$\overline{V}_T$	tail plane total velocity $(m/s,\ ft/s)$
X_T, Y_T, Z_T	tail rotor forces (N, lbf)
α_{TP}	tail plane incidence angle (rad)
h_{FN}	negative z component of fin centre of pressure
l_{FN}	location aft of fuselage reference point $(m,\ ft)$
S_{FN}	fin area $(m^2,\ ft^2)$
θ_{FN}	fin setting (positive nose starboard)
C_{YFN}	fin side-force function
L_{FN}, M_{FN}, N_{FN}	fin aerodynamic rolling, pitching and yawing moments $(N\,m\,,\ ft\,lb\ )$
$\overline{V}_{FN}$	fin total velocity $(m/s,\ ft/s)$
β_{FN}	fin sideslip angle (rad)
C_{YS}	aerodynamic side-force coefficient
$k_{\lambda F}$	main rotor downwash factor
l_F	fuselage reference length $(m,\ ft)$
S_P	fuselage plan area $(m^2,\ ft^2)$
S_S	fuselage side area $(m^2,\ ft^2)$

C_{MF}	fuselage pitching moment function
C_{NF}, C_{NAF}, C_{NBF}	fuselage yawing moment functions
C_{XF}, C_{ZF}	fuselage force functions
L_F, M_F, N_F	fuselage aerodynamic rolling, pitching and yawing moments $(N\,m\,,\ ft\,lb\ )$
V_F	fuselage total velocity $(m/s,\ ft/s)$
$w_{A\lambda}$	fuselage normal velocity incorporating rotor downwash
X_F, Y_F, Z_F	fuselage aerodynamic forces $(N\,m,\ \ ft\,lb)$
α_F	fuselage incidence angle (rad)
β_F	fuselage sideslip angle (rad)
ϕ	euler roll angle (rad)
I_{xx}, I_{yy}, I_{zz}	moment of inertia $(kg\,m^2,\ slug\ ft^2)$
I_{xz}	product of inertia $(kg\,m^2,\ slug\ ft^2)$
M_a	mass of the helicopter (kg, lb)
g	gravitational constant
L, M, N	overall aircraft rolling, pitching and yawing moments $(N\,m,\ ft\,lb)$
p, q, r	aircraft roll, pitch and yaw rates about body reference axes. (rad/s)
X, Y, Z	overall aircraft force components (N, lbf)

References

[1] Aracil, J., "Describing Function Method for Stability Analysis of PD and PI fuzzy controllers, IFAC Digital control: Past, Present and Future of PID control, Terrassa, Spain, 2000.

[2] Astrom, K.J. and Wittenmark, B., "Adaptive Control, 2nd Edition, Reading, MA: Addision-Wesley, 1995.

[3] Avila-Vilchis, J.C., Brogliato, B., Dzul, A., and Lozano, R., "Nonlinear modelling and control of helicopter", Automatica, April, 2003.

[4] Anonymous, "Handling qualities requirements for military rotorcraft", ADS-33-D, U.S. Army aviation and Troop Command, St.Louis, MO, May 1996.

[5] Antsaklis.P.J., and Passino.K.M., (Eds,) "An introduction to intelligent and autonomous control", Kluwer academic publishers, Norwell, MA, 1993.

[6] Anthony.T.C., Wie.B., and Carroll.S., "Pulse modulated control synthesis of a flexible spacecraft", AIAA Journal of guidance, control and dynamics, Vol.13, No.6, pp.1014 ~ 1022, 1990.

[7] Atherton.D.P., "Nonlinear control engineering", Van-Nostrand, 1975.

[8] Bagnell, J.A. and Schneider, J.G., "Autonomous Helicopter Control using Reinforcement Learning Policy Search Methods", Proceedings of the IEEE Conference on Robotics & Automation, Seoul, Korea, pp 1615 ~ 1620, 2001.

[9] Barve.J.J., Interval methods for analysis of linear and nonlinear control systems, PhD thesis, Indian Institute of technology, Department of Electrical Engineering, December 2003.

[10] Bhattacharyya.S.P., Chapellat.H., and Keel.L.H., "Robust control-the parametric approach", Prentice Hall, New York, 1995.

[11] Blight, J.D., Dailey, R.L., and Gangsaas, D., "Practical control law design for aircraft using multivariable techniques" In Tischler, M.B., (Ed.) Advances in aircraft flight control, pp 231 ~ 267, 1996.

[12] Bossi, J.A., and Langehough, M.A., "Multivariable autopilot designs for a bank-to-turn missile", in proceedings of American control conference, Atlanta, Georgia, USA, pp 567 ~ 572, 1988.

[13] Boyle, D.P., and Chamitoff, G.E., "Autonomous manoeuvre tracking for self piloted vehicles", AIAA Journal of guidance, control and dynamics, Vol.22, No.1, pp.58 ~ 67, 1999.

[14] Bramwell, A.R.S., Done, G., and Balmford, D., "Bramwell's helicopter dynamics" Butterworth-Heinemann, 2001.

[15] Bramwell, A.R.S., "Helicopter Dynamics", Edward Arnold 1976.

[16] Bryson, A.E., "New concepts in control theory 1959-1984", Journal of guidance, control and dynamics, Vol.8, No.4, pp.417 ~ 425, 1985.

[17] Buskey, G., Wyth, G. and Roberts, J., "Autonomous Helicopter Hover Using an Artificial Neural Network", Proceedings of the IEEE International conference on Robotics & Automation , Seoul, Korea, pp1635 ~ 1640, 2001.

[18] Cameron, N., "Identifying pilot model parameters for an initial handling qualities assessment", PhD Thesis, University of Glasgow, Department of Aerospace Engineering, April 2002.

[19] Carr, J., "Applications of centre Manifold theory", Springer-Verlag, Newyork, 1981.

[20] Cicolani, L.S., and Kanning.G., " Equations of motion of slung load systems with results for dual lift", NASA, TM 102246, Feb 1990.

[21] Cicolani, L.S., Kanning.G., and Synnestvedt.R., "Simulation of the Dynamics of helicopter slung load systems", Journal of the American helicopter society, Oct 1995.

[22] Cicolani, L.S., McCoy, A.H., Tischier, M.B., Tucker, G.E., Gatenio, P., and Marmar, D., "Flight time identification of a UH-60A helicopter and slung load", NASA TM-11231, 1998.

[23] Cicolani, L.S., Sahai, R., Tucker, G.E., McCoy, A.H., Tyson, P.H., Tischier, M.B., and Rosen, A., "Flight test identification and simulation of a UH-60A helicopter and slung load", NASA/TM-2001-209619, USAAMCOM-TR-01-A-001, January 2001.

[24] Cheng, R., "Rotorcraft flight control design using quantitative feedback theory and dynamic crossfeeds, Msc thesis, California Polytechnic State University, San Luis Obispo, 1995.

[25] Chen.B.S., Cheng.Y.M., and Lee.C.H., "Genetic approach to mixed H_2 / H_∞ optimal PID control", IEEE control system magazine, pp 51 ~ 60, October, 1995.

[26] Driankov, D., "Fuzzy Gain scheduling, in C. Bonivento, C. Fantuzzi and R. Rovatti (Ed.) Fuzzy logic control: Advances in methodology", Singapore: World Scientific, 1998.

[27] Driankov, D., Palm, R., and Rehfuss, U., A TakagiSugeno Fuzzy Gain-Scheduler, Proc. IEEE conf. Fuzzy systems, NewOrleans, pp 1053 ~ 1059, 1996.

[28] Doyle, J.C., and Stein, G., " Multivariable feedback design: Concepts for a classical/Modern synthesis", IEEE Transactions on automatic control, Vol. AC-26, No 1, pp. 4 ~ 16, Jan. 1981.

[29] Dorling, C.M., and Zinober, A.S.I., "Two approaches to hyperplane design in multivariable variable structure control systems", International journal of control, Vol. 44, No.1, pp65 ~ 82, 1986.

[30] Dukes, T.A., "Maneuvering heavy sling loads near hover- part 1: Damping the pendulous motion", Journal of the American helicopter society, pp2 ~ 11, April 1973.

[31] Enns, D.F., "Multivariable flight control for attack helicopter" IEEE control system magazine, Vol. 7, no 2, pp. 34 ~ 38, 1987.

[32] Enns.D.F., "Multivariable flight control for an attack helicopter" in the proceedings of ACC'86, Seattle, WA, pp858 ~ 863, June 1986.

[33] Edwards, C. and Spurgeon, S.K., "Sliding mode control: Theory and application", Taylor & Francis, London, 1998.

[34] Feedback Instruments Ltd., "Twin rotor MIMO system: Reference Manual", Park road, Crowborough, E. Sussex, TN6 2QR, UK, 1997.

[35] Fletcher, J.W., "A model structure for identification of linear models of the UH-60 helicopter in hover and forward flight", NASA/TM 110362, August 1995.

[36] Fletcher, J.W., "Identification of UH-60 stability derivative models in hover from flight test data" AHS, May 1993.

[37] FLIGHTLAB user manuals, Advanced Rotorcraft Technology, Inc., Mountain View, CA 94043, April 2000.

[38] Fusato, D., Guglieri, G., and Celi, R., "Flight dynamics of an articulated rotor helicopter with an external slung load", AHS, 1999.

[39] Garrard, W.L., Low, E., and Prouty, S., "Design of attitude and rate command system for helicopters using eigenstructure assignment", AIAA Journal of guidance, control and dynamics, Vol.12, no. 6, pp. 783 ~ 791, December 1989.

[40] Garrard, W.L., and Liebst, B.S., "Design of a multivariable helicopter flight control system for handling qualities enhancement", Proc. 43rd AHS forum, St. Louis, pp 677 ~ 696, May 1987.

[41] Ghosh., R., and Tomlin., C., "Nonlinear inverse dynamic control for model based flight" AIAA-2000-4066, American institute of aeronautics and astronautics, 2000.

[42] Goodall, D.P. and Ryan, E. P. "Feedback controlled differential inclusions and stabilizations of uncertain dynamical systems", SIAM journal on control and optimization, 26, pp 1431~1441, 1988.

[43] Goodall, D.P., "Asymptotic Sabilization of a Class of Uncertain Composite Systems", Dynamics and Control, 4, pp 311 ~ 326, 1994.

[44] Goodall, D. P. and Wang, J., "Stabilization of a class of uncertain nonlinear affine systems subject to control constraints", International J. Robust and Nonlinear Control, 11, pp 797 ~ 818, 2001.

[45] Gribble, J.J., "Linear quadratic Gaussian / loop transfer recovery design for a helicopter in law-speed flight", Journal of Guidance, control and dynamics, Vol. 16, No.4, Aug. 1993.

[46] Gribble, J.J., and Murray-Smith, D.J., "Command following control law design by linear quadratic optimisation", 16th European Rotorcraft Forum, Glasgow, Paper NO. III.5.3, 1990.

[47] Gubbels, A.W., "Preliminary slung load investigation on the NRC Bell 412 Advanced systems research aircraft", Journal of the American helicopter society, vol 46, No.2, pp 161 ~ 165, April 2001.

[48] Gupta, N.K., and Bryson, A.E., "Near-hover control of helicopter with a hanging load", Journal of Aircraft vol. 13, pp217 ~ 222, March 1976.

[49] Harvey, C.A., and Stein, G., "Mulitvariable feedback design: concept for a classical/modern synthesis", IEEE Transactions on automatic control, Vol. AC-23, No 2, pp 378 ~ 387, 1978.

[50] Houpis, H., "Quantitative feedback theory; fundamentals and applications", Marcel dekker publishers, New York, 1999.

[51] Horowitz, "Survey of quantitative feedback theory (QFT), International journal of control, Vol. 53, No.2, pp255 ~ 291, 1991.

[52] Innocenti, M., and Schmidt, D.K., "Quadratic optimal cooperative control synthesis with flight control application" AIAA Journal of guidance, control and dynamics, Vol.7, no. 2 , March 1984.

[53] Isidori, A., Marconi, L., and Serrani, A., "Robust nonlinear motion control of a helicopter", IEEE Transactions on automatic control, Vol. 48, No 3, pp 413 ~ 425, March 2003.

[54] Jun, M., Roumeliotis., and Sukhatme., G.S., "State estimation of an autonomous flying helicopter", in IEEE/RSJ international conference on intelligent robots and systems, pp 1346 ~ 1353, October, 1999.

[55] Kadmiry, B. and Driankov, D., "Autonomous Helicopter Control Using Linguistic and Model-Based Fuzzy Control", Proceedings of the IEEE International symposium on Intelligent control, Mexico City, Mexico, pp 348 ~ 352, 2001.

[56] Khalil, H.K., "Nonlinear systems", Macmillan publishing company, 1992.

[57] Khalil, H.K., Nonlinear Systems, 2nd Ed., Englewood Cliff, NJ: Prentice-Hall, 1996.

[58] Kwatny, H. G., and Blankenship, G.L., "Nonlinear control and analytical mechanics", Birkhauser, 2000.

[59] Lane., S.H., and Stengel.,R.F., "Flight control design using nonlinear inverse dynamics", Automatica, Vol. 24, No.4, 1988.

[60] Ledin.J., Ledin.P.E., Dickens.M., and Sharp.J., "Single modelling environment for constructing high-fidelity plant and controller models", AIAA, 2003.

[61] Leishman, G., "The Principles of Helicopter Aerodynamics", Cambridge University Press, 2000.

[62] Leva, A. and Colombo, A.M., "Method for optimising set-point weights in ISA-PID autotuners, IEE proceedings: Control theory and applications, Vol. 146, No. 2, pp 137 ~ 146, 1999.

[63] Mahony, R., Hamel.T., and Dzul.A., "Hover control via Lyapunov control for an autonomous helicopter", Proceedings of the 38th IEEE cont. on Decision and Control, pp 3490 ~ 3495, December1999.

[64] Manness, M.A., Gribble, J.J., and Smith, D.J.M., "Multivariable methods for helicopter flight control law design", Proceedings of the 16th Annual society European rotorcraft forum, paper no. III.5.2, Glasgow, UK, 1990.

[65] Marquez, H.J., "Nonlinear control systems: Analysis and Design", John Wiley & sons, Inc., 2003.

[66] Mayajima, K., "Analytical design of a high performance stability and control augmentation system for a hingeless rotor helicopter", JAHS, Vol. 24, No.3, pp29 ~ 36, 1979.

[67] McCoy, A.H., "Flight testing and real-time system identification analysis of a UH-60A Black Hawk helicopter with an instrumented external slung load", NASA/CR-1998-196710, RTOP-581-30-22, June 1998.

[68] Meyer, G., Hunt, R.L., and Su, R., "Design of a helicopter autopilot by means of linearizing transformations" Guidance and control panel 35th symposium, AGARD CP 321, paper no. 4, 1983.

[69] Musch.H.E., and Steiner.M., "Tuning advanced PID controllers via direct H_∞-norm minimization", in the proceeding of ECC'97, 1997.

[70] Nagabhushan, B.L., "Systematic investigation of models of helicopters with a slung load", Ph.D. Thesis, Dept. of Aerospace Engineering, Virginia Polytechnic Institute and State University, Feb 1977.

[71] Newman, S., The Foundations of Helicopter Flight, Arnold, A member of the Hodder Headline Group, London 1994.

[72] Newman, B., "Dynamics and control of limit cycling motions in boosting rockets" Journal of guidance control and dynamics Vol. 8, No. 2, pp 280 ~ 286, 1995.

[73] Padfield, G.D., and White, M.D., "Flight Simulation in Academia; HELIFLIGHT in its first year of operation-The Challenge of Realistic Rotorcraft Simulation" RAeS Conference, London, Nov. 2001.

[74] Padfield.G.D., "Helicopter flight dynamics", Blackwell science Ltd., 1996.

[75] Padfield.G.D., "A theoretical model of helicopter flight mechanics for application to piloted simulation", Royal Aircraft Establishment, TR/81048, 1981.

[76] Postlethwaite.I., Prempain.E., Turkoglu.E., and Turner.M., "Various H-infinity controllers for the Bell-205 helicopter: Design and Flight test", IFAC world congress, 2002.

[77] Prabhaker, A., "Stability of helicopter carrying an under-slung load", Vertica, Vol. 2, pp 121 ~ 143, 1978.

[78] Prasad, J.V.R., Schrage, D.P., and Calise, A.J., "Comparison of helicopter flight control system design techniques", Helicopter handling qualities and control, International conference, RAS, London, Paper No.12, November, 1988.

[79] Prouty, R., Helicopter Performance, Stability and Control, PWS Publishers, 1986.

[80] Qu, Z. "Robust control of nonlinear uncertain systems under generalized matching conditions", Automatics, 29, pp 985 ~ 998, 1993.

[81] Ryan, E.P. and Corless, M., "Continuous and asymptotic stability of a class of uncertain dynamical systems via continuous and discontinuous feedback control", IMA J. Math.Control and information, 1, PP 223 ~ 242, 1984.

[82] Rubio, F.R., and Aracil, J., "Design of a combined tracking control systems", Control Engineering practice, Vol. 5, No. 1, pp 23 ~ 31, 1997.

[83] Sahai, R., Cicolani, L.S., Tischiler, M.B., Blanken, C.L., Sullivan, C., Wei, M.Y., Sun Ng.Y., and Pierce.L.E., "Flight-time identification of helicopter-slung load frequency response characteristics using CIFER," AIAA, 1999.

[84] Sanders.C.P., DeBitetto.P.A., Feron.E., Vuong.H.F., and Leveson.N., "Hierarchical control of small autonomous helicopters", 37th IEEE conference on decision and control, vol. 4, pp3629 ~ 3634, Tampa, FL, December 16 ~ 18, 1998.

[85] Shaughnessy, J.D., Deaux, T.N., and Kenneth, R.Y., "Development and validation of a piloted simulation of a helicopter and external sling load" NASA Technical paper 1285, NASA-LRC, Jan 1979.

[86] Sheldon, D.F., "An appreciation of the dynamic problems associated with the external transportation of loads from a helicopter- state of the art", Vertica, vol.1, pp 281 ~ 290, 1977.

[87] Shim, H., Koo, T.J., Hoffmann, F. and Sastry, S., "A Comprehensive Study of Control Design for an Autonomous Helicopter", Proceedings of the 37th IEEE conference on Design & control, Tampa, Florida, USA, pp 3653 ~ 3658, 1998.

[88] Shtessel, Y., and Shkolnikov, I. A., "Aeronautical and space vehicle control in dynamic sliding manifolds", International Journal of control, Vol. 76, Issue 10, pp 1000 ~ 1017, 2003.

[89] Shtessel, Y., Buffington, J., and Banda, S., "Tailless aircraft flight control using multiple time scale re-configurable sliding models", IEEE transaction on control system technology, Vol. 10, No.2, pp 288 ~ 296, 2002.

[90] Shtessel, Y., Buffington, J., and Banda, S., "Multiple time scale flight control using reconfigurable sliding modes", AIAA Journal on guidance, control, and dynamics, Vol.22, No.6, pp 873 ~ 883, 1999.

[91] Shkolnikov, I. A, and Shtessel, Y.,"Aircraft nonminimum phase control in dynamic sliding manifolds", AIAA Journal on guidance, control, and dynamics, Vol.24, No.3, pp 566 ~ 572, 2001.

[92] Skogestad, S. and Postlethwaite, I., Multivariable Feedback control-Analysis and Design, John wiley & sons, Chichester, England, 1996.

[93] Slotine, J-J.E., and Li, W., "Applied nonlinear control", Prentice-Hall, 1991.

[94] Smith, G.A., and Meyer, G., "Aircraft automatic flight control system with model inversion", AIAA Journal of guidance, control and dynamics, Vol.10, No. 3, pp. 269 ~ 275, 1987.

[95] Steinberg, M., "Potential Role of Neural Networks and Fuzzy logic in flight control design and development", AIAA 92-0999, Washington, DC, 1992.

[96] Stepniewski, W.Z., and Keys, C.N., Rotary-Wing Aerodynamics, Dover Publications, Inc, New York, Vol. 2, 1984.

[97] Stengel, R.F., "Intelligent flight control systems" in Aerospace vehicle Dynamics and control, M. Cook and M. Rycroft, ed. Oxford University Press, Oxford, pp. 33 ~ 80, 1994.

[98] Saripalli.S., Roberts.J.M., Croke., P.I., Buskey.G., and Sukhatme.G.S., "A tale of two helicopters", in IEEE/RSJ international conference on intelligent robots and systems (IROS), pp 805 ~ 810, October, 2003.

[99] Snell, S.A., Enns, D.F., Jr, W.L.G., Nonlinear inversion flight control for a super-manoeuvrable aircraft", Journal of guidance, control and dynamics, Vol.15, No. 4, pp. 976 ~ 984, 1992.

[100] Snell, S.A., and Stout, P.W., "Flight control law using nonlinear dynamic inversion combined with quantitative feedback theory", Journal of dynamic systems, measurement and control, Vol.120, No.2, pp208 ~ 214, 1998.

[101] Sugeno, M., Hirano, I., Nakamura, S. and Kotsu, S., "Development of an intelligent unmanned helicopter", In IEEE International Conference on Fuzzy systems, Vol. 5, pp 33 ~ 38, 1995.

[102] Thanapalan, K., Wang, J., and Nuttall, K., "A study of helicopter dynamics with an external load", Proceeding of the 16th International conference on System Engineering, Coventry, UK, pp 697 ~ 702, September 2003.

[103] Thomson, D.G., and Bradley, R., "The principles and practical application of helicopter inverse simulation" Simulation practice and theory, Journal of the Federation of European simulation societies, pp 47 ~ 70, 1998.

[104] Thompson, D.F., Pruyn,J.S., and Shukla, A., "A feedback design for robust tracking and robust stiffness in flight control actuators using a modified QFT technique, International journal of control, Vol. 72, No. 16, pp 1480 ~ 1488, 1999.

[105] Turner, M.C., "Robust control of systems subject to input nonlinearities with application to high performance helicopters", PhD Thesis, University of Leicester, Department of Engineering, July 2000.

[106] Tyson, P.H., Cicolani, L.S., Tischler, M.B., Rosen, A., Levine, D., and Dearing, M., "Simulation prediction and flight validation of UH-60A Black Hawk slung load characteristics" AHS, May 1999.

[107] Vidyasagar, M., "Nonlinear systems analysis", Prentice hall International Inc., 2nd Edition, 1993.

[108] Visioli, A., "Adaptive tuning of fuzzy set-point weighting for PID controllers", IFAC Digital Control: Past, Present and Future of PID control, Terrassa, Spain, 2000.

[109] Walker, D.J., "Multivariable control of the longitudinal and lateral dynamics of fly-by-wire helicopter", Control Engineering practice, vol. 11, pp 781 ~ 795, July 2003.

[110] Wan, E.A. and Bogdanov, A.A.," Model predictive neural control with applications to a 6 DoF helicopter model", Proceedings of the American Control Conferences", Arlington, VA, pp 488 ~ 493, 2001.

[111] Wang, J., Practical Stabilization of Uncertain Dynamical Systems with Application to Feedback Control of a Robotic Manipulator, PhD Thesis, Coventry University, Control Theory & Applications Centre, September 1995.

[112] Watkins, T.C., Sinacori, J.B., and Kesler, D.F., "Stabilization of externally slung helicopter load" USA AMRDL TR-74-42, Aug 1974.

[113] Wendel, T., and Schmidt, D., "Flight control synthesis for unstable fighter aircraft using the LQG/LTR methodology", Proceedings of AIAA Guidance, navigation and control conference, Boston, MA, Aug. 14-16, pp.247 ~ 254, 1989.

[114] Woodley.B., Jones.H., Frew.E., LeMaster.E., and Rock.S., "A contestant in the 1997 international aerial robotics competition aerospace robotics laboratory Stanford University", in the proceeding of AUVSI'97, July, 1997.

[115] Yue, A., Postlethwaite, I., and Padfield, G.D., "H-infinity design and the improvement of helicopter handling qualities" Vertica, Vol. 13, pp. 119 ~ 132, 1989.

[116] Yue, A., and Postlethwaite, I., "Improvement of helicopter handling qualities using H-infinity optimisation" IEE Proceedings, Vol. 137, part D, No3, pp. 115 ~ 129, 1990.

[117] Xie, J., "MIMO twin rotor fuzzy control", MSc Thesis, Department of Electrical Engineering and Electronics, University of Liverpool, UK, July 2002.

[118] Xie, J., Wang, J., Jia, L., Zhong, M. and Thanapalan, K., "Robust Fuzzy Controller Development for a Nonlinear Twin rotor MIMO system", Proceeding of the 16th International conference on System Engineering, Coventry, UK, pp 761 ~ 766, September 2003.